7-13-2009

Removing Arsenic from Landfill Leachate in Batch Reactors with Kemiron Adsorbent, a Commercially Available Iron Oxide

Douglas Oti
University of South Florida

Removing Arsenic from Landfill Leachate in Batch Reactors with Kemiron Adsorbent, a Commercially Available Iron Oxide

by

Douglas Oti

A dissertation submitted in partial fulfillment
of the requirements for the degree of
Doctor of Philosophy
Department of Civil and Environmental Engineering
College of Engineering
University of South Florida

Major Professor: Maya Trotz, Ph.D.
Daniel Yeh, Ph.D.
Mark Stewart, Ph.D.
Norma Alcantar, Ph.D.
Jeffrey Cunningham, Ph.D.

Date of Approval:
July 13, 2009

Keywords: Adsorption, Langmuir, Freundlich, Diffusion coefficient, Electron potential.

This dissertation is dedicated to my wife, Joyce, and to my two daughters; Aba and Effia. It is also dedicated to my mum, my dad and to all my siblings.

Acknowledgments

First of all I would like to acknowledge my wife, Joyce, whose deep love got me through the times associated with doing my Ph.D. Her support has been unwavering and priceless. My two daughters, Aba and Effia have always been, and continue to be my source of joy.

I also wish to express my sincere appreciation to Dr. M. Trotz whose capacity as a Principal Advisor has been of great value. I would like to thank my committee members Drs. Jeffrey Cunningham , Daniel Yeh, Norma Alcantar, and Mark Stewart whose thoughtful suggestions and encouragement have been a significant motivator for making this possible.

Finally, I wish to thank Joniqua Howard, Erlande Omisca, and Ken Thomas and all those who worked in Dr. Trotz's laboratory while I was there for their help and suggestions on my work. I again express my appreciation to all my colleagues, especially Roland Okwen, Mr. Jean Cobbold, Mr. Gilbert Koume and to their families. Thanks also to Mr. Ackah for his priceless help throughout this process.

This work was supported by Florida Center for Solid and Hazardous Waste Grant No. 1933-082.

Table of Contents

List of Tables

List of Figures

Removing Arsenic from Landfill Leachate in Batch Reactors with Kemiron Adsorbent, a Commercially Available Iron Oxide

Douglas Oti

ABSTRACT

This research evaluated the effectiveness of a commercially available adsorbent, Kemiron, to remove arsenic from conditions representative of landfill leachate. Kemiron was identified as an iron oxide of 39.8 m^2/g surface area, 44 % of which resided in the less than 3 nm pore size range. Batch experiments of As(V) and As(III) were conducted with particle sizes either ≤38 μm and in the range 500 – 600 μm with equilibrium being reached in the smaller particles in ~ 36 hours and estimated at 374 hrs for the larger particles. Ionic strength did not affect the mass loadings of As(V) and As(III) which approached 80 mg/g sorbent and greater than 90 mg/g respectively at pH 7. The effect of Se(IV) and Ni(II) was greater on As(III) than on As(V) sorption with as much as a 40% reduction in As(III) sorption in the presence of a similar amount of Se(IV). Sulfate, calcium and carbonate reduced As(III) sorption whereas calcium enhanced As(V) sorption. As removal tested in synthetic landfill leachate under both young and old landfill conditions indicated that pH, ORP, and Se(IV) as a co-contaminant with 1:1 mg/L concentration to As were the most significant key factors that influence As adsorption. Over 90% of 5 mg/L As(V) as initial concentration was removed at pH 7.2 within an operating range of 197 and 371.6 mV of ORP and 99% removal was also

achieved at ~ pH 11 under the range of -335.7 and 9.1 mV of ORP where the latter condition would be unlikely in real leachate. Preliminary experiments with real leachate solutions show similar sorption behavior for As(V) though the total amount removed was reduced. Whilst this work shows the potential for sorption technology as a treatment option for heavy metal removal from landfill leachate, further tests are definitely needed to determine the various pre-treatment options needed before real leachate solutions can be treated. Many commercially available sorbents have been developed for contaminated drinking waters and this is the first study that has looked at their application to the more complex leachate matrix.

Chapter 1

Introduction

1.1 Motivation

Arsenic (As) contamination in surface and groundwater is a major problem of our time, affecting large populations around the world, including the United States. The outbreaks of As-related diseases in Bangladesh and in some parts of West Bengal elevated consciousness of its deleterious health effects like Blackfoot disease (Lamm and Kruse 2005), gastrointestinal disorders, cardiac damage, chronic vascular disorders (Simeonova and Luster 2004), and skin cancer (Rossman *et al.* 2004). Table 1.1 summarizes concentrations of As detected in various water resources and the health impacts on users in various parts of the world. Other heavy metals also pose health concerns. For instance, selenium (Se) is an essential nutrient at low levels, but ingestion at concentrations above 55 μg/L can damage the nervous system (Letavayova *et al.* 2006). Arsenic contamination of potable water is due to both natural and man made sources. Landfills are an emerging concern in Florida and other parts of the United States because of the potential leakage of leachate contaminated with arsenic and other contaminants into aquifers (Christensen *et al.* 2000, Pujari and Deshpande 2005).

The leachate from lined landfills is either sent to an external waste water treatment facility, recycled back through the landfill, or treated on site. Figure 1.1 depicts a typical lined landfill in which some leachate is recycled through the landfill to assist

Table 1.1: Arsenic and its related health effects.

Ranges of As concentration	Place	Health effect seen	References
Unknown cumulative amount	Southwestern coast of Taiwan	Blackfoot disease	Tseng (1989)
10 – 100 µg/L for less than 20 years and between 20 and 40 years for 100,000 people	Taiwan	Urinary cancer	Chiou *et al.* (1995)
Unknown cumulative amount	Chile	Lung cancer and bronchiectasis in young adults	Smith *et al.* (2006)
0.41 mg/L or greater	China	Induction of oxidative Stress	Sugden *et al.* (2004)
Unknown cumulative amount	Finland	Bladder cancer	Kurttio *et al.* (1999)
Unknown cumulative amount	Taiwan and Bangladesh	Diabetes	Navas-Acien *et al.* (2008)
300 µg/L or greater	West Bengal, India	Skin lesions	Chowdhury *et al.* (2000)
1 – 3644 µg/L	West Bengal, India	Skin lesions	Rahman *et al.* (2006)
50 µg/L or greater	Araihazar, Bangladesh	Intellectual impairment of children	Wasserman (2004)
50 – 400 µg/L for over 20 years	West Bengal	Bronchiectasis	Mazumder *et al.* (2005)
1200 µg/L or greater	Bangladesh	Abdominal pain, vomiting, diarrhea, muscular weakness and cramping.	Mead (2005)

Table 1.1 (continued)

Unknown cumulative amount	New Hampshire (USA) and Sonora (Mexico)	Decreased DNA Repair in Vitro	Andrew *et al.* (2006)
Unknown cumulative amount	Utah, USA	Increased mortality from hypertensive heart disease, nephritis and nephrosis, and prostate cancer	Lewis *et al.* (1999)
Unknown cumulative amount	West Virginia, USA	Accelerates atherosclerosis	Simeonova and Luster (2004)
100 µg/L or greater	Nevada and California, USA	People with diets deficient in protein and other nutrients are more susceptible than others to arsenic-caused cancer	Steinmaus *et al.* (2005)

with biodegradation processes.Unlike organic compounds, heavy metals like arsenic do not degrade. An opportunity exists to capture the heavy metals released from a degenerating solid waste into leachate in an onsite treatment step. Such a process would minimize the volume occupied by the heavy metal, making it easier to recycle it or easier to dispose of it in a controlled environment like a more contained, lined landfill cell. Wastewater treatment facilities have limits on the volume of leachate they can process based on the leachate quality. High concentrations of As content attract surcharges and a presence of high levels of total dissolved solids are sometimes rejected by some treatment facilities. These factors lead to expensive disposal costs for some Florida landfill facilities. For example, in 2005, the Polk County Landfill in Lakeland, Florida transported approximately half of its leachate to a treatment facility in Jacksonville at a significant cost to the landfill facility because the local waste water treatment plant did

not have the capacity to accept the high total dissolved solids concentration coupled with the concentrations of toxic metals like arsenic. Recycling of the leachate through the landfill is a potential low cost option for disposal, but the non-degradable nature of heavy metals like arsenic means that the landfill will be a continual source of arsenic, and will always have to be monitored, even after the degradation of toxic organic compounds. Recycling of heavy metals through the landfills may also increase their concentration to levels where microbial activity is significantly reduced due to toxic effects.

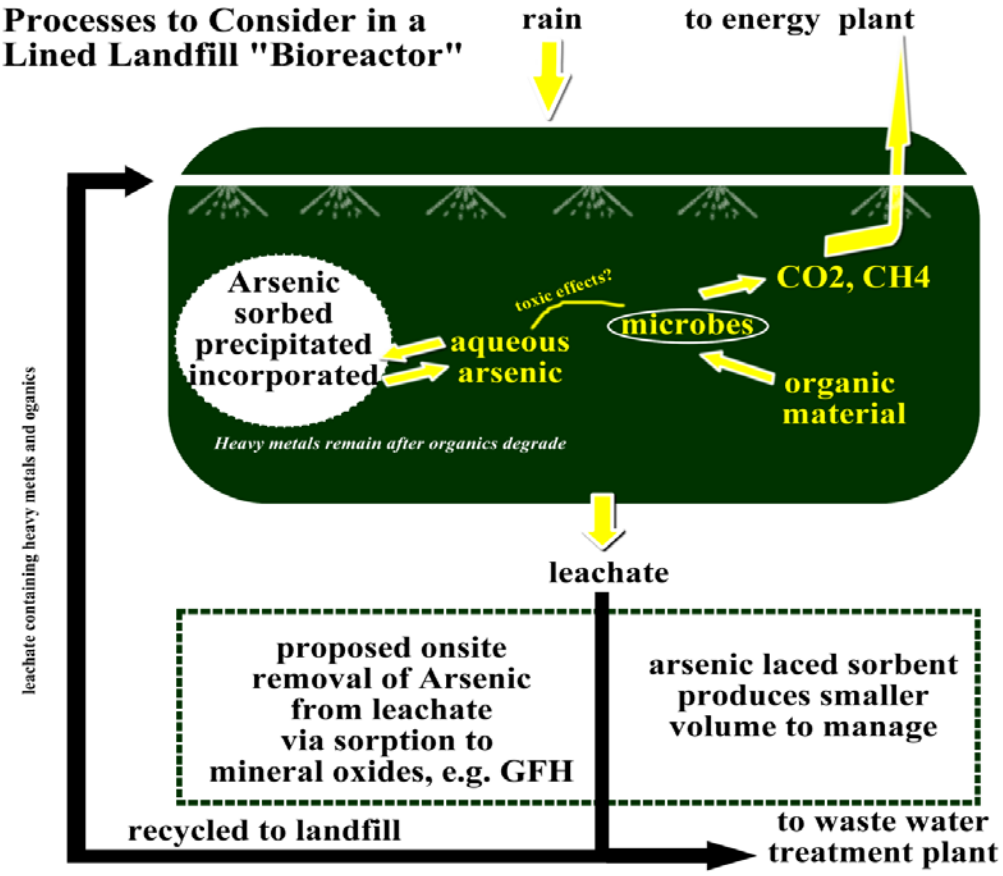

Figure 1.1: Schematic diagram of on-site treatment of landfill leachate. Collected leachate can be treated onsite via a technology like sorption to mineral oxides in a packed column (Fixed Bed Reactor). Once arsenic is removed, the leachate can either be sent to a wastewater treatment facility for further treatment or recycled through the landfill. Overall, arsenic from the entire site can be collected by the packed columns and used appropriately (recycled or disposed of more carefully).

There are onsite treatment methods adopted for leachate treatment so far. These methods include precipitation, oxidation-sedimentation, coagulation-filtration, reverse osmosis, and adsorption. However, treatment of As or other heavy metal contaminants in landfill leachate remains a significant challenge. Adsorption onto mineral oxide sorbents packed into fixed bed reactors is particularly attractive because of the small equipment footprint, efficiency and cost effectiveness. This technology is now popular to combat the widespread As contamination of potable water around the world (Wiszniowski *et al.* 2006), but has not been applied to more complex matrices like landfill leachate.

There is extensive background literature on As removal from drinking water sources through sorption to mineral oxides (Bajpai and Chaudhuri 1999, Thirunavukkarasu *et al.* 2003b, Cincotti *et al.* 2006, Bang *et al.* 2005, Zhang and Lindan 2003, Xu *et al.* 2006, Entezari and Bastami 2006, Agrawal and Sahu 2006), but little is known of the performance of these adsorbents with complex mixtures like landfill leachate. Some investigations on adsorption processes involving other contaminants in landfill leachate have been done. For example, NH_3-N (Ashrafizadeh *et al.* 2008, Kargi and Pamukoglu 2003), organic content in the form of Biochemical Oxygen Demand (BOD), Chemical Oxygen Demand (COD) (Kargi and Pamukoglu 2003, Fan *et al.* 2007, Rivas *et al.* 2003) and Total Organic Carbon (TOC) (Fan *et al.* 2007) among others have been studied in adsorption processes. Preliminary results from tests I did with real landfill leachate spiked with As indicated that As in landfill leachate could be removed by mineral oxide surfaces.

Landfill leachate is mostly characterized by high organic content and high concentrations of inorganic ions. The organics are measured in terms of Chemical

Oxygen Demand (COD), or Total Organic Carbon (TOC) (Weber *et al.* 2002; Wiszniowski *et al.* 2006, Kuleyin and Ergun 2007, Fan *et al.* 2006). The concentrations of organics present vary widely with landfill age (Alvarez-Vazquez *et al.* 2004, Cooke *et al.* 2001). The older landfill leachate generally contains lower concentrations of organic and inorganic ions than the younger landfill leachate (Alvarez-Vazquez *et al.* 2004, Statom *et al.* 2004). The pH range has also been found to fall between 5 and 8.5 (Fan et al. 2006) with the lower pH associated with younger landfill leachate and the higher pH related to older leachate. The leachate characteristics differ significantly from the geochemistry of contaminated groundwater drinking water sources, the focus of most arsenic removal technology.

1.2 Research Goal and Objectives

The goal of this research was to evaluate the effectiveness of a commercially available adsorbent, Kemiron, to remove arsenic from conditions representative of landfill leachate. It involved laboratory batch experiments coupled with modeling and focused on the adsorption capability of Kemiron in a synthetic leachate under various physico-chemical conditions. The considered environmental and chemical conditions for the experiments were pH, oxidation reduction potential (ORP), ionic strength, Chemical Oxygen Demand (COD), and the presence of co-contaminants. Ions like carbonate (CO_3^{2-}), sulfate (SO_4^{2-}), ammonium (NH_4^+ - N) and Ca^{2+} were evaluated for their impact on arsenic sorption since they represent the most commonly occurring species in landfill leachate or are representative of common types of inorganics in landfill leachate. Nickel (Ni^{2+}) and selenite (Se(IV)) were used as trace co-contaminants, representing cationic and

anionic type trace metals. The specific objectives were:

1) Adsorbent (Kemiron) characterization. This adsorbent characterization was needed for modeling sorption data and for comparison with published research results of As sorption by other adsorbents. The adsorbent characterization included the following experiments and analyses:

a) Determination of the BET surface area, particle density, and skeletal porosity of Kemiron.

b) Determination of Kemiron composition and mineral identification.

2) As sorption characterization under a range of conditions (pH, ionic strength, presence of other ions (Se(IV), Ni^{2+}, Ca^{2+}, CO_3^{2-}, SO_4^{2-}, NH_4^+ - N, CH_3COO^-, $C_2H_5COO^-$where the last two ions represent COD). This sorption characterization highlighted the optimum conditions for the As treatment, identified limitations of the adsorption technology, and provide data needed for modeling. The experiments included:

a) Determination of uptake equilibration time of As(V) and As(III) onto Kemiron ($\leq$ 38 μm, 500-600 μm) in clean batch and in synthetic landfill leachate systems at various pH, and at initial solute concentrations.

b) Modeling of As(V) and As(III) onto Kemiron in batch systems using isotherm data.

c) Determination of the effect of co-contaminants, represented by Se(IV) and Ni^{2+}, on As removal.

Chapter 2 discusses background information on leachate characteristics and geochemistry of the systems under study, Chapter 3 presents the models used to interpret

experimental data, Chapter 4 summarizes materials and methods used, Chapter 5 presents and discusses experimental results and modeling efforts and Chapter 6 summarizes the major findings of this work and discusses opportunities for further research.

Chapter 2

Background

2.1 Introduction

This chapter provides background information on different components of this project. It first reviews the literature on landfill leachate characterization (Sections 2.1 to 2.5) with a special emphasis on some of the factors (type of waste, age of landfill, Oxidation Reduction Potential, pH) that contribute to general leachate composition. It then discusses the relevance of this work by placing it in the context of landfills in the State of Florida, which is by no means the only geographic location where the presence of arsenic in leachate either is, or will be an issue. Section 2.7 describes arsenic chemistry and provides the thermodynamic constants and construct used to interpret experimental data of the work. Sections 2.8 and 2.9 introduce the concept of the mineral oxide adsorbent, especially previous research on arsenic interactions with and removal by mineral oxide adsorbents.

2.2 Landfill Leachate Characterization

Kjeldsen *et al.* (2002) characterized landfill leachate into four major components: 1) inorganic macro components, including cations like magnesium, calcium, iron and anions like bicarbonate, sulfate, chloride and phosphate; 2) heavy metals like arsenic, cadmium, selenium and many others; 3) dissolved organic matter, usually expressed as

Table 2.1: Landfill leachate characteristic parameters (Reitzel *et al.* 1992, Pohland and Harper 1989).

Parameter	Purpose
Physical	
pH	Acid-base/stabilization phase indicator
ORP	Oxidation-Reduction/stabilization phase indicator
Conductivity	Ionic strength/activity indicator
Temperature	Reaction indicator
Chemical	
COD, TOC, TVA	Substrate indicator
TKN, NH_3-N, PO_4^{3-}/P	Nutrient indicator
SO_4^{2-}/S, NO_3^-/NH_3	Stabilization phase indicator
TS, Chloride	Dilution/mobility indicator
Total alkalinity	Buffer capacity indicator
Alkali/alkaline earth metals	Toxicity/environmental effect
Heavy metals	Toxicity/environmental effect
Biological	
BOD_5	Substrate/biodegradability
Total/faecal coliforms	Health effect indicators
Faecal streptococci	Health effect indicator
Viruses	Health effect indicator
Pure/enrichment culture	Stabilization phase indicators

biochemical oxygen demand (BOD), chemical oxygen demand (COD) and total organic carbon (TOC); and 4) anthropogenic organic contaminants including xenobiotics. While Christensen *et al.* (1994) disregarded the relevance of pathogens in landfill leachate characterization, Mor (2006) and others considered the presence of fecal indicator bacteria as relevant, but whose number decreased with increasing landfill leachate age. Reitzel *et al.* (1992), Pohland and Harper (1989) characterized landfill leachate with the parameters shown in Table 2.1. The full meanings of the acronyms in the Table 2.1 can be found in Appendix D. Most authors characterize landfill leachate with fewer than the parameters in Table 2.1 using only BOD, COD, TOC, BOD/COD ratio, pH, ammonium nitrogen (NH_4^+- N), total Kjeldahl nitrogen (TKN) and heavy metals. The results of these parameters depend on the following: 1) constituting waste composition (Kargi and Pamukoglu 2003, Weber *et al.* 2002), 2) age of the landfill (Alvarez-Vazquez *et al.* 2004), 3) amount of precipitation or moisture content in the landfill (Renou *et al.* 2008), 4) the presence of active microorganisms (Kargi and Pamukoglu 2003), 5) Oxidation-reduction potential (ORP) in the landfill (Bayard *et al.* 2006), and 6) pH of the landfill (Pokhrel and Viraraghavan 2004). Some of these contributing factors are discussed further in sections 2.2 to 2.5.

2.3 Effect of Waste Composition on Landfill Leachate Characteristics

Landfill leachate characteristics are reflections of landfill waste composition (Salem *et al.* 2008, Xiao *et al.* 2007). Given that landfill leachate is characterized by parameters like BOD, COD, and NH_3 - N, and the concentrations of organic and inorganic species, the values of these parameters depend on proportional compositions of

the parent waste material (Duggan 2005, Mor, 2006). Despite the variability of the waste compositions and their subsequent variations in the proportions of the characteristic parameters, TOC (particularly cellulosic material) mostly constitutes the largest percentage (Boni *et al.*, 2006). The knowledge of leachate composition of a landfill enabled Kjeldsen *et al.* (1998) to characterize the expected chemical composition of the leachate in time and space in the United States. Contents and concentrations of organic substances in landfill leachate in many cases, determine the nature of pretreatment processes needed to be undertaken. The wastes in hazardous landfills (generally classified as Class 1 Landfills requiring liners and leachate collection systems) are quite different from that of non hazardous municipal solid waste landfills. Consequently, the content of their leachate differ from each other, especially in the levels of toxic elements and compounds that each produce.

2.4 Effect of Age on Landfill Leachate Characteristics

The age of landfill leachate from municipal, mixed industrial and non hazardous commercial solid waste impacts values of BOD, COD, TOC, and NH_3-N (Alvarez-Vazquez et al. 2004, Kjeldsen et al. 2002). Young landfill leachate (< 1-2 years old) are normally dominated by organics of lower molecular weights that generally have high values of BOD and COD (Zhang and Selim 2005). As landfill leachate matures organics of higher molecular weight (i.e. COD) dominates while BOD drops in value. This is due to biodegradation of the lower molecular weight organics. The biodegradation continues until the contaminant constituents become resistant to biodegradation or are simply no longer degraded by microbes under the conditions existing at that time. BOD and COD

both degenerate as leachate ages, however, the rate of the degeneration is higher with BOD than with COD. Al Yaqout and Hamoda (2005) showed that the average BOD/COD of a younger landfill leachate in Kuwait was 0.13 while the BOD/COD of older landfill leachate was 0.04. Generally, a BOD/COD of 0.5 of landfill leachate indicates a young age of the leachate while BOD/COD of 0.1 and lower points to older and stable landfill leachate (El-Fadel *et al.* 2002).

2.5 Effect of pH on Landfill Leachate Characteristics

According to Renou *et al.* (2008), pH of landfill leachates usually lies between 5.8 and 8.5. The differences in pH of landfill leachate are related to different levels of biological (aerobic or anaerobic) activities inside the landfills (Poulsen *et al.* 2002). Salem *et al.* (2008) related the pH changes of landfill leachate to biochemical evolution occurring in the landfill. Poulsen *et al.* (2002) discovered that pH of a landfill leachate decreased in the first 3 to 5 months, when the high concentration of oxygen was consumed to produce high and increasing concentrations of leached material. In a situation when oxygen is limited, the landfill undergoes acidogenesis to produce high concentrations of organics (BOD and COD), CO_2 with increasing Cl^- and NH_3/NH_4^+, leading to a drop in pH. In an aerobic environment, the pH remained constant to about the 50^{th} month and rises to 8 at about the 150^{th} month. The pH remains high thereafter and coincides with the growth of a methanogenic microbial population that creates high levels of methane and leaching out of heavy metals (Poulsen *et al.* 2002).

2.6 Effect of Oxidation-Reduction Potential (ORP) on Landfill Leachate Characteristics

ORP characterizes the strength of an oxidizing agent (electron acceptor) or reducing agent (electron donor). Some examples of oxidizers include chlorine, hydrogen peroxide, ozone, bromine, and hypochlorite and examples of reducers include sodium sulfite, sodium bisulfate, and hydrogen sulfide. ORP measurement in soils and rocks has been used to detect leakage of landfill leachate in the subsurface and ORP gradients in soils/rocks by leachate migrations have resulted in remobilization of ions in the neighboring rocks (Christensen *et al.* 2000). Studies have also indicated that As and Fe species are sensitive to ORP in their environments. For instance, As(III) and Fe^{2+} are dominant in reduced environments while As(V) and Fe^{3+} are prevalent in oxidized environments. Thus high Fe^{3+}/Fe^{2+} and As(V)/As(III) ratios in a landfill leachate is indicative of higher values of ORP of landfill. In methanogenic, sulfate-reducing, and iron-reducing landfill leachate plumes, ORP consistently results between -70 and -100 mV while in aerobic plumes ORP yields readings of 200 to 300 mV (Christensen *et al.* 2000).

2.7 Arsenic in Landfill Leachate

Arsenic (As) contamination in landfill leachate is a major concern in Florida and many other parts of the United States. In 2005, an attempt was made to contact 68 Florida landfills (not only active Class 1 landfills) via email and phone to learn about their leachate disposal practices and total arsenic concentrations. Of the 68 landfills on the list, 26 responses were obtained and of those 26 responses 7 landfills in Florida had

leachate with arsenic concentrations greater than 10 μg/L combined with a disposal issue related to arsenic. The seven landfills identified were:

- Alachua County
- Lake County
- Marion County
- Martin County
- Orange County
- Polk County
- Santa Rosa County

These seven landfills paid for offsite leachate disposal and sometimes had an additional surcharge fee because arsenic concentrations were above permissible limits. Though leachate contained a list of other heavy metals, arsenic concentrations were closer to or above permissible limits.

Arsenic inorganically exists as As(III) and As(V) and organically as methylarsonic acid [MMA(V)], dimethylarsinic acid [DMA(V)], methylarsonous acid [MMA(III)], and dimethylarsinous acid [DMA(III)] (Sierra-Alvarez *et al.* 2005). As(III) converts to As(V) in oxidizing (oxygen-rich) environments and As(V) reduces to As(III) in reducing (anaerobic) environments where As(V) acts as an electron acceptor (Rittmann and McCarty 2001). The methylated organoarsenicals [MMA(III)], [DMA(III)], [MMA(V)], and [DMA(V)] occur from biotransformation of the inorganic arsenicals. As(III) is more mobile and more toxic than arsenate As(V) and its toxicity has been linked to the fact that the human skin contains several sulfhydryl groups to which As(III) binds (Maji *et al.* 2007). Sierra-Alvarez *et al.* 2005 have postulated the following three

mechanisms by which As leaches out from solid waste in landfills under aerobic conditions: 1) oxidation of metal sulfides to the more soluble metal sulfates, 2) oxidation of metal sulfides to sulfuric acid which results in pH reduction, hence dissolving the metals on contact, and 3) complexation of metals with humic acid leading to metal mobilization. Most metals or metalloids in solid waste landfills leach out to the highest degree at pH 3 and below (Moghaddam and Mulligan, 2008). This pH range, however, is not necessary for arsenic, or other heavy metal mobilization in landfill leachate.

2.8 Chemistry of Arsenate, Arsenite, Selenite and Other Chemical Constituents

Equilibrium constants are used to predict and understand speciation of chemicals in aqueous environments as a function of solution pH and pe, where pe applies onlt to redox sensitive ions. Table 2.2 provides a list of log K values for some of the chemicals used in this study and Figures 2.1 - 2.5 show the distribution of various species of relevant to this with a function of pH and/or pe. Geochemical Workbench and NIST software were used to calculate these equilibrium speciation diagrams using the (Gimenez *et al.* 2007, Jones and Pichler 2007).

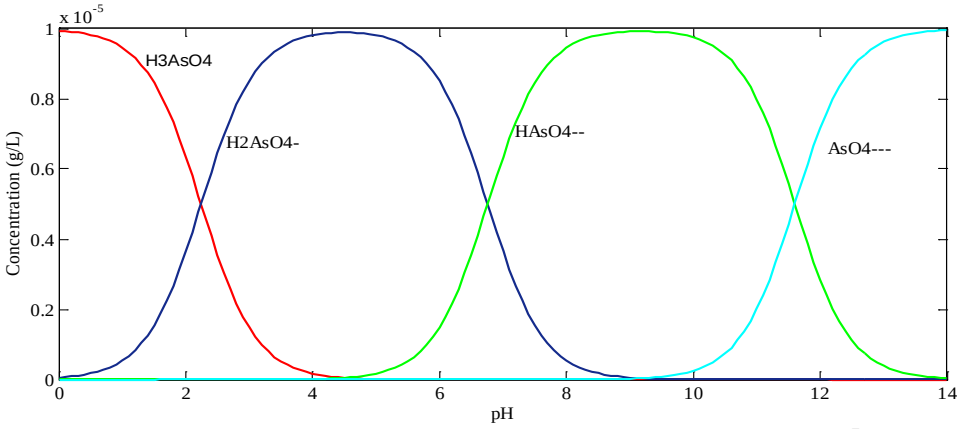

Figure 2.1: Arsenate speciation diagram with total As(V) of 10^{-5} M

Table 2.2: Thermodynamic constants for As(III), As(V), Se(IV), CO_3^{2-} and others. Assuming Ionic strength = 0, T = 25°C.

Formation Reaction	**pK**
$H_2AsO_3^- + H^+ = H_3AsO_3$	9.32
$HAsO_3^{2-} + H^+ = H_2AsO_3^-$	12.13
$AsO_3^{3-} + H^+ = HAsO_3^{2-}$	13.41
$H_2AsO_4^- + H^+ = H_3AsO_4$	2.22
$HAsO_4^{2-} + H^+ = H_2AsO_4^-$	7.00
$AsO_4^{3-} + H^+ = HAsO_4^{2-}$	11.54
$SeO_3^{2-} + H^+ = HSeO_3^-$	8.40
$HSeO_3^- + H^+ = H_2SeO_3$	2.63
$HCO_3^- + H^+ = H_2CO_3$	6.35
$CO_3^{2-} + H^+ = HCO_3^-$	10.33
$CH_3COO^- + H^+ = CH_3COOH$	4.76
$NH_4^+ + OH^- = NH_3$	-9.25

In the acidic and alkaline regions of Figures 2.1 – 2.2, the dominant As(V) species is $H_2AsO_4^-$ and $HAsO_4^{2-}$, respectively. It is often assumed that the dominant solution species is also the dominant adsorbing species. As a result, several authors have proposed mechanisms involving one or both of these species for the adsorption of arsenic onto various minerals (Villalobos *et al.* 2003, Goldberg 2002). Similarly H_3AsO_3 and $H_2AsO_3^-$ predominate all the other species of As(III) in acidic and alkaline regions. For Se(IV) in Figure 2.3, $HSeO_3^-$ and SeO_3^{2-} dominate in acidic and alkaline regions respectively. Whilst As(V) and Se(IV) exist as charged species above pH 2.22 and 2.63

respectively, As(III) remains a fully unspeciated until pH 9.32 and above. In a reducing environment, As exists predominantly as As(III), while in an oxygen rich environment arsenic exists as As(V). Figures 2.4 and 2.5 show carbonate and ammonium speciation respectively.

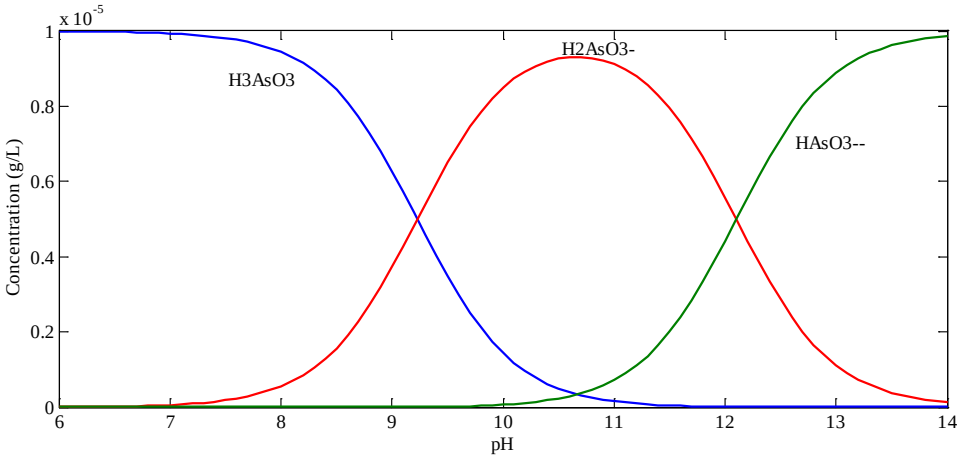

Figure 2.2: Arsenite speciation diagram with total As(III) of 10^{-5} M.

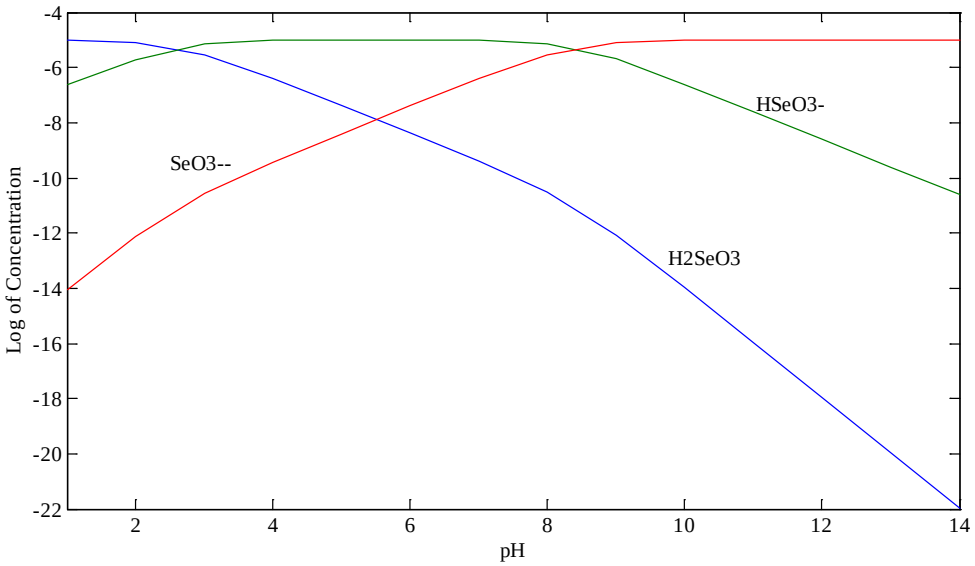

Figure 2.3: Selenite speciation diagram with total Se(IV) of 10^{-5} M.

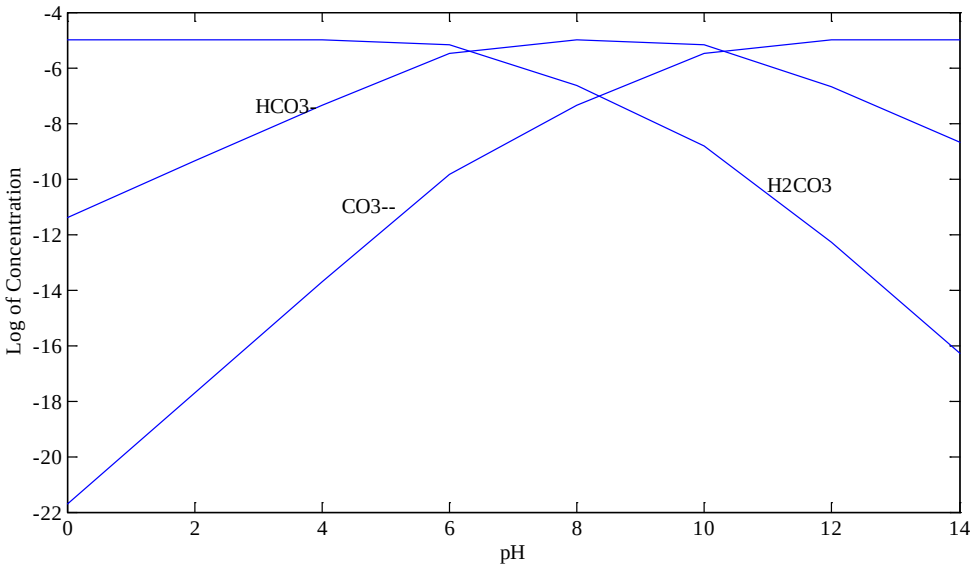

Figure 2.4: Carbonate speciation diagram with total CO_3^{2-} of 10^{-5} M.

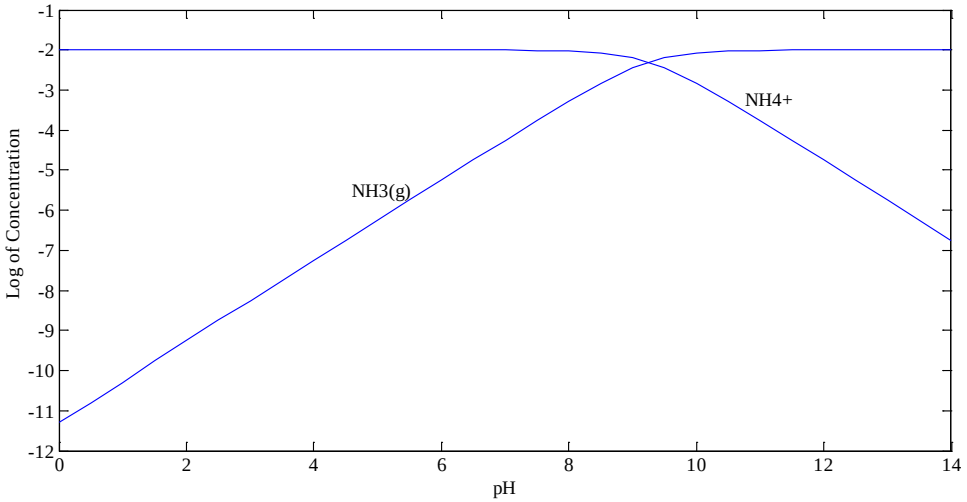

Figure 2.5: Ammonia – ammonium speciation diagram with total NH_4^+ of 10^{-5} M.

Like the As(V) species carbonate would have a negative charge in solution and hence could compete with Asfor the surface sites. Ammonium ($NH4^+$) on the other hand would be positively charged across most of the pH range studied. The speciation diagrams allow us to interpret experimental data and this type of analysis will be invoked in chapter 5.

2.9 Iron Oxide/Hydroxide Surface Chemistry

Surfaces of hydrated iron oxide are usually assigned +1 and -1 charges. These charges can be neutralized by binding of OH^- to ≡Fe sites and H^+ to the ≡O sites. Again, hydrated as ≡FeOH group in solution may be protonated as $\equiv FeOH_2^+$, neutral as ≡FeOH°, or deprotonated to form $\equiv FeO^-$ species depending on the pH of the solution. The surface acidity reaction can be written as shown in table 2.3 below.

Table 2.3: Speciation reaction of iron hydroxide

Formation Reaction	Log K
$\equiv FeOH + H^+ = \equiv FeOH_2^+$	7
$\equiv FeO^- + H^+ = \equiv FeOH$	9.2

From Table 2.3, $\equiv FeOH_2^+$ dominates below the point of zero charge (pH_{pzc}) while $\equiv FeO^-$ dominates at above the pH_{pzc}. Many iron based adsorbents have their pH_{pzc} between 8 and 9.5 (Naeem *et al.* 2007; Smith 1998; Sperlich *et al.* 2005). Villalobos *et al.* (2003) however found that surface area determination method, particle sizing procedure and adsorbent pretreatment methods affected the pH_{pzc} of goethite. Thus a universal pH_{pzc} value for sorbents may introduce errors in surface modeling attempts. For the most part, however, the neutral FeOH dominates iron species in water at pH 8. In adsorption studies, the amount of anions sorbed decreased as a function of pH. This has been explained with electrostatic influence. The charges on iron hydroxide surfaces are neutral at pH_{pzc}. An increase in pH induces negative charges on the adsorbent surface and this repels As species, a negatively charged adsorbate species.

2.10 Arsenic Adsorption Studies

Iron based sorbents are used as adsorption media because of their net positive surface charge at low pH and again because the active surfaces form bonds with many anions. Batch equilibrium sorption of As, and Se(IV) onto iron oxide/hydroxide has been extensively studied. As(V) and Se(IV) are most effectively adsorbed at lower pH, while As(III) and Ni^{2+} adsorption are rather higher at higher pH level. This is because the pH at which oxides of iron possess zero charge (i.e., pH_{PZC}) is generally between 8.0 and 9.0. At pH below these values the solid surfaces acquire a net positive charge. Consequently, much of the adsorption of As(V) on these surfaces is by electrostatics attraction, while As(III) is sorbed by weak Van der Waal forces. This is because As(V) speciate into oxyanions at 2.2 and 2.6 respectively but As(III) speciates at 9.3.

Studies also show that adsorption of As onto iron oxide/hydroxide is either unaffected by increasing ionic strength or decreases with increasing ionic strength (Zhang *et al.* 2007, Payne and Abel-Fattah 2005). Typically, As(III) is more sensitive to changes in ionic strength than As(V). Several spectroscopic investigations regarding the binding of As to various solid surfaces have led to a proposed inner-sphere (ligand-exchange) type reaction mechanisms for As sorption onto adsorbent surfaces. Kanel *et al.* (2005) described adsorption mechanism of As(III) onto zero valent iron as inner sphere. Again inner sphere mechanism has been reported on As(III) adsorption onto gibbsite (Oliveira *et al.* 2006). Duc *et al.* (2006) have also shown that ionic strength have no effect on the adsorption of selenium onto haematite. Martinez *et al.* (2006), Catalano *et al.* (2006) respectively have described the sorption mechanism of Se(IV) onto hematite and magnetite as inner sphere. This supports the inference made by Goldberg (2002) on the

description of sorption mechanism of ions onto metal surfaces based on the knowledge of ionic strength responses. Others have demonstrated that anions such as sulfate, phosphate, carbonate, and molybdate may compete with arsenite, and to a lesser degree arsenate, for available surface sorption sites. Consequently, arsenite sorption is significantly hindered in the presence of co-adsorbing anions.

Chapter 3

Theoretical Considerations of Adsorption

3.1 Introduction

This chapter will introduce the basic concepts of adsorption and describe two common models used to describe adsorption behavior under equilibrium conditions, the Langmuir and Freundlich isotherms. It then explains the methodology used to calculate and compare mass transfer parameters that characterize the rate at which species of interest are removed by the mineral oxide surface. The models described here are used in Chapter 5 to interpret experimental data and provide comparisons with published research on other systems of interest. Finally, Oxidation Reduction Potential (ORP) is explained in a way that relates experimental measurements with theoretical concepts.

3.2 Adsorption and Adsorption Isotherms

Adsorption refers to the accumulation of ions or molecules at the interface between two phases in relation to the concentrations of the ions or the molecules in a bulk solution. Generally, chemical, physical or electrostatic interactions influence the adsorption behavior of inorganic adsorbates onto the surfaces of adsorbents. Chemical interactions include covalent and hydrogen bonding, while electrostatic forces are involved in ion – ion and ion – dipole interactions. Physical attractions involving relatively weak Van der Waals forces include dipole – dipole, dipole – induced dipole

interactions. The Van der Waals forces are involved in the sorption of nonionic organic and inorganic molecules from aqueous solutions.

Figure 3.1 depicts adsorption processes as they relate to the solid-liquid interface. The left hand side of the first scenario, (a), represents a solid (e.g. a mineral oxide) in solution with dissolved ions, where ≡ represents sites on the solid surface capable of binding a dissolved ion. The right hand side of the first scenario depicts the dissolved ion binding to the surface site through the process of adsorption. Scenario (b) depicts the surface sites as hydrated species $\equiv SH_2O$ and replaces the symbol for dissolved species used in scenario (a) with real species one would expect in a simple solution containing water, sodium nitrate ($NaNO_3$) and some dissolved species A (shown here as an uncharged species). The adsorption of species A to the surface site results in the formation of ≡SA. Scenario (c) depicts the surface sites with different charges represented as $\equiv SOH_2^+$, $\equiv SO^-$ and ≡SOH and adsorbed species as ≡SOA and $\equiv SO^-\ldots Na^+$ where the difference between the latter two species lies in the strength and type of bond between the adsorbent surface site and the adsorbing species The representations given in Figure 3.1 are only some of the ways in which adsorption processes are conceptualized and are simpler than other models (e.g. Constant Capacitance Model, The Diffuse Layer Model, The Triple Layer Model, CD-MUSIC Model) which incorporate changes in the electric potential as a function of distance from the surface of the adsorbent and/or require more detailed information on the specific surface site types (Hayes and Leckie 1987; Hiemstra et al. 1989; Davis and Kent, 1990).

Isotherms are commonly used to describe equilibrium adsorption behavior . To accurately represent the adsorption of an adsorbate over a wide range of conditions,

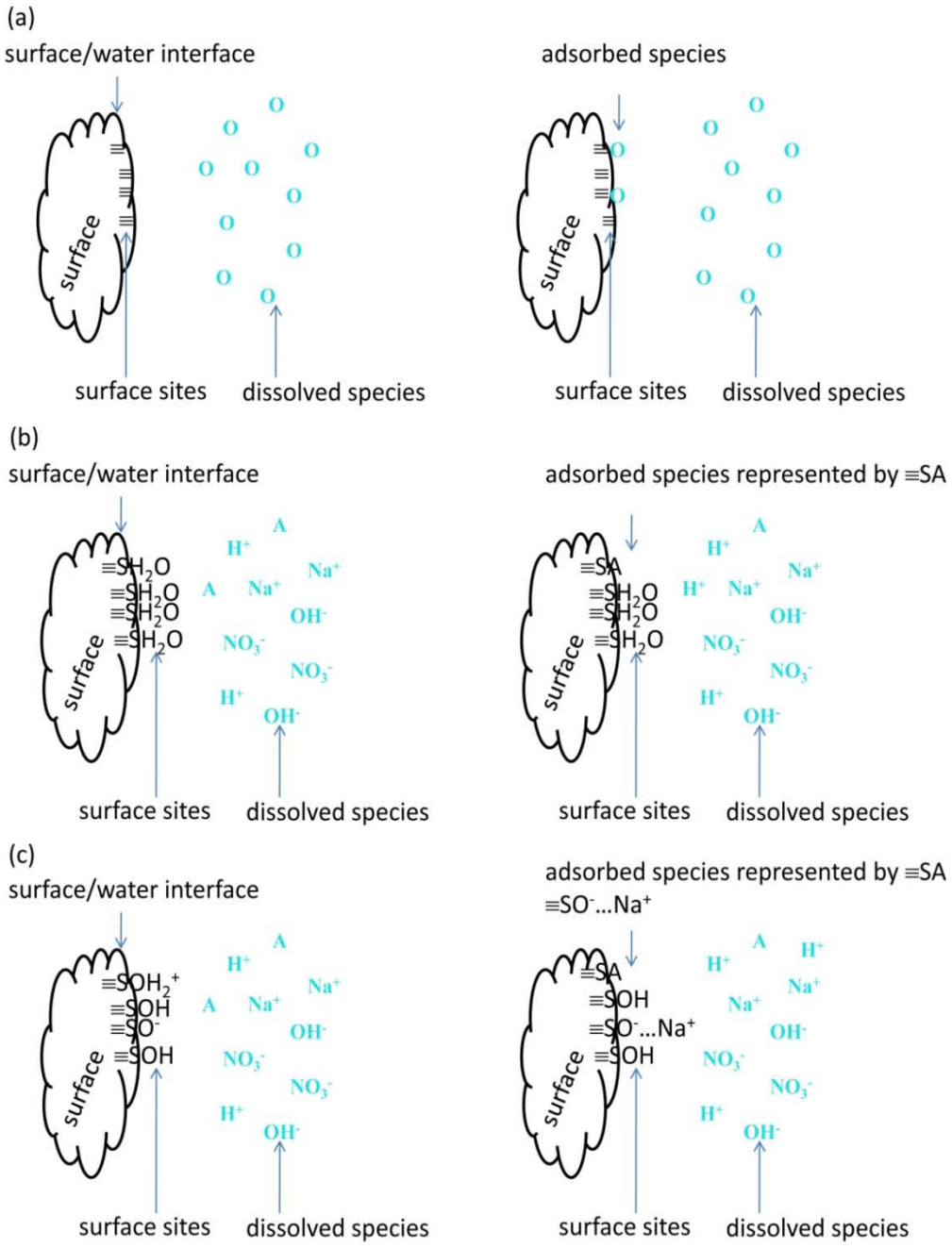

Figure 3.1: Schematic representation of the adsorption process. The solid-water interface for surface sites, dissolved species and adsorbed species represented as (a) ≡, O and, ≡O respectively; (b) $\equiv SH_2O$, various species like Na^+, H^+, A, OH^-, and ≡SA respectively; and (c) $\equiv SOH_2^+$, ≡SOH, $\equiv SO^-$, various species, and ≡SA or $SO^-\ldots Na^+$ respectively.

the following factors are considered:

1) Characteristics of the adsorbent
2) Characteristics of the solution
3) Characteristics of the adsorbate
4) The interactions of the adsorbent with the solution and the adsorbate

The two most frequently used isotherm models for heavy metal adsorption are Langmuir and Freundlich models.

3.2.1 Langmuir Model

The use of the Langmuir isotherm model is based on the following assumptions (Benjamin, 2002):

1) All sites have equal binding energy.
2) The binding sites are uniformly distributed on the adsorbent surface.
3) The affinity of the sites for the adsorbate is independent of the solution condition.
4) There is no effect of the adsorbed species on the adjacent sites.
5) A single value is used to represent the reaction between a given adsorbate and all the surface sites.

In a binary system, Benjamin (2002) used a simple equilibrium surface complexation reaction model and a corresponding constant to illustrate the occupation of the sites by an adsorbate in a system. The equilibrium reaction equation was written as:

$$A_{(aq)} + \equiv SH_2O \leftrightarrow \equiv SA + H_2O \qquad (3.1)$$

where $A_{(aq)}$ = aqueous adsorbate, $\equiv SH_2O$ is the unoccupied site by the adsorbate, $\equiv SA$ is the occupied site by the adsorbate. From equation (3.1), adsorption coefficient,

K_{ads} is given by:

$$K_{ads} = \frac{\{\equiv SA\}}{\{A_{(aq)}\}\{\equiv SH_2O\}} \quad (3.2)$$

where the total number of site is given by:

$$\{\equiv TOTS\} = \{\equiv SA\} + \{\equiv SH_2O\} \quad (3.3)$$

Manipulation and substitution of equation (3.3) into equation (3.2) leads to

$$\{\equiv SA\} = \frac{K_{ads}\{A_{(aq)}\}}{1+K_{ads}\{A_{(aq)}\}}\{\equiv TOTS\} \quad (3.4)$$

Equation (3.4) can also be written as

$$q_{eq} = \frac{K_L\{A_{(aq)}\}}{1+K_L\{A_{(aq)}\}}\{q_{max}\} \quad (3.5)$$

Equation (3.5) is known as the Langmuir model where q_{eq} = $\{\equiv SA\}$, the mass loading of the contaminant per mass of the adsorbent; $K_L = K_{ads,}$ is the coefficient of the Langmuir model that measures the affinity of the adsorbent for the adsorbate; and q_{max} = $\{\equiv TOTS\}$, the maximum loading capacity of a given mass of the adsorbent. If $K_L\{A_{(aq)}\} \ll 1$, then the adsorbent has a very low affinity for the adsorbate and equation (3.5) becomes equal to $K_L\{A_{(aq)}\}\{q_{max}\}$. Testing of experimental data fits to the Langmuir Isotherm is usually done by transforming data to fit Equation 3.6.

$$\frac{1}{qA} = \frac{1}{q_{max}K_L\{A_{(aq)}\}} + \frac{1}{\{q_{max}\}} \quad (3.6)$$

In this work data fitting was actually done using the Gauss-Newton to fit Equation 3.5. This was done in MATLAB and Appendix D provides the script for running this analysis. In a ternary system involving two adsorbates A and B along with the adsorbent, Benjamin (2002) derived the competitive Langmuir isotherm model from two simple complexation reactions:

$$A_{(aq)} + \equiv SH_2O \leftrightarrow \equiv SA + H_2O \quad (3.7)$$

$$B_{(aq)} + \equiv SH_2O \leftrightarrow \equiv SB + H_2O \quad (3.8)$$

The ratio of adsorbate B sorbed to adsorbate A sorbed is written as:

$$\frac{\{\equiv SB\}}{\{\equiv SA\}} = \frac{K_{ads,B}\{B_{(aq)}\}}{K_{ads,A}\{A_{(aq)}\}} \quad (3.9)$$

The site balance for this case is:

$$\{\equiv TOTS\} = \{\equiv SH_2O\} + \{\equiv SA\} + \{\equiv SB\} \quad (3.10)$$

By substitution of equations (9) and (10) into equation (7), Langmuir isotherm derived is given by:

$$q_A = \frac{K_{ads}\{A_{(aq)}\}}{1 + K_{ads,A}\{A_{(aq)}\} + K_{ads,B}\{B_{(aq)}\}} q_{max} \quad (3.11)$$

Langmuir sorption model of an adsorption indicates limited adsorption capacity of an adsorbent as per an adsorbate. The limited adsorption capacity occurs as a result of limited number of sorption sites the adsorbent possesses as per the adsorbate. Linear and Freundlich models on the other hand indicate unlimited sorption capacity. This may be due to a presence of infinite number of sites on an adsorbent per an adsorbate. Linear and Freundlich models also indicate lower affinity of the adsorbent for the adsorbate. Although there is infinite numbers of sorption site types present in many adsorbent solid surfaces, only fewer types of the sites are usually dominant while most of the sites types are insignificant in the amount of adsorbate adsorbed in the removal processes. For instance, Dzombak and Morel (1990); Papini *et al.* (1999) identified more than one sorption site type in some adsorbents with respect to some adsorbates. Dzombak and Morel (1990) reported of two types of sites on iron oxide adsorbent in arsenic adsorption tests while Papini *et al.* (1999) reported of three site types on a heterogeneous natural

medium (red pozzolan) at a constant ionic strength of 0.1 mol/L for lead (Pb) adsorption. For multisite Langmuir isotherm, (ex. Two sites), the total adsorbate loading, $q_{A,tot}$, is given by:

$$q_{A,tot} = q_{A,1} + q_{A,2} = \frac{q_{max,1}K_{ads,A,1}\{A_{(aq)}\}}{1+K_{ads,A,1}\{A_{(aq)}\}} + \frac{q_{max,2}K_{ads,A,2}\{A_{(aq)}\}}{1+K_{ads,A,2}\{A_{(aq)}\}} \qquad (3.12)$$

where $q_{A,1}$ = total loadings onto site type 1 and $q_{A,2}$ = total loadings onto site type 2.

3.2.2 Freundlich Model

There are other instances when the binding sites cannot be represented as discrete or by some few dominating sites. The surfaces behave as if the sites present are associated with continuous distribution of binding energies. Here Langmuir isotherm fails but one of the isotherm functions that fit such scenario is Freundlich. Freundlich isotherm model is given by:

$$q_{tot} = k_f\{A_{(aq)}\}^n \qquad (3.13)$$

where

$$k_f = \frac{\propto RT\pi}{\sin(n\pi)} \qquad (3.14)$$

and R and T are universal gas constant and absolute temperature respectively. The failure of the Langmuir isotherm equation is attributable to the various assumptions upon which the model was derived. For instance, Langmuir model assumes that the adsorbent binding surface sites are uniformly distributed, identical and all can be represented with a single value under all conditions. The Langmuir equation again assumes that binding of an adsorbate to any site has no effect on the equilibrium constants for binding of other molecules to the surface. However, these assumptions are not always true.

3.3 Hydroxide Surfaces and Ionic Adsorbate

In solution of hydroxyl surfaces are usually represented as $\equiv SOH_2^+$, $\equiv SOH$, and $\equiv SO^-$ for one type sorption site species. Depending on pH there is always a relative dominance of one or two site species over the other. Typically surface site species of iron hydroxide groups are written as $\equiv FeOH_2^+$, $\equiv FeOH$, and $\equiv FeO^-$. During adsorption ionic adsorbates are presumed to bind directly to oxide surface or the Fe ion, displacing the $\equiv OH_x$ group. Surface complexes formed by such reactions are relatively strong and are reffered to as innersphere complexes. H^+ and OH^- ions are always presumed to bind to oxide surfaces by innersphere complexes. Some other ions on the other hand are presumed to bind to water molecule which in turn binds to the Fe surfaces. The adsorbates here are not directly linked to the Fe oxide surface but by connection through water molecules. Such binding forms weaker complexes with the surface and is known as outer sphere complexes.

3.4 ORP and E_h Measurements

ORP or redox potential (E_h) studies are of importance in environmental chemistry. This importance stems from the changes in the characteristic properties of the elements that are involved in this adsorption process. ORP changes have effect on the original properties of both the adsorbent and the adsorbate of a system. For instance, low ORP values change S(VI) as in SO_4^{2-} to is S(-II) in H_2S. S(VI) is highly soluble, non volatile and relatively innocuous. However, S(-II) in H_2S forms insoluble metal precipitation and is also quite toxic (Benjamin, 2002). ORP is measured in millivolts (mV) or in volts (V) with ORP electrodes containing a silver/silver chloride (Ag/AgCl)

reference. The values obtained are then converted into oxidation potential or redox potential E_h voltage values. E_h voltage values are the values that would be obtained if Standard Hydrogen Electrode was used. For the Orion ORP electrode that was used in this work, the ORP (mV) values obtained were converted to E_h (mV) by adding absolute value of 219 mV to the ORP readings values at a temperature of 20°C or 220 mV at 25°C. Like pH, pe is defined in relation to activity. The relationship between E_h and pe is given by $pe = E_h\left(\frac{F}{2.30259RT}\right)$ where F is Faraday's constant, given by 96485.309, T is temperature in Kelvin, and R is molar gas constant given by 8.314 J/mol-K.

3.5 Batch Kinetics Studies

For non-equilibrium adsorption processes in porous solid media the migration of the contaminant species from bulk solution into the solute particle encounters two resistances in series: a resistance due to the external film, and intraparticle resistance. In a fast stirred batch system the thickness of the film surrounding the adsorbent particles is assumed to be thinned out. Consequently, resistance to adsorbate migration across an external boundary layer is considered negligible. In the pores of an adsorbent, the dissolved adsorbate migrates towards the center of adsorbent due to either concentration gradient in the pore water (pore diffusion) on the pore walls (surface diffusion). The rate of diffusion in the pores is usually described by Fick's law. The intra particle solute concentration under unsteady state with a fixed diffusivity in a spherical adsorbent is given by:

$$\frac{\partial q_p}{\partial t} = D_{app}\left(\frac{\partial^2 q_p}{\partial r^2} + \frac{2}{r}\frac{\partial q_p}{\partial r}\right) \qquad (3.15)$$

where q_p is solute concentration in the pore water [M/M], D_{app} is apparent diffusion coefficient [L^2/T], r is the radial position of the adosrbate in the spherical solid particle [L], and t is time [T]. With initial condition:

$$q_p(r, t = 0) = 0 \tag{3.16}$$

and with boundary conditions:

$$q_p(t = \infty, r = a) = C_b \tag{3.17}$$

where $VC_b + M.\frac{3}{a^3}\int_0^a r^2\, q(r,t)dr = VC_b$, C_b= As concentration in the bulk solution [M/L] and M = mass of the adsorbent [M].

$$\frac{\partial q_p(r = 0, t)}{\partial r} = 0 \tag{3.18}$$

Crank (1975) established the analytical fractional uptake solution to linear diffusion equation in a limited volume with the same initial and boundary conditions as written above for the equation (3.15). The linear diffusion equation, also known as the Fick's first law of diffusion is given by:

$$Flux = D_{app}\left(\frac{\partial q_p}{\partial r}\right) \tag{3.19}$$

and Crank's (1975) solution is also given by:

$$\frac{M_t}{M_\infty} = 1 - \sum_{n=1}^{\infty} \frac{6\alpha(1+\alpha)}{9 + 9\alpha + q_n{}^2\alpha^2} \exp\left(\frac{-D_{app} q_n{}^2 t}{a^2}\right) \tag{3.20}$$

where M_t and M_∞ are the masses of the solute in the adsorbent at time t and at equilibrium time (infinite time) respectively. The parameter q_n are non- zero roots [-] of $\tan q_n = \frac{3q_n}{3 + \alpha q_n{}^2}$ and $\alpha = \frac{3V}{4\pi a^3 K_d}$. α [-] is also expressed in terms of final fractional

uptake of solute by the spherical adsorbent as: $\frac{M_\infty}{VC_0} = \frac{1}{1+\alpha}$. This analytical solution to adsorption model assumed a linear isotherm. The most frequently used mathematical algorithm by which the non-zero roots of $\tan q_n = \frac{3q_n}{3+\alpha q_n^{\ 2}}$ is estimated is Newton – Raphson method. Equation 3.16 states that initially there was no contaminant in the pores of the adsorbent. Equation 3.17, also states that at time infinity the solute concentration on the periphery of the spherical adsorbent is in equilibrium with the bulk solution. Finally, Equation 3.18 indicates that the solute concentration gradient in the core of the spherical sorbent is zero. Ball and Roberts (1991) experimentally determined fractional uptake from:

$$f_d = \frac{C_{bi} - C_b}{C_{bi} - C_{be}} \tag{3.21}$$

where C_{bi}, C_b, and C_{be} are the solute concentrations [M/L] observed in the bulk solution initially, at time t, and at equilibrium respectively. For no instantaneous adsorption and no partioning into to the headspace or otherwise lost from solution, equation (3.20) becomes

$$f_d = \frac{C_T - C_b}{C_T - C_{be}} = \frac{M_t}{M_\infty} \tag{3.22}$$

where C_T is the total initial concentration of the solute in the bulk solution [M/L], M_t and M_∞ are the masses of solute loading onto the adsorbent at any given time and at equilibrium respectively. Solute diffusion in porous media is hindered by such factors as tortuous pathways, dead end pores, and variable pore diameters.

According to Ball and Roberts (1991), apparent diffusion coefficient relates to effective pore diffusion coefficient by:

$$D_{app} = D_e * R_{\text{int}} \tag{3.23}$$

where D_e is effective diffusion coefficient [L^2/T], R_{int} is the internal retardation factor [-] within the internal pores of the adsorbent and is also given by:

$$R_{\text{int}} = [1 + (\frac{\rho_p}{\varepsilon_i})K_{di}] \tag{3.24}$$

where ε_i is internal porosity [-], and K_{di} is linear equilibrium adsorption coefficient [L/M]. Equation 3.12 was derived on the assumption that adsorption is linear in the pores of the adsorbents. Diffusion in the bulk is however assumed to be faster than pore diffusion for two reasons. Bulk diffusion involves simple geometries and a straight path. Pore coefficient thus relates to bulk diffusion coefficient as:

$$D_e = \frac{D_b K_r}{\chi} \tag{3.25}$$

where K_r is constrictivity factor [-] (≤ 1), and χ is tortuosity factor [-] (≥ 1). In this research equilibrium tests were performed with both 500 - 600 µm and 38 µm grain sizes. The purpose for using fine grain size in the equilibrium experimentation was to attain a shorter equilibration time. There have been reported situations when the adsorption capacity of an adsorbent had dropped with the increase in the adsorbent grain size (Giammar *et al.* 2007). One possible way this can occur is when the fine grain sizes of the adsorbents used are far smaller the smallest pore sizes of the bulk such that the fine grain particles become non porous. For instance, nano sized fine grain adsorbent derived from microporous bulk adsorbent as was the case with Giammar *et al.* (2007). Other

possible causes that have been reported include constrictivity and dead ends. Such case could imply that equilibrium experimentation with the fine grain size is not representive of that of the coarser grains. Internal constrictivity and dead ends (steric effect) are difficult to determine separately and so are usually determined as a lump sum (Ball and Roberts, 1991).

3.6 Experimental Data Fitting

There are two types of applications adopted in experimental data fitting. These are trend analysis and hypothesis testing. In this work trend analysis was used and this presents a process of using a pattern of data to make a prediction. Least squares regressions are used in a trend analysis to predict imprecise data while interpolations are used to determine data with high precision (Chapra and Canale 2002). Some of the tools of least squares regression for a best fit are minimization of sum of squares of residual errors and coefficient of determination (r^2) for all the available data. The coefficient of determination is given by:

$$r^2 = {}^{(S_t - S_r)}/_{S_t} \qquad (3.26)$$

where $S_t = \sum(y_i - \bar{y})^2$ and $S_r = \sum(y_i - y_p)^2$, S_t = the total sum of the squares of the residuals between the data points and the mean, S_r = the sum of squares of the residual errors, $\bar{y}$ = arithmetic mean of a sample, y_p = predicted values. For a perfect fit $S_r = 0$ and $r^2 = 1$.

Gauss Newton algorithm is also another method that has been employed by many in fitting non-linear data. This method which uses minimization of the sum of squares of residual errors was adopted in this work.

Chapter 4

Materials and Methods

4.1 Introduction

This chapter describes the materials and the methods adopted for this research. The approach to the experiments conducted was grouped into two main categories: Kemiron particle characterization, and batch sorption tests. The batch adsorption tests were subcategorized into rate of sorption and equilibration tests. Both the rate of sorption and the equilibration tests were initially done in binary systems (only arsenic present) and then further tested in more complex systems containing more than one contaminant and in the presence of synthetic landfill leachate.

4.2 Materials

4.2.1 Adsorbent

Kemiron is an adsorbent that is manufactured by Kemiron Company, with a local distributor in Florida. The adsorbent particles were ground in a ceramic mortar and sieved through American Society for Testing and Materials (ASTM) stainless steel sieves to obtain two particle sizes referred to as fines ($\leq$ 38 μm) and coarse (500 – 600 μm) fractions. The Kemiron adsorbent was chosen for this research because it was a newly

developed product with little known about its adsorption performance with arsenic remediation and its availability in Florida.

4.2.2 Reagents and Stock Solutions

All the reagents used were of analytical grade and purchased from Fisher scientific. The stock solutions were made by dissolving the given solid reagent in ultrapure water (Barnstead) with resistance of 18.2 M-ohm. The reagents also included sodium hypochlorite, NaOCl, sodium sulfide, Na_2S, sodium arsenate heptahydrate, $Na_2HAsO_4.7H_2O$, sodium nitrate, $NaNO_3$, nitric acid, HNO_3, sodium hydroxide, NaOH, sodium acetate, CH_3COONa, sodium propionate,C_2H_5COONa, sodium carbonate, Na_2CO_3, magnesium chloride, $MgCl_2$, sodium sulfate, Na_2SO_4, ammonium nitrate, NH_4NO_3, sodium chloride, NaCl, calcium carbonate, $CaCO_3$, and sodium selenite, Na_2SeO_3. A stock solution of 150 mg/L Ni ($Ni(NO_3)_2.6H_2O$) was used as modifier solution in the determination of arsenic using GFAAS analysis. Prior to use, $NaNO_3$ was dried at 80°C for 4 hours and stored in a dessicator. pH adjustments were done with the nitric acid, HNO_3 and NaOH and ORP adjustments were done with NaOCl and Na_2S. CO_2 free milliQ water was prepared by boiling ultrapure (Barnstead) water and sparging with ultra high pure argon gas (Airgas Incorp.) until cool and maintained under an Argon atmosphere. All slurries were also purged with Argon gas for 24 hours prior to spiking with various stock solutions which were freshly prepared for each experiment.

The synthetic landfill leachate was made by combination of various salts partly based on papers and reports from Kjeldsen *et al.* (2002), Kjeldsen and Christophersen (2001). Table 4.1 shows the resulting species composition and their concentrations.

Table 4.1: Synthetic landfill leachate constituents.

Parameter	Concentrations (mg/L)		Classification
	Young phase (acidogenic)	Old phase (methanogenic)	
CH_3COO^-	11000 COD	1500 COD	Organic species
$C_2H_5COO^-$	11000 COD	1500 COD	
Na^+	3270.5	4971.9	
Mg^{2+}	470	180	
Ca^{2+}	1200	60	
NH_4^+ - N	740	740	Inorganic species
CO_3^{2-}	2115.5	4190	
SO_4^{2-}	500	80	
Cl^-	2120	2645.1	
NO_3^-	2544.3	2544.3	
Ni^{2+}	0.17	0.17	Co-contaminant
SeO_3^{2-}	5	5	

4.2.3 Instrumentation

A Hitachi H-7010 coupled to an electron counting sensor (Joel JSM-840) was used for Scanning Electron Microscopy (SEM) and Energy Dispersive Spectroscopy (EDS). SEM provides information on Kemiron particle morphology and EDS provides information on the percentage by mass of the elemental constituents of the Kemiron. An X-ray diffractometer (XRD) (Philips) was used to identify mineralolgy of Kemiron. A copper target was used for the x-ray source with a strongest characteristic radiation ($K\alpha_1$) at a wavelength of about 1.54 angstroms. The effective pore size, the total pore volume as

well as the total pore surface area of Kemiron were determined with mercury intrusion porosimetry by Micromeritics in Atlanta, Georgia. BET multipoint surface area and pore analyses with nitrogen intrusion were also measured. Kemiron was dried at 80°C for 18 h and degassed at 80°C for 3 h prior to these characterizations.

A Ross semi micro gel filled electrode coupled to an Orion 940 pH meter was used for pH measurements after being calibrated with Fisher Scientific pH buffers, 4.0, 7.0, and 10.0. Oxidation reduction potential of the system was measured with an ORP probe (ORION 9678BNWP) connected to the ORION 940 meter in the relative millivolt mode. Potassium iodide solution (ORION) was used as the standard solution. A Graphite Furnace Atomic Absorbance spectrometer (GFAA), Varian Spectra AA 640 DUO model which was equipped with automated sample injection (GTA 100) was used to measure total arsenic concentrations.

4.3 Methods

Figure 4.1 illustrates the experimental setup used for batch experiments in this study. Ultra high purity (UHP) nitrogen gas was scrubbed to remove CO_2 prior to bubbling into the reactor vessel to remove CO_2 and maintain a CO_2 free system. An overhead stirrer was used for experiments with the 500 – 600 μm particle sizes to reduce mechanical alterations on the particle size.

Prior to the start of the experiments all glassware was washed with Liquinox detergent and then soaked in 1 N sodium hydroxide for more than 1 hour, rinsed with milliQ water and soaked again in 10% nitric acid overnight before finally being rinsed with, and left soaking in milliQ water overnight. Cleaning of polycarbonate (PC)

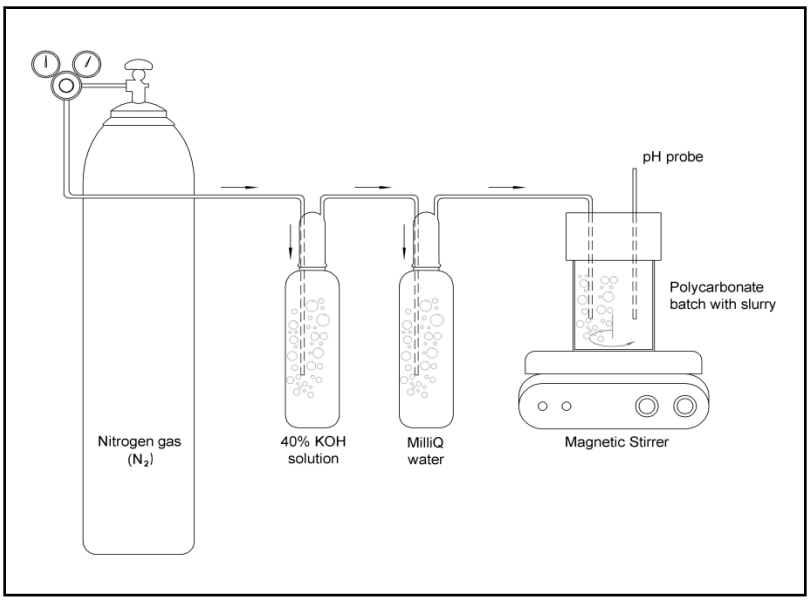

Figure 4.1: Ultra high pure nitrogen gas sparging setup for a batch system.

containers was similar to that of glassware except the concentrations of acid and base were both 0.1 N.

4.3.1 Batch Adsorption Characterization

Batch kinetic studies in binary systems were undertaken on two grains sizes of Kemiron (≤ 38 and 500 - 600 μm). The objectives for these were to establish equilibration times and also to estimate diffusion rate constants for As removal in both the binary and in more complex systems involving these two grain sizes. All experiments involving the 500 - 600 μm grain size were done with 1000 mL solutions and an overhead stirrer and all of the binary experiments involving the ≤ 38 μm were done in 200 mL solutions. The experiments involving the synthetic landfill leachate were done in 1000 mL solutions irrespective of the adsorbent grain size. In the binary systems the pH of the solution was first lowered to ~5.5 with 0.1 N HNO_3 before it was sparged with the

ultra high pure nitrogen gas overnight. The pH was then raised to 7 with 0.1 N NaOH and then 5 mg/L As was spiked into it. The pH was maintained at 7 using both 0.001 N NaOH and 0.1 N HNO_3. Samples of 2 ml were taken as a function of time for every experiment and also for each of the grain sizes. The results from the analyses were modeled with mass transfer equations. The kinetic studies of the landfill leachate were done at pH 9.4 and at ORP of 240 mV.

Equilibration tests were conducted on As in both the binary and in the complex systems involving only the ≤ 38 μm and the 500 – 600 μm grain sizes of Kemiron. In the binary system and with only the fine slurries, the tests were done at ionic strengths of 0.001 N and 0.1 N of $NaNO_3$. The objectives were to evaluate the impacts of: 1) ionic strength on As removal in the binary system, 2) initial As concentration on amount of As adsorbed, and 3) the effect of particle size (≤ 38 μm and the 500 – 600 μm grain sizes) on the As removed. In each case the system was made of 0.1 g/L Kemiron in a polycarbonate (PC) batch reactor with CO_2 free ultrapure water. The gas sparging with the pH before and after were the same as described in the kinetic studies. 15 Samples of 8 mL were removed into 10 mL PC tubes at various pH levels. The head spaces in the 10 mL PC tubes were filled with ultra pure nitrogen gas. After 72 hours the sample pH was recorded and the samples were filtered with 0.20 μm MILLIPORE filters. The filtrate was acidified with concentration HNO_3 to 0.7% and analyzed for total As. The equilibration binary batch experiments were carried out on initial As concentrations of 5, 10, 15, 20, 30, and 40 mg/L.

With the synthetic landfill leachate the equilibration tests were done for two different categories on the based on landfill age. Young (acidogenic) landfill leachate

contained higher concentrations of the constituent ions while old (methanogenic) landfill leachate contained less concentrations of constituent ions. Batch equilibration tests on the synthetic leachate were similar to those of the binary systems in ultrapure water. The ultrapure water used for the leachate preparation was simultaneously boiled and sparged with UHP nitrogen gas to remove dissolved CO_2 and O_2. pHs in the synthetic leachate were changed with concentrated HNO_3. In the competing batch sorption experiments, concentrations of various ions from their respective salt solutions were spiked into the batch slurries along with arsenic. The competing ions used were SeO_3^{3-}, Ni^{2+}, NH_4^{+}, CO_3^{2-}, SO_4^{2-} and the objective was to evaluate the impact of the presence of the ions on As removal. Samples of 8 mL were then taken into the 10 mL PC tubes at various pH levels. The head spaces in the 10 mL PC tubes are filled with ultra pure nitrogen gas. After 72 hrs of equilibration on an end over end rotator, the pH was measured and the samples filtered through 0.20 μm MILLIPORE. The filtrate was acidified with concentrated HNO_3 to 0.7% and analyzed for As.

Batch isotherm experiments were also done at room temperature on As with initial concentrations of 5 mg/L, 10 mg/L, 20 mg/L, 30 mg/L, 40 mg/L and 50 mg/L at various pH values (6,7, and 9), for 72 h and with the ionic strength of 0.001 N $NaNO_3$. The objective for this experiment was to evaluate the impact of initial concentrations of As on the mass density of As adsorbed onto Kemiron. Multiple samples each having a volume of 8 mL were taken from the slurry into 10 mL PC tubes. The preparations and the filtrations of the samples for analysis for the isotherm were similar to those for the batch equilibration experiments. Batch equilibration tests in the synthetic landfill leachate were done with two objectives. The first objective was to verify the increased As

adsorption impact as exhibited by the various conditions in binary systems in the landfill leachate system. The second objective was to select the two parameters that had the most impact on As removal in the the binary systems. By applying a 2^2 factorial experimentation method, optimum conditions for maximum As removal in the synthetic landfill leachate were determined.

A set of preliminary experiments were also done using real landfill leachate collected from the North Central Landfill in Polk county, Florida. The leachate was collected in 1L HDPE containers and stored on ice during transport. Once in the laboratory it was filtered through a 0.45 µm filter and used for experiments. The leachate was also analyzed for total arsenic concentrations. Leachate was digested on an Environmental Express Hotblock set at 105^{o}C (sample temperatures were 95^{o}C). 100 ml of leachate sample was placed in a 250 ml beaker to which 3 ml concentrated HNO_3 was added and the mixture boiled down to ~ 5 ml. 3 ml more of concentrated nitric acid were added and the mixture boiled until constant color. 10 ml of concentrated HCl was then added along with ultrapure water and the mixture boiled for 15 minutes after which the cooled mixture was made to mark in a 100 ml volumetric flask. This procedure was repeated using a 100 ml Environmental Express polyprophene container, and then 1 mL of 30% H_2O_2 plus 2.5 mL of concentrated HNO_3 was added and the samples allowed to heat for 2 hours after which they were cooled, diluted and analyzed on the GFAA.

Chapter 5

Results and Discussion

5.1 Introduction

This chapter describes and discusses the characterization studies of Kemiron and the results from the adsorption experiments performed. Kemiron characterization was done with X-Ray Diffraction (XRD), Scanning Electron Microscopy (SEM), Electron Dispersion Spectroscopy (EDS), Mercury porisimetry and nitrogen adsorption Brunauer Emmett Teller (BET) surface area determinations. The impacts of various experimental variables on batch equilibrium, and batch kinetics of the As adsorption onto Kemiron were evaluated. Variables such as As concentration, pH, ionic strength, ORP, and solution composition were tested for their impact on both clean systems and on synthetic landfill leachate at room temperature. The suitable parameters for maximum adsorption were adopted from clean systems and tested in the systems using synthetic landfill leachate.

5.2 Kemiron Surface Characterization

The surface characterization of Kemiron was done on ≤ 38 and 500 – 600 μm grain sizes. Three commonly used pore size classifications are micropores (pore diameter smaller than 2 nm), mesopores (pore diameter 2 – 50 nm) and macropores (pore diameter larger than 50 nm) (Sing *et al.*, 1985). Gases like nitrogen (0.15 nm diameter) can access

pore sizes ranging from 0.3 to 300 nm whereas molecules of mercury (0.314 nm diameter) access pores ranging from 3 nm to 200 μm. Table 5.1 summarizes the Kemiron surface characteristics based on mercury porosimetry and BET nitrogen intrusion performed by Micromeritics, Georgia.

Table 5.1: Properties of Kemiron particles. For the 500-600 μm diameter particles and mercury porisimetry analysis.

Property	Quantitative value
Total Pore Volume (ml/g)	0.42
Bulk Density @ 55 psia (g/ml)	1.32
Porosity (%)	55
Max Pore Diameter (μm)	327
Min Pore Diameter (nm)	3
Median Pore Diameter (nm)	7
Mean Pore Diameter (nm)	76
Total Surface Area (m^2/g)	22.1
BET Surface Area (m^2/g)*	39.8
Skeletal Density (g/ml)	2.94

* BET nitrogen gas intrusion method.

The surface area obtained from mercury porisimetry was 22.1 m^2/g for the 500 - 600 μm particle sizes (see Figure 5.1 and Appendix A). The BET surface areas were 37.6 ± 0.2 m^2/g and 39.8 ± 0.2 m^2/g for ≤ 38 and 500 - 600 μm Kemiron particles grain sizes respectively. There was a 44% difference between the surface area obtained for the 500-

600 μm particle size fraction using mercury porisimetry and nitrogen intrusion with the latter method giving the higher of the two surface areas. This can be explained in terms of the pore size distribution, where mercury porisimetry is unable to access pores less than 3 nm (minimum pore diameter observed in Table 5.1 was 3 nm using mercury porisimetry and shown in Figure 5.1). N_2 adsorption BET surface area analysis accesses pore sizes down to 0.3 nm and the discrepancy between the two surface areas suggests that roughly 44% of the pores lie in the 0.3 to 3 nm range. It is possible that some of these micropores are inaccessible to ions like $H_2AsO_4^-$ which has an average diameter of around 0.8 nm, however, their contribution to total surface area is significant (Bodek *et al.*, 1988). There was only a 5% difference between the surface areas obtained for the two size fractions studied and this is expected since crushing of particles should not change surface area when the majority of that surface is within the pore structure.

Research on the nature of material pores and sorption isotherm characteristics has been done by Rigby (2005); Gregg and Singh (1982) and the interpretations here are based on these sources. The hysteresis loops presented in both the mercury and the nitrogen gas sorption (lower curve) and desorption (upper curve) are shown in Figures 5.2 and 5.3. The hysteresis characteristic features are associated with capillary condensation occurring in pores. According to the sorption classification of Gregg and Singh (1982), Figures 5.2 and 5.3 conform to Type IV of the adsorption isotherm. However; the linear part of the graph below the hysteresis loop which indicates a stage of monolayer coverage is missing in Figure 5.2 (mercury adsorption graph) but is present in Figure 5.3 (nitrogen adsorption graph). The reason for the missing stage of the graph is unclear but might be suggestive of mercury's inability to access the micropores. Another

thing that the hyteresis loop indicates is pore structure type present in the adsorbent particles. In comparison with the classification of Gregg and Singh (1982), Figure 5.2

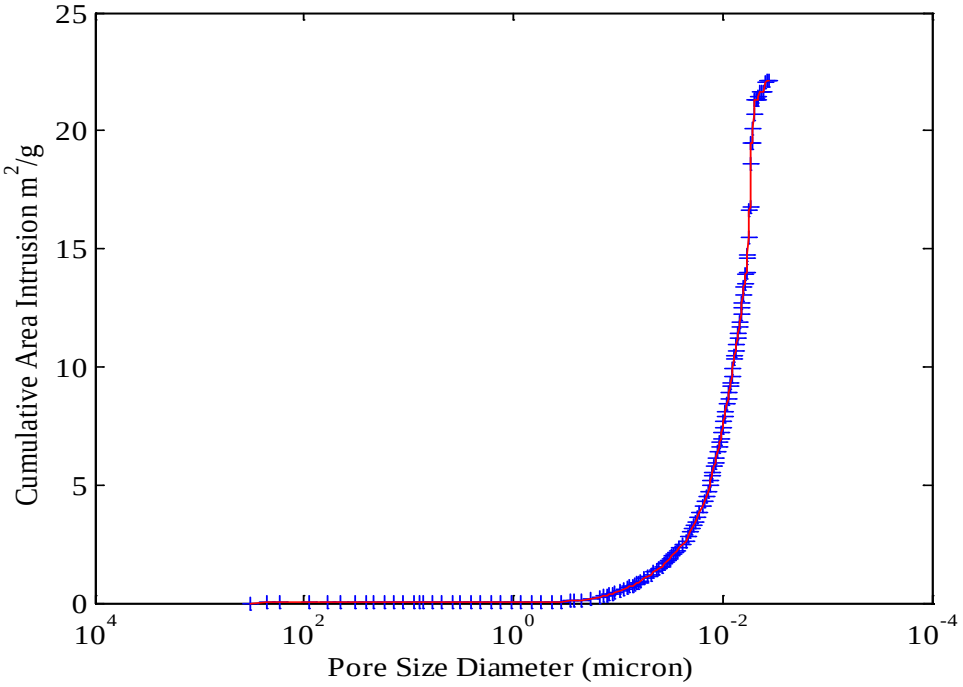

Figure 5.1: Cumulative area mercury porosimetry of 500 – 600 µm particle size.

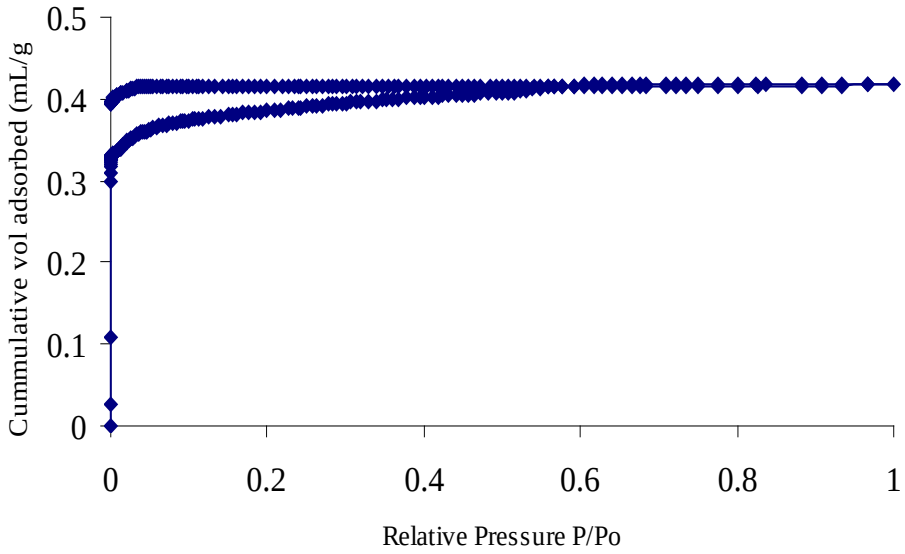

Figure 5.2: Mercury adsorption isotherm onto 500 – 600 µm particle size of Kemiron.

indicates H1 Type pores which are often associated with porous materials consisting of agglomerates of approximately uniform spheres in a fairly regular array, with a narrow

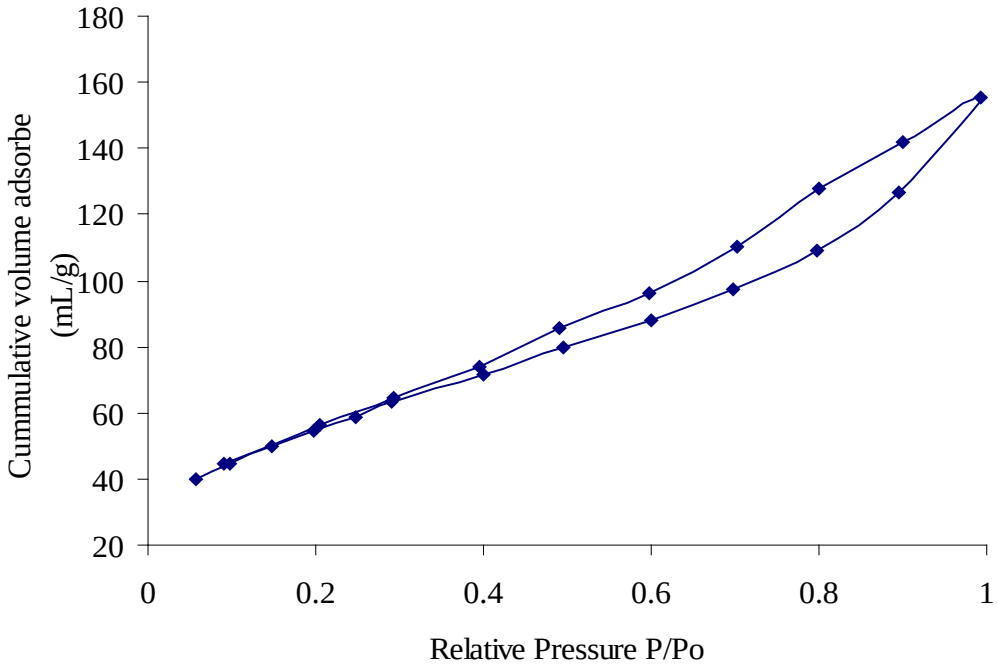

Figure 5.3: Nitrogen adsorption isotherm onto 500 – 600 μm particle size of Kemiron.

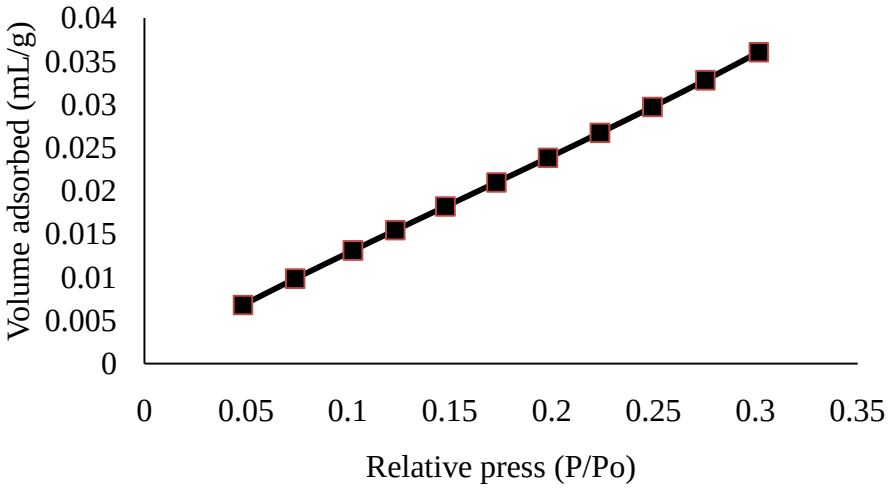

Figure 5.4: Nitrogen adsorption isotherm onto ≤ 38 μm particle size of Kemiron.

distribution of pore sizes. Figure 5.3 on the other hand indicates a Type H3 loop which does not exhibit any limiting adsorption at high relative pressure (P/P_o). This is associated with aggregates of plate like particles with slit-shaped pores. Figure 5.4 shows no hysteresis associated with the ≤ 38 μm particle size with relative pressure up to 0.33. This suggests the sorption test ended prematurely when compared with Figure 5.3.

5.2.1 Scanning Electron Microscopy (SEM)

Particle morphology for Kemiron was determined using a Hitachi H-7010 Scanning Electron Microscope (SEM) with Joel JSM-840 attached. A representative micrograph of Kemiron is shown in Figure 5.5. The surface of the 500 – 600 μm particle appear to consist of aggregates of smaller particles which look rounded and fluffy. This observation is in agreement with the Type H1 pore structure interpretation of Figure 5.2.

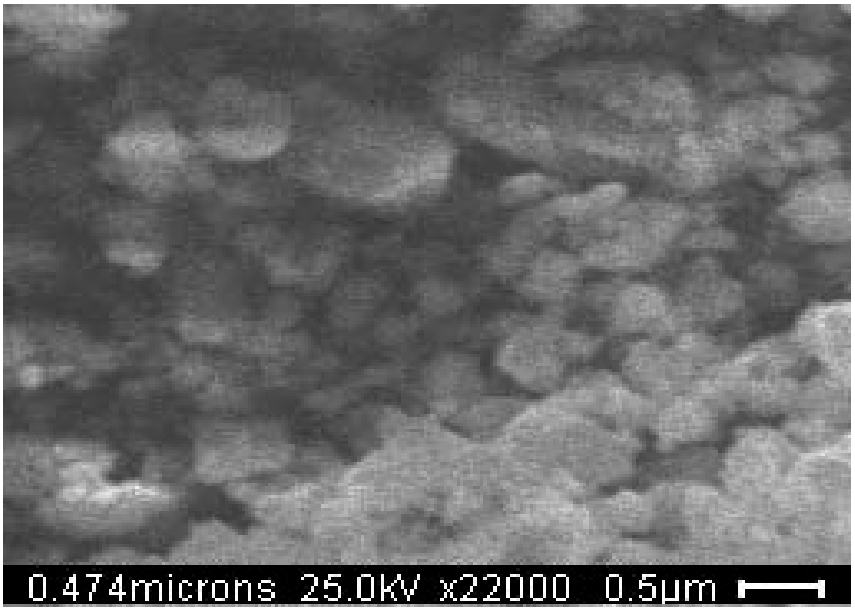

Figure 5.5: Scanning Electron Microscope (SEM) Micrograph of a 500 – 600 μm Kemiron particle.

5.2.2 X-Ray Diffractometry (XRD)

The X-Ray Diffractogram of Kemiron (Figure 5.6) lacked very well defined peaks and had a noisy baseline. This suggested that Kemiron could be amorphous. The closest iron based compound in the database of International Committee Coal Organic Petrology (ICCP) on which high peaks coincided was goethite. The noisy peak characteristics may also depict agglomeration of very fine particles (Alcantar and Pichler, 2007). This interpretation of particle aggregates is supported by the H1 type pore structure classification of Figure 5.2 and the SEM as well.

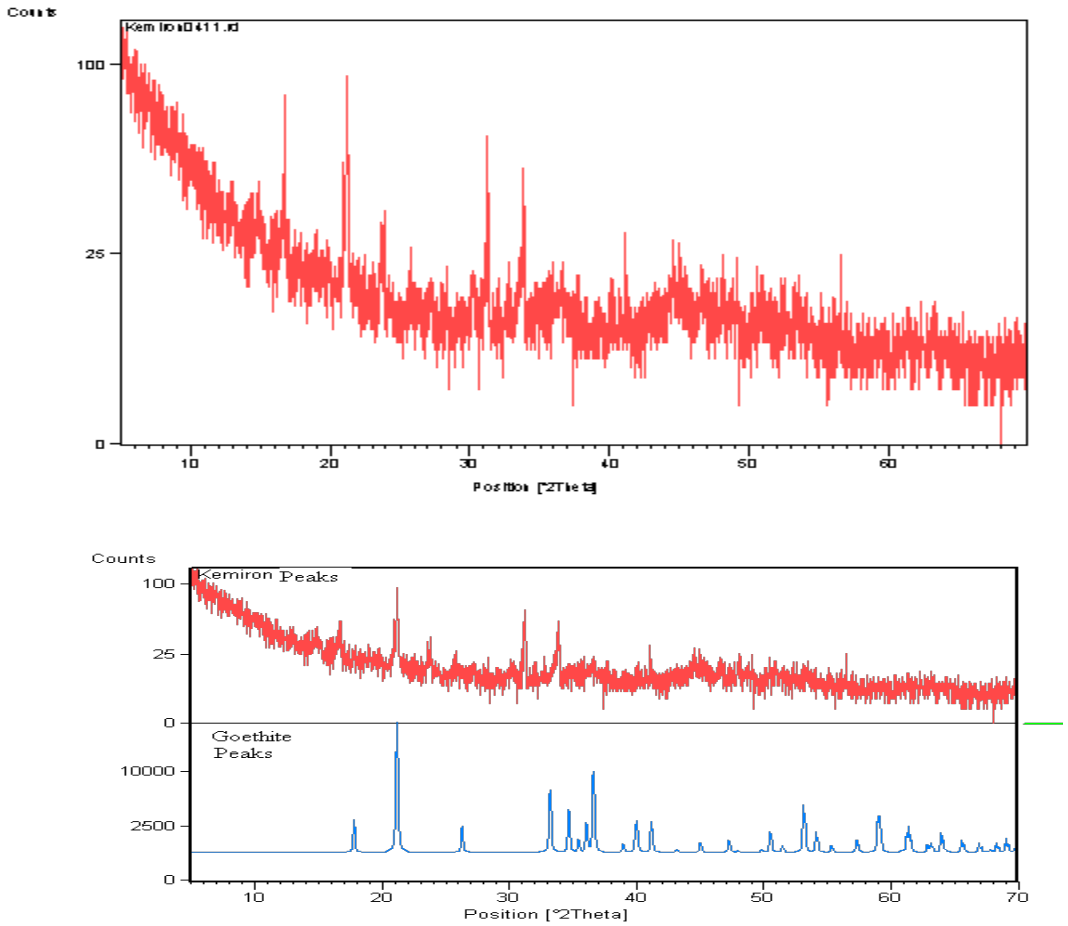

Figure 5.6: X-Ray diffractogram (XRD) of Kemiron powder (≤ 38 μm particle size) and goethite for comparison.

Table 5.2 contains some surface area data of goethite and granular ferric hydroxide (GFH) reported by some researchers. The BET N_2 adsorption surface area of goethite presented ranges from 27.5 m^2/g to 94 m^2/g and depends on factors like the rate of base addition during the precipitation process (Villalobos *et al.*, 2003). The surface area of the Kemiron also falls within the range seen in the literature for goethite and is much lower than what has been reported for the amorphous iron oxides (ferrihydrite in Table 5.2).

Table 5.2: BET surface areas reported on some iron based adsorbents.

Adsorbent	Surface area (m^2/g)	Reference
Goethite	27.5	Campo *et al.* (2008)
Goethite micro rod	40 ± 3	Cwiertny *et al.* (2009)
Goethite 25	40.2	Kosmulski *et al.* (2003)
Goethite 140	47.05	Kosmulski et al. (2003)
GFH	235 ± 8	Badruzzaman *et al.* (2004)
Ferrihydrite	280 ± 30	Hiemstra and van Remsdjk (2009)

5.2.3 Electron Dispersion Spectroscopy (EDS)

Energy Dispersive Spectroscopy (EDS) revealed the major elemental weight percentages in Kemiron as 40.37 % iron, 42.25 % oxygen, 7.92 % carbon and 5.90 % sulfur. Figure 5.7 shows the number of emitted electrons per second of Kemiron at a given amount of electron volts generated. The percentages by weight analysis were done by quantitative methods using Atomic number, Absorption and Fluorescence (ZAF) correction.

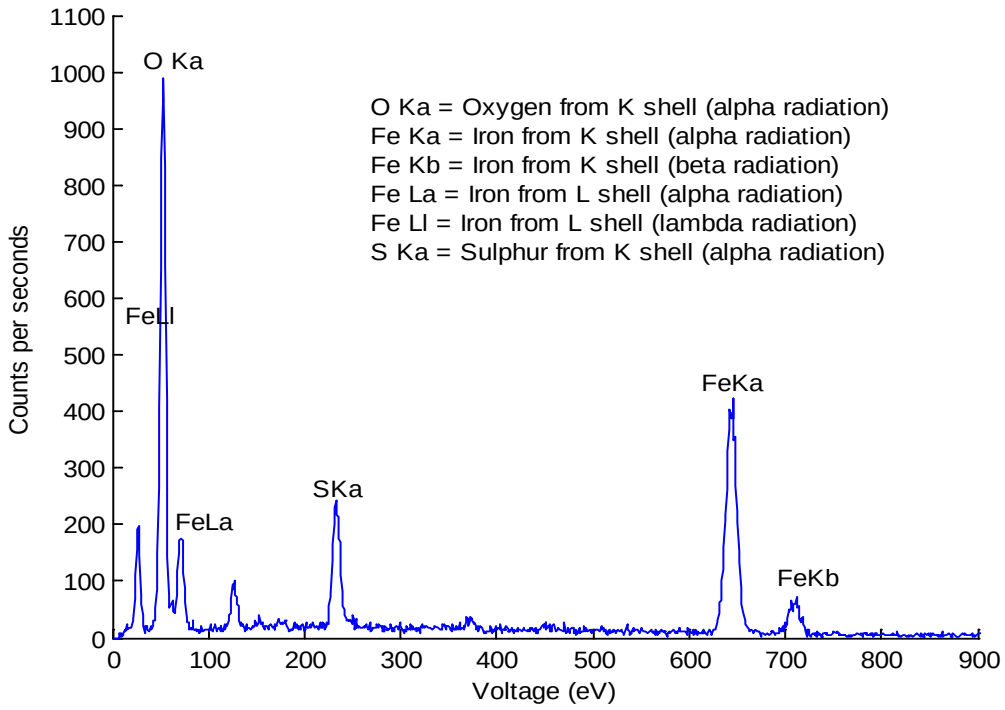

Figure 5.7: Energy Dispersive Spectroscopy (EDS) scan of < 38 μm Kemiron.

5.3 Kinetics of Arsenic Adsorption in Binary System

The kinetics of adsorption has received several interpretations in terms of the processes responsible for observed phenomenon. LaBolle and Fogg (2001) explained the process of contaminant transport in a quiescent system by means of molecular diffusion which is enhanced by mechanical dispersion (e.g. stirring). During contaminant transport into a porous medium from a bulk solution the contaminant migration proceeds through an assumed external boundary between the bulk solution and the solid surface and then into internal pores toward the center of a porous solid. Mass transfer resistance to the migration of the solute into the pores of the adsorbent result from the external boundary layer surrounding the solid particle and also from diffusional processes in the internal pores of the adsorbents.

In the batch experiments involving continuous stirring, external film resistance is minimized and the rate of removal depends on the resistance in the internal pores. Thus in this experiment, the rapid rate step which completed within a few minutes might be due to resistance in the macro and meso pore structures (see Figure 5.1). The slower and mass transfer rate limiting step took hours to days to reach equilibrium and might be due to resistances in micropores of the adsorbents (Cunningham *et al.* 1997). Bulk diffusion is assumed to be faster than pore diffusion and is also assumed to involve simple geometries as well as straight paths while pore diffusion involves complex, tortuous pathways, dead-end pores and variable pore diameters (Ball and Roberts 1991). This means the longer the microscale length, the longer the time for equilibrium.

In this research, continuous stirred batch kinetic experiments were done on As with 0.1 g/L Kemiron, at pH 7, and with ionic strength of 0.001 N $NaNO_3$. The particle sizes of Kemiron used for these experiments were ≤ 38 μm and 500 – 600 μm in diameter. The objectives for the kinetic studies were to: 1) determine the As adsorption equilibration time, 2) evaluate the impact of the grain size on the adsorption capacities, and 3) estimate diffusion coefficients. The kinetics of adsorption of As onto Kemiron was expected to be intraparticle diffusion controlled. Also the equilibration time was expected to depend on the diffusional length. The dependence of the equilibration time on diffusional length was based on an assumption that the diffusion coefficient of As migration into the pores of Kemiron is unaffected by the size of the adsorbent. Again, the adsorption capacity of Kemiron was expected to remain unchanged for all grain sizes under the same physico-chemical conditions.

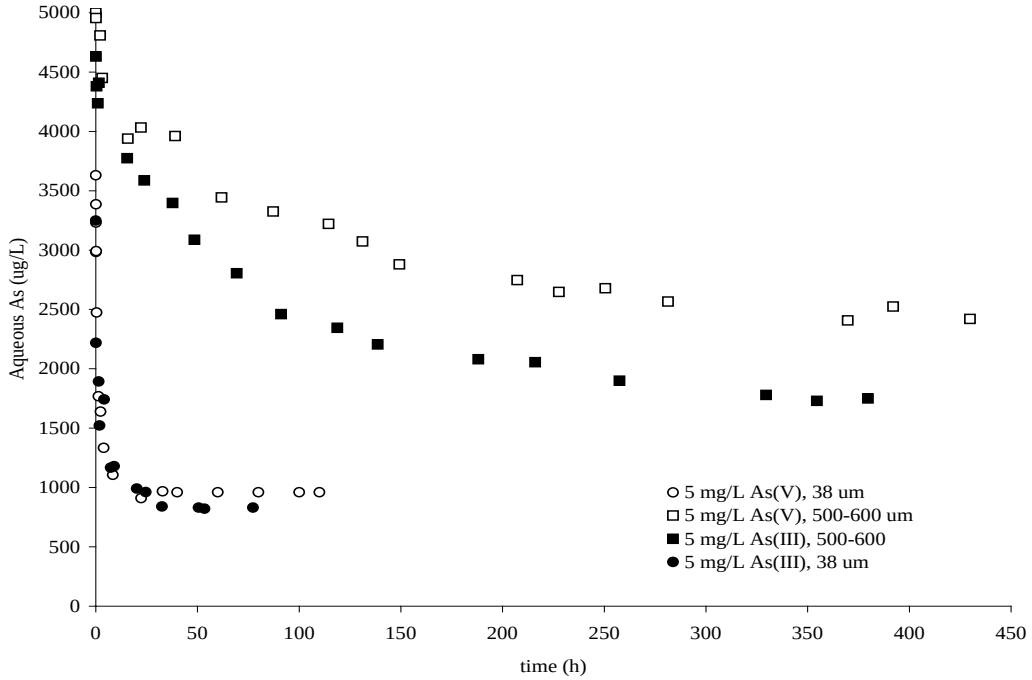

Figure 5.8: Rate of uptake of As onto 0.1 g/L Kemiron. Conditions: pH = 7, As_T = 5 mg/L, I = 0.001 N $NaNO_3$, no CO_2, and at room temperature.

Figure 5.8 plots the rate of uptake results which clearly indicate that the equilibration time of sorption of both As(V) and As(III) depends on the diffusional length of the Kemiron particles. The experimental time scale of the sorption of both As(V) and As(III) onto the 500 – 600 µm particle size of the adsorbent was not long enough for equilibrium to be achieved. The assumptions made during the equilibration times were that the diffusion coefficient was constant, the equilibration time was directly proportional to the square of the diameter of the adsorbent, and the sorption capacity remains the same for all grain sizes where that capacity was determined from sorption data of the ≤ 38 µm particle size. The equilibration time estimated from Figure 5.7 for both As(V) and As(III) sorption onto the ≤ 38 µm particle size was 36 h but for As(III) sorption onto the 500 – 600 µm particle size, the estimated time for the equilibration was determined mathematically to be 8975 h (374 days).

In addition to showing that there was a higher rate of As removal involving the ≤ 38 μm particle size than of the 500 – 600 μm grain size, Figure 5.7 also shows that As(V) and As(III) adsorption onto the 500 - 600 μm had two gradients, with the initial one being more steep. This suggests an initial fast rate step followed by a slower rate step. The slower rate step as explained by LaBolle and Fogg (2001) and Cunningham et al. (1997) could be due to internal pore diffusion. Figure 5.7 shows that Kemiron adsorption capacity appears equal for the two As species onto ≤ 38 μm grain size but not for the adsorption onto the 500 – 600 μm size in the timeframe of the experiment. While there is ~ 80% sorption of 5 mg/L initial concentrations of both As(V) and As(III) onto ≤ 38 μm, there was about 70% sorption of As(III) and 50% sorption of As(V) onto the 500 - 600 μm particle size by the end of the experiments.

The rate of removal of As(V) was slower than As(III) in the 500 – 600 μm grain size. As(III) is known to exist as an undissociated, uncharged molecule at pH 7 while As(V) exists as speciated ions with net negative charge. Wet chemistry tests to determine binding strength usually looks at the effect of ionic strength which was done for this research and the results are shown in Figures 5.18 and 5.19. There appears to be no significant effect of ionic strength on the binding strength of either As(V) or As(III) to the Kemiron surface. The strength of the bond between Kemiron and either As(V) or As(III) can also be assessed through the influence of a competing ion. Section 5.8 presents results on arsenic sorption in the presence of competing ions which show As(III) to be more sensitive to the presence of such ions (e.g. selenite). This can be interpreted to mean that As(III) forms weaker complexes with the surface than As(V). The faster rate of removal of As(III) compared to As(V) from the 500-600 μm grain size could be due to

its weaker surface complexes which are more “mobile” if a surface diffusion type mechanism (i.e. arsenic diffusion results from concentration gradients along the particle surface) explains movement into the particle micropores. On the other hand, a pore diffusion model (i.e. arsenic diffusion results from concentration gradients in the pore water) could also explain why the uncharged As(III) species sorbs faster than the charged species whose movement would depend on counterions diffusing out of the micropores.

Sections 5.4-5.8 delve into modeling details of the rate of uptake data. For the subsequent experiments presented after section 5.8, an equilibration time of 72 hours was used given that all experiments were conducted on the 38 μm grain size. This time was longer than that observed in the previous discussion, but was used to account for any effects that might occur due to the presence of competing ions in the more complex systems.

5.4 Modeling Rate of Arsenic Adsorption

The rate of As loading onto the Kemiron grain particles was modeled with Crank’s analytical solution to Fick’s law of diffusion in a limited volume. The objective for the modeling was to estimate a diffusion coefficient for As removal onto Kemiron in both DI water systems and in synthetic landfill leachate systems. According to Ball (1990) organic solute transport depends among other factors, on the rate of sorption of solute onto an adsorbent and the capacity of the adsorbent for the adsorbate. It was assumed that this relationship also applies to an inorganic solute like As and in an adsorbent like Kemiron.

5.4.1 Diffusion Coefficient Estimation

The diffusion coefficient estimation using Crank's (1975) model required two dimensionless parameters: fractional uptake and dimensionless time, τ, defined by $\tau = D_{app}t/a^2$. Ball and Roberts (1991) used K_d^{app}/K_d^{ult} on the ordinate instead of f_d and the τ for the abscissa instead of time, t. The reason was that the ultimate fractional uptake (F) affects f_d and consequently affects the diffusion coefficient. K_d^{app}/K_d^{ult} equals $\left(C_{be}/C_b\right) * f_d$ where C_{be} is the aqueous concentration at equilibrium and C_b is the aqueous concentration at time t of the sorbate ion of interest. The dimensionless $K_d{}^{app}/K_d{}^{ult}$ was thus used in order to normalize the effect of F. The diffusion rate constants of As transport onto the various grain sizes of Kemiron were estimated with the assumption that the transfer mechanism was intraparticle diffusion controlled and that the external film resistance was negligible. Crank's (Crank, 1975) model adopted for the coefficient estimation was based on a linear isotherm adsorption model and the results of Crank's model are shown in Figures 5.9 – 5.15 and in Table 5.3. Crank's (1975) analytical solution fitted well onto the fractional mass loaded on both 38 μm and 500 – 600 μm grain sizes. To obtain the best fit nonlinear curve onto the experimental data points, a least squares procedure was adopted using Gauss – Newton method. For Crank's model one fitting parameter, D_{app}/a^2, was used. The fitting computation steps can be obtained upon request. However, the computations of the Gauss-Newton method can be found in Appendix D.

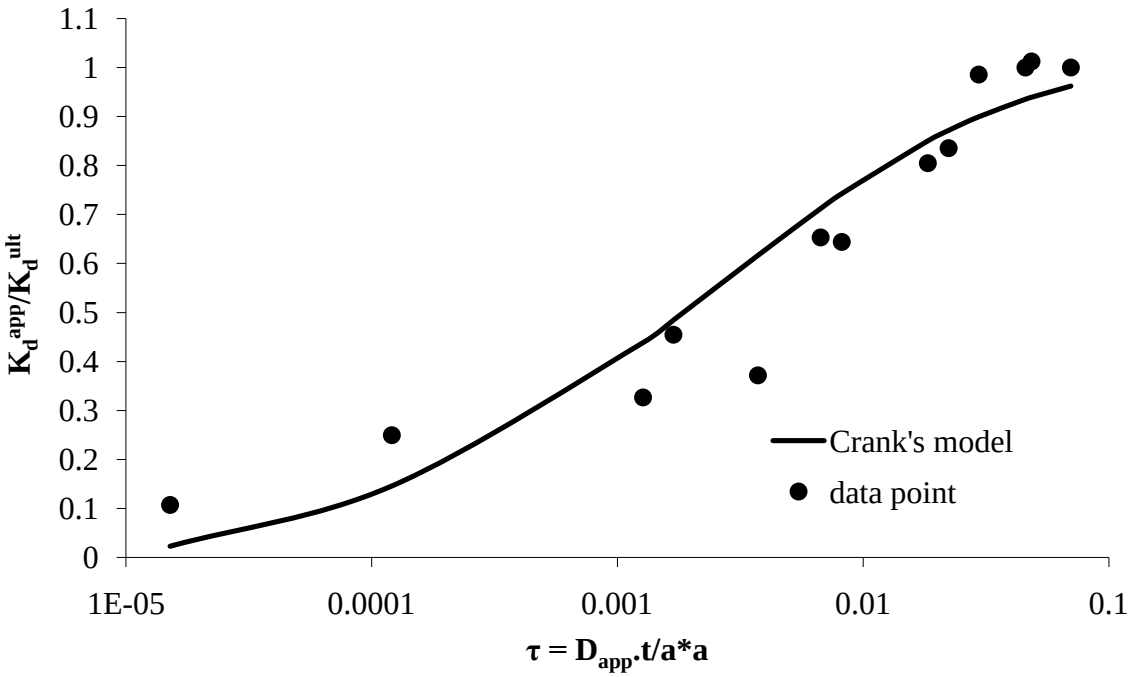

Figure 5.9: Fractional mass of As(III) removal onto ≤ 38 μm grain size in a batch system. Conditions: 5 mg/L $As(III)_T$, 0.1 g/L Kemiron, I = 0.001 N $NaNO_3$, at fixed pH of 7, and Kemiron adsorbent.

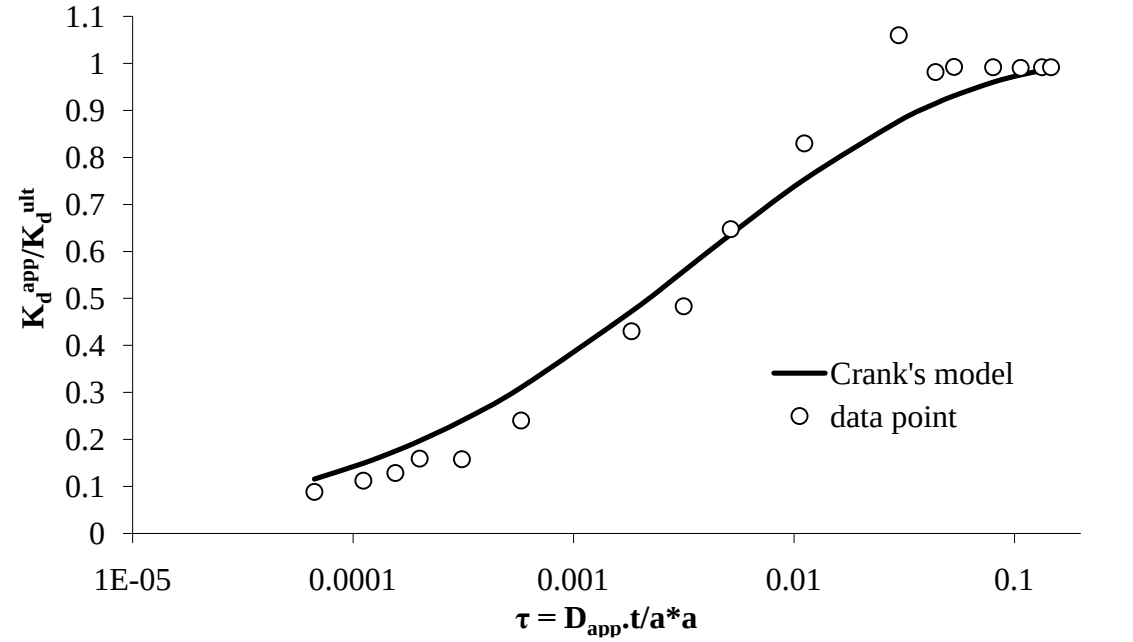

Figure 5.10: Fractional mass of As(V) removal onto ≤ 38 μm grain size in a batch system. Conditions: 5 mg/L $As(V)_T$, 0.1 g/L Kemiron, I = 0.001 N $NaNO_3$, pH = 7, and Kemiron adsorbent.

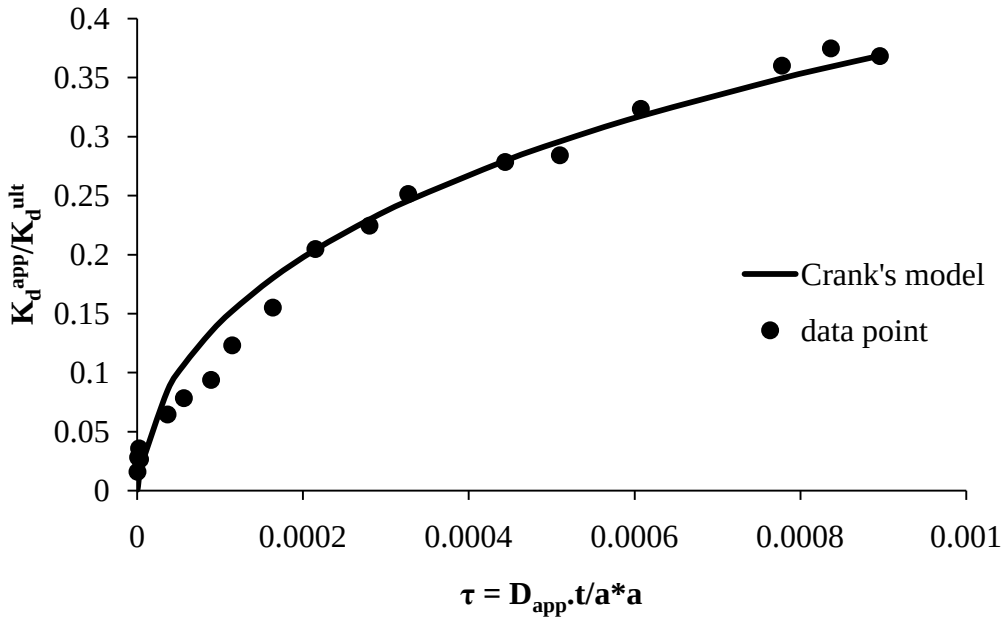

Figure 5.11: Fractional mass of As(III) removal onto 500 – 600 μm grain size in a batch system. Conditions: 5 mg/L $As(III)_T$, 0.1 g/L Kemiron, I = 0.001 N $NaNO_3$, at fixed pH of 7, and Kemiron adsorbent.

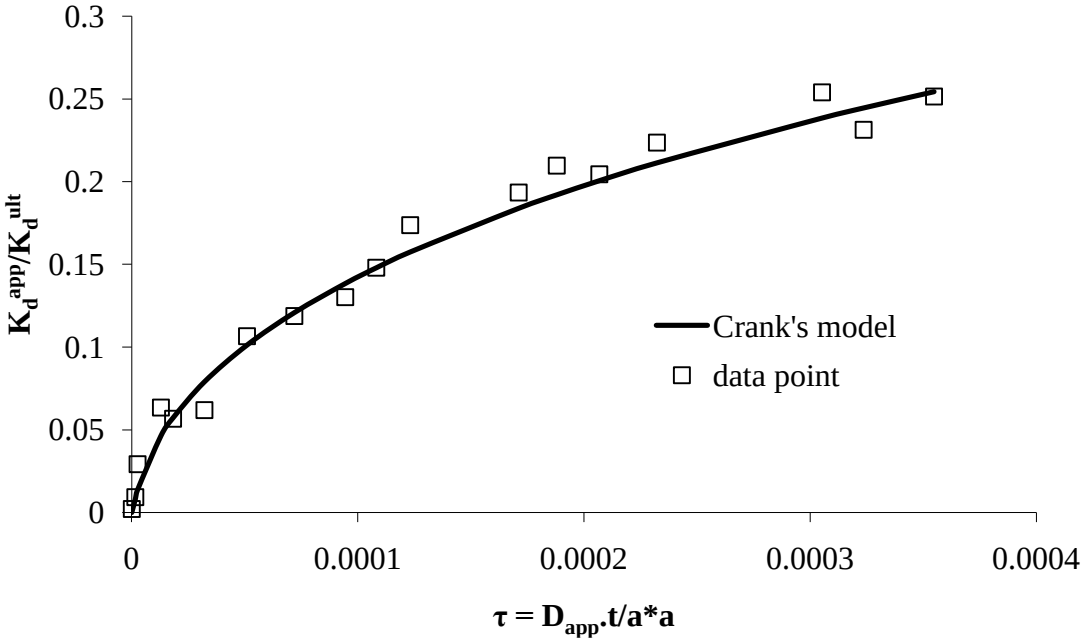

Figure 5.12: Fractional mass of As(V) removal onto 500 – 600 μm grain size in a batch system. Conditions: 5 mg/L $As(V)_T$, 0.1 g/L Kemiron, I = 0.001 N $NaNO_3$, at fixed pH of 7, and Kemiron adsorbent.

The fractional removal models of As(III) and As(V) onto the less than 38 μm particles are shown in Figures 5.12. Figure 5.13 and 5.14 compare the results for the model fits of As(V) and As(III) removal onto the less than 38 μm and the 500 – 600 μm grain size.

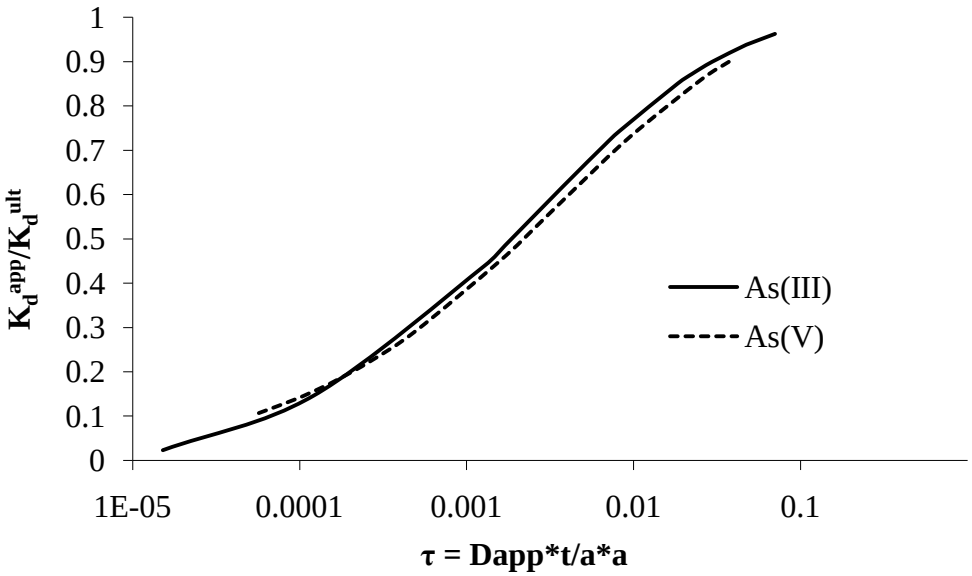

Figure 5.13: Fractional mass of As removal model in a batch system. Conditions: 5 mg/L As_T, 0.1 g/L Kemiron, I = 0.001 N $NaNO_3$, at fixed pH of 7, and Kemiron grain size ≤ 38 μm.

There have been some reported cases of various diffusion coefficients for the same adsorbent but with different grain sizes or with different initial concentrations. According to Ball (1990), situations like these indicate one of the following three possible reasons: 1) the diffusion coefficient may be a function of the particle size; 2) the length scale may not be actually the particle radius; and 3) the kinetic experimental data may not be good. In Table 5.3, the relatively low value of D_{app}/a^2 of As(V) onto the 500 – 600 μm was expected because of the high values of the particle radius, a.

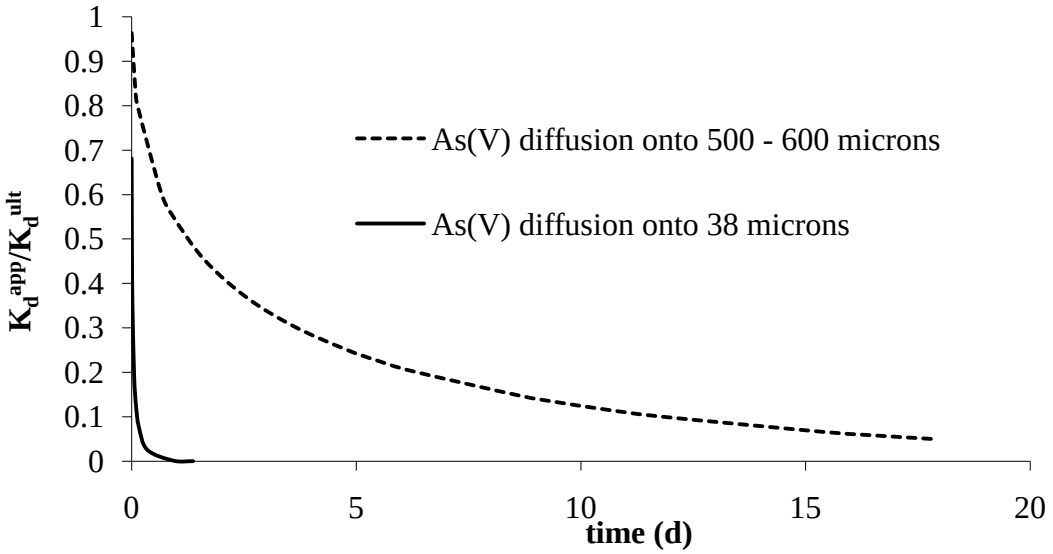

Figure 5.14: Kinetics of As(V) removal model in a batch system. Conditions: 5 mg/L $As(V)_T$, 0.1 g/L Kemiron, I = 0.001 N $NaNO_3$, at fixed pH of 7, and Kemiron grain sizes used are 38 μm and 500 – 600 μm.

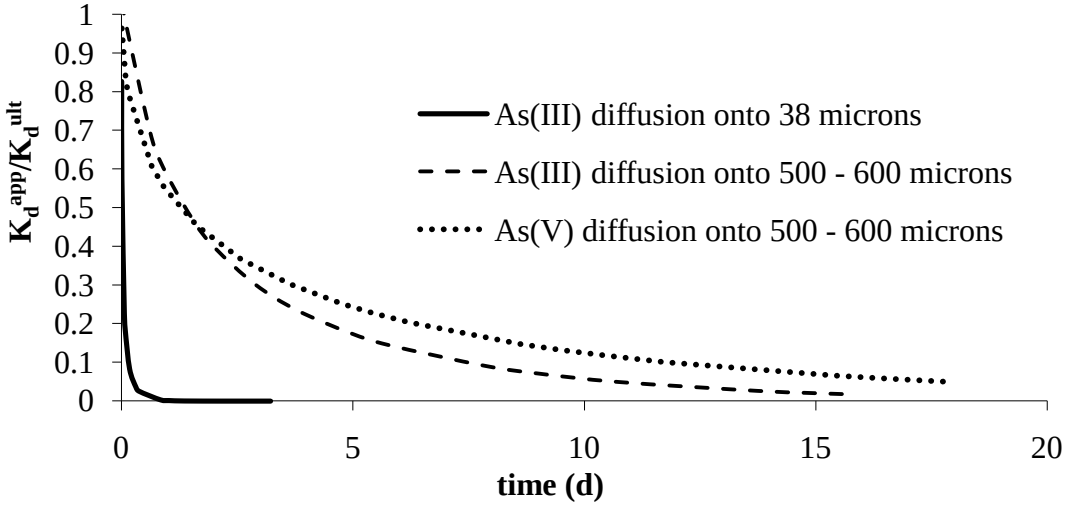

Figure 5.15: Kinetics of As removal model in a batch system. Conditions: 5 mg/L As_T, 0.1 g/L Kemiron, I = 0.001 N $NaNO_3$, at fixed pH of 7, and Kemiron grain sizes used are 38 μm and 500 – 600 μm.

For a constant value of D_{app} for diffusion into the pores of both 38 μm and 500 – 600 μm particles, the value of D_{app}/a^2 is expected to be lower for the 500 – 600 μm when compared with the 38 μm adsorbent grain size (Table 5.3).

Table 5.4 shows diffusion rate constants of As adsorption reported by others in relation to the grain sizes of the adsorbents. Granular Ferric Hydroxide (GFH) shows three orders of diffusion coefficients for As(V) adsorption onto the grain size range of 0.6 – 2.0 mm.

Table 5.3: Grain sizes and intraparticle diffusion rate constants of As removal. Conditions: in binary systems, pH 7, I = 0.001 N $NaNO_3$, CO_2 absent, room temperature.

Kemiron size fraction (μm)	Solute	D_{app}/a^2 (10^{-8} s^{-1})
≤ 38	As(V)	32
≤ 38	As(III)	25
500 – 600	As(V)	0.02
500 – 600	As(III)	0.07

Table 5.4: Intraparticle diffusion coefficients of As removal onto other iron oxide. Conditions: pH = 7 at room temperature.

Adsorbent	Grain size	Adsorbate	D_{app} (10^{-11} cm^2/s)	Source
GFH	0.8 – 1.0 mm	As(V)	203.0 324.0	Badruzzaman *et al.* (2004)
GFH	0.6 – 2.0 mm	As(V)	6.4	Vaughan *et al.* (2007)
Iron oxide		As(V)	1.0	Hristovski *et al.* (2009)
Iron oxide modified GAC	0.6 mm	As(V)	90.5	Thirunavukkarasu *et al.* (2003a)

5.4.2 Effect of Arsenic Concentration on Diffusion

This test was limited to As(V) adsorption onto 500 – 600 μm. The assumption made here was that the trend as exhibited by As(V) would also be exhibited by As(III)

under the same conditions. It was expected that the rate of As(V) uptake would increase with increasing initial concentrations of As(V) due to larger concentration gradients onto particle surfaces.

The rate of As(V) adsorbed was subsequently observed to have higher removal gradients with higher initial As concentrations as shown in Figure 5.16. This suggests that the As(V) removal rate depended on the initial concentration. While the slopes leveled off between the 300th and 400th hour after the spiking of the 5 mg/L initial concentration, the times for the leveling off seemed to shift to the right as the initial As concentration increased from the 5 mg/L to the 20 mg/L As(V). Sorption of only the 5 mg/L and 10 mg/L As(V) concentrations were done on the ≤ 38 μm fraction, hence limiting the determination of D_{app}/a^2 to only these two concentrations since equilibrium was not reached over the duration of the experiment for the 500-600 μm fraction. The results are given in Table 5.5. For the two initial concentrations used D_{app}/a^2 differed by an order of magnitude.

Table 5.5: Effect of initial As(V) concentration on mass loadings. Effects on intraparticle diffusion rate constants in binary systems at pH 7, I = 0.001 N $NaNO_3$ onto 500 – 600 μm Kemiron particle grain size.

As(V) conc. (mg/L)	Mass of As(V) sorbed (mg/g)	D_{app}/a^2 (10^{-8} /s)
5	25.49	0.02
10	35.50	0.5
15	40.00	Not determined
20	51.00	Not determined

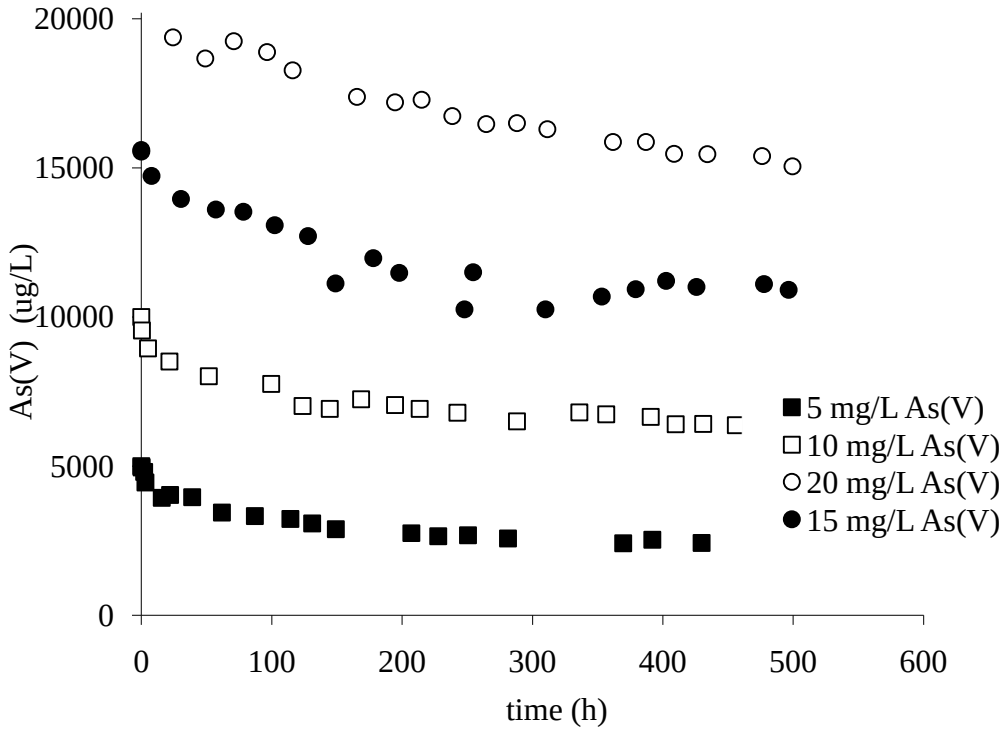

Figure 5.16: Effect of initial As(V) concentration on rate of uptake. Conditions: As(V) at pH 7, I = 0.001N $NaNO_3$, particle size of 500 – 600 μm, and at room temperature.

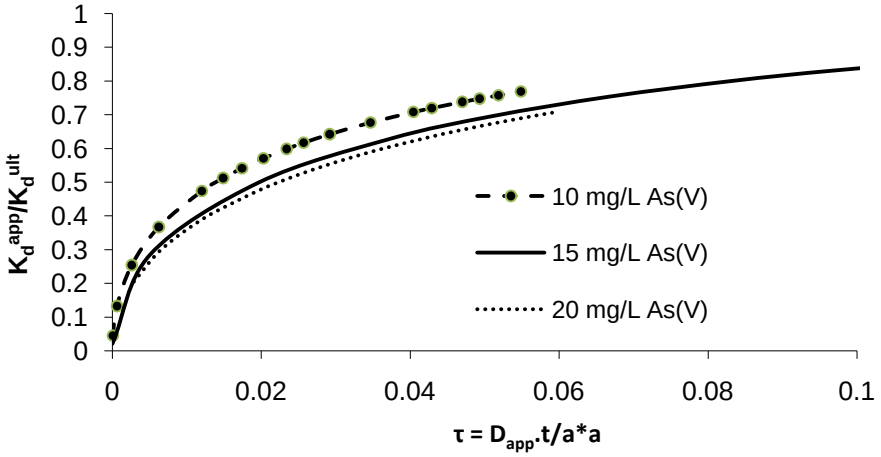

Figure 5.17: Model of Fractional mass of As(V) removal. Conditions: batch system for 5 m& 10 g/L $As(V)_T$, 0.1 g/L Kemiron, I = 0.001 N $NaNO_3$, at fixed pH of 7, and Kemiron grain size = 500 – 600 μm

5.5 Batch Equilibrium Sorption of Arsenic

Batch As adsorption studies were conducted under the following sets of conditions: 1 mg/L, 5 mg/L, and 10 mg/L initial As concentrations; 0.001 N $NaNO_3$ and 0.1 N $NaNO_3$ for ionic strength; over a range of pH of 4 – 10; 0.1 g/L Kemiron dose with grain size of 38 µm for shorter equilibration time, and the absence of CO_2 for adsorption competition prevention in the systems unless otherwise noted. The objectives of these experiments were to evaluate the impact of pH on As adsorption onto Kemiron and to evaluate the impact of background ionic strength on the adsorption. For another set of batch experiments the objective was to determine the impact of the presence of competing ions on the adsorption of arsenic. Ions like CO_3^{2-}, SO_4^{2-}, NH_4^{+}- N, and Ca^{2+}, were used to represent the commonest competing bivalent inorganic ions found in landfill leachate. The impact of Ni^{2+}, and Se(IV) were also evaluated as representatives of trace co-contaminants.

The equilibrium sorption experiments in the binary systems shown in Figure 5.18 were conducted for 5 mg/L and 10 mg/L total As(V) concentrations while As(III) concentrations of 1 mg/L, 5 mg/L and 10 mg/L were conducted and are shown in Figure 5.19. The adsorption of As(V) increased as a pH decreased as shown in Figure 5.18 which can be explained in terms of a combination of a positive surface charge as pH decreases and the negatively charged As(V) species. The dominating species of As(V) up to pH 2.2 was H_3AsO_4. Between pH 2.2 and 7.0, $H_2AsO_4^{-}$, species dominated while $HAsO_4^{2-}$ dominated between pH of 7.0 and 12.1.

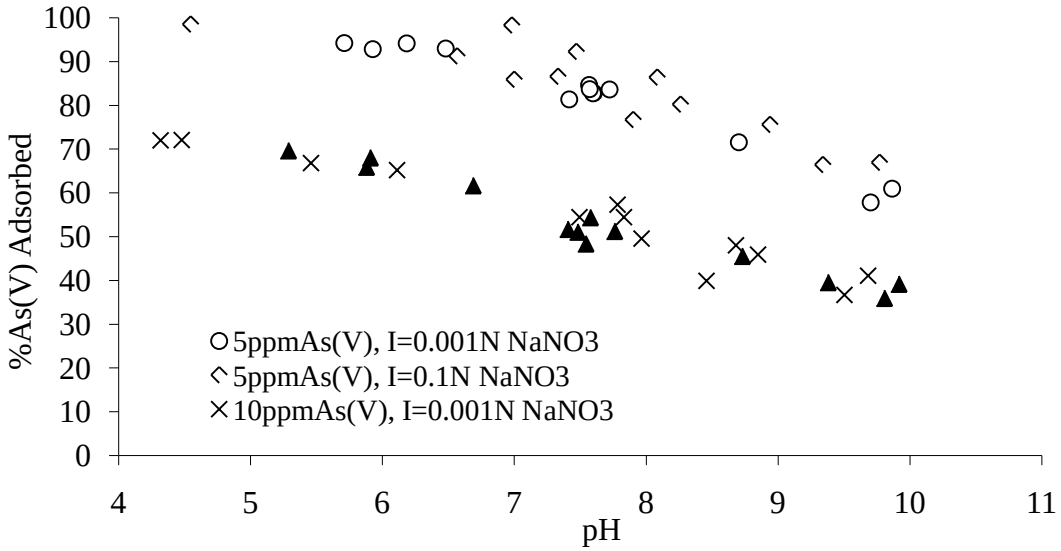

Figure 5.18: Batch equilibration tests of As(V) onto 38 µm Kemiron grain size. Conditions: in CO_2 free binary systems and at room temperature.

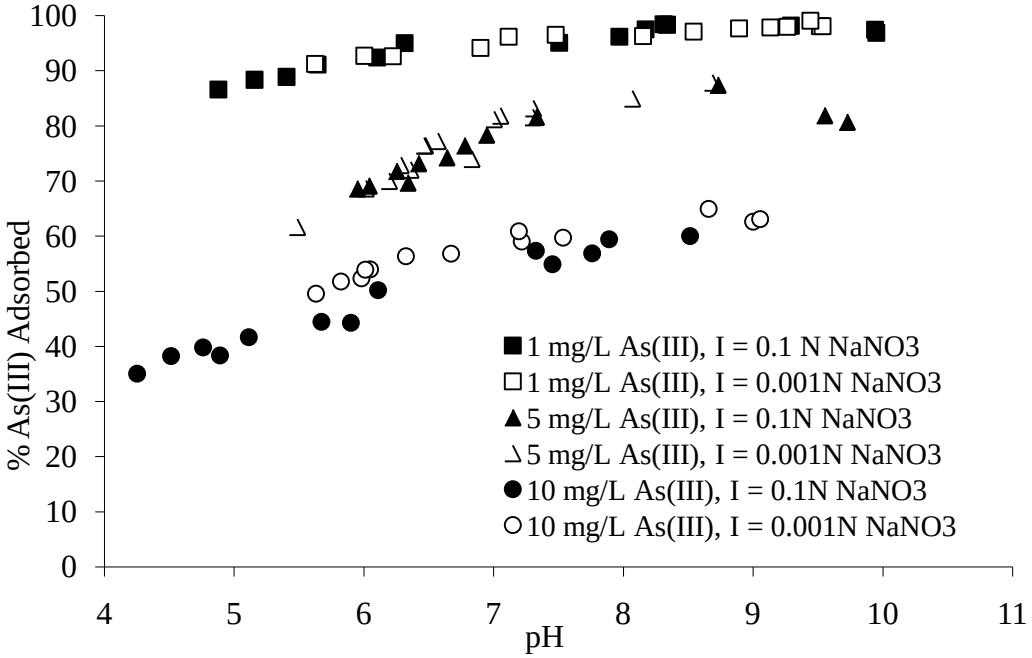

Figure 5.19: Batch equilibration tests of As(III) onto 38 µm Kemiron grain size. Conditions: in CO_2 free binary systems and at room temperature.

Figure 5.19 shows the variation of As(III) sorption with pH, the effect of ionic strength and the effect of total As(III) concentration. Like other studies, the sorption is dome shaped and peaks in the pH 8 to 9 region for all total concentrations, though at 1 mg/L As(III) this was least pronounced (Chakraborty *et al.* 2007). This peak can be explained in terms of both the aqueous speciation of As(III) and the surface charge as a function of pH. Under the solution conditions studied, As(III) remains as an uncharged H_3AsO_3 species until the first pK_a (9.32) after which it becomes the negatively charged $H_2AsO_3^-$ species. The pzc of iron oxide surfaces occurs around pH 8-9.5 where they are positively charged below the pzc and negatively charged above (Naeem *et al.* 2007, Sperlich *et al.* 2005). Hence, the maximum sorption between As(III) species and the surface occurs in the vicinity where the As(III) is negatively charged and the surface is positively charged, which is expected.

For all of the total initial As(III) and As(V) concentrations studied the adsorption behavior was also unaffected when the background ionic strength varied from 0.001 N $NaNO_3$ to 0.1 N $NaNO_3$, an observation seen by others (Smith and Naidu 2009). Ionic strength has usually been used as a wet chemical diagnosis for whether an ion was bound strongly (usually referred to as an inner-sphere complex) or weakly (usually referred to as an outer-sphere complex) where unchanged sorption as a function of ionic strength was attributed to inner-sphere type sorption mechanisms (McBride 1997; He *et al.*, 1997; Hayes et al., 1998). The results shown in Figure 5.19 suggest that As(III) binds in an inner-sphere type mechanism to Kemiron.

Many iron based adsorbents have their pH point of zero charge (pH_{pzc}) between 8.0 and 9.5 (Naeem *et al.* 2007, Sperlich *et al.* 2005). At the pH_{PZC}, the charges on the

adsorbent surface are neutral and pH values below and above the pH_{pzc} result in net positive and net negative surface charges respectively. In our equilibration experiment, the adsorption edge showed a considerable drop around pH 7.5 for As(V) which is mainly found as negatively charged species in this pH range. The sorption edges of both As(V) and As(III) crossed near pH 7.5 shown in Figure 5.20 with higher As(III) sorption above pH 7.5. In this pH region where the surface changes from a net positive to a net negative/neutral charge, sorption of the uncharged As(III) species is favored over sorption of the dominant negatively charged As(V) species.

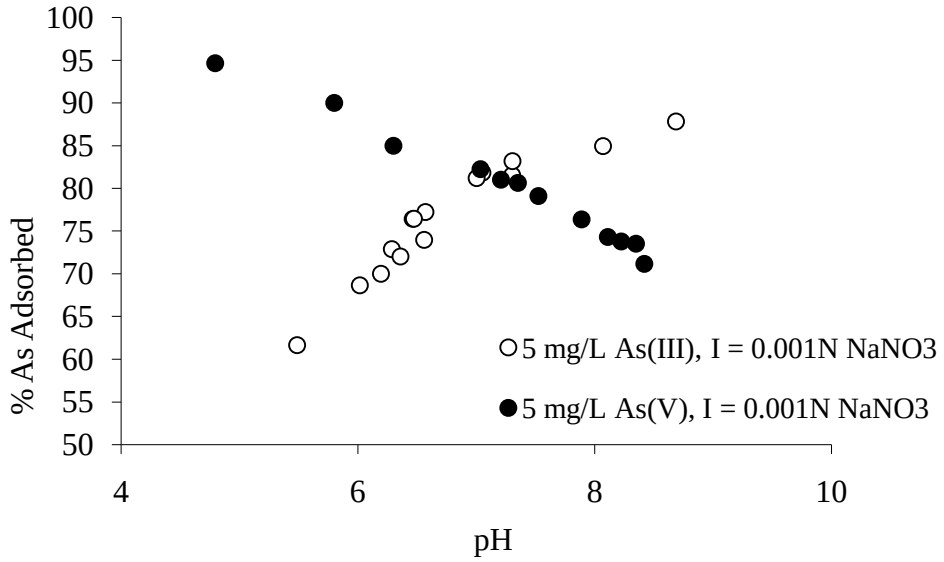

Figure 5.20: Batch equilibration tests of both As(V) and As(III) onto 38 µm Kemiron. Conditions: in CO_2 free binary systems and at room temperature.

5.6 Arsenic Adsorption Isotherms

Adsorption isotherms are usually used to determine the density of surface hydroxyl sites (sites per unit surface area), and to determine the type of adsorption model that best fits the contaminant removal data. In this work, As(V) and As(III) adsorption data were analyzed using Langmuir and Freundlich models and Table 5.6 lists some of

the previous research conditions and model fits used. These models were adopted to describe and to compare the relationship between the amount of As loadings on the Kemiron surface and the concentration of arsenic in solution at equilibrium, for constant pH and temperature. Figures 5.21 and 5.22 show As(III) and As(V) sorption isotherms at pH values that range from 6 to 9. The best fits to the experimental data using the Freundlich model for As(III) and Langmuir model for As(V) are also shown in those figures as lines.

Table 5.6: Isotherms of As adsorption onto various adsorbents.

Adsorbate species	**Adsorbent**	**Isotherm model**	**Reference**
As(V)	GFH	F	Abdallah and Gagnon (2009)
As(III)	U. cylindricum	L	Sari & Tuzen (2009)
As(III)	U. cylindricum	D – R	Sari & Tuzen (2009)
As(III)/(V)	Fe(III) – Ti(IV)	L/F	Ghosh *et al.* (2004)
As(III)	Kemiron	F	This work
As(V)	Kemiron	L	This work

F – Freundlich, L – Langmuir, D-R – Dubinin-Radushkevich.

The experimental data in Figure 5.21 shows that As(III) sorption capacity continues to increase under the conditions studied and that for a given pH value, the corresponding amount of arsenic on the surface increases as a function of pH. The differences in the amount sorbed at a given pH is not great and can be explained by referring to Figure 5.19 which plotted As(III) sorption edges as a function of pH. For the pH range presented in Figure 5.21, As(III) sorption is at its maximum which represents a plateau on the dome shaped sorption curve. It is obvious from the isotherm plots that a Linear model (q =KC) would apply to neither As(III) or As(V) across the full range of sorption densities. The As(V) adsorption isotherms shown in Figure 5.22 begin to

plateau under the experimental conditions, and for a given aqueous equilibrium condition the sorption capacity increases as pH decreases. This is consistent with the results shown in Figure 5.18. Compared with As(III) for the same pH value, the maximum As(V) sorption capacity observed is lower. For example, the capacity for As(V) at pH 7 is somewhere around 86 mg As/ g sorbent whereas it is greater than 90 mg As/ g sorbent for As(III). At lower pH values As(V) is favored and the capacity for sorption by Kemiron would be greater. It is also possible that a "cluster effect" causes the lower capacity observed for the case of As(V). While at the pH 7 As(III) exists as an uncharged molecule, As(V) exists as a charged ion. It is possible that the binding between the As(V) and the surface during diffusion into the pores forms clusters which hinder the movement of other dissolved ions.

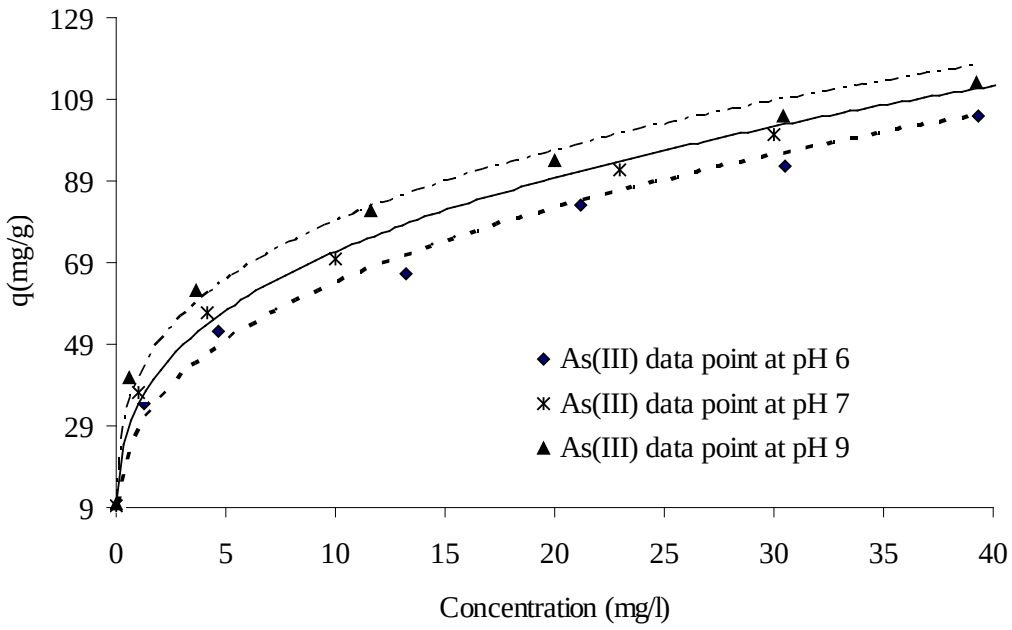

Figure 5.21: Effect of pH on As(III) adsorption isotherm in pure system. Freundlich Model fits and experimental data. Conditions: room temperature, I = 0.001N $NaNO_3$, adsorbent grain size of ≤ 38 μm.

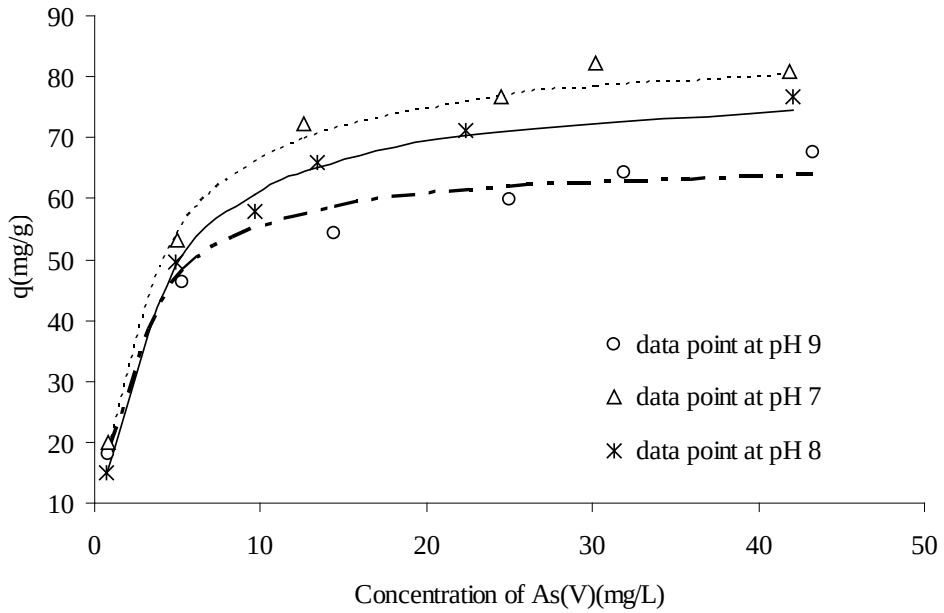

Figure 5.22: Effect of pH on As(V) adsorption isotherm in pure system. Langmuir model fits (lines) and experimental data shown. Conditions: room temp, I = 0.001N $NaNO_3$, adsorbent grain size of ≤ 38 μm.

The use of Langmuir and Freundlich models to fit the As(V) and As(III) sorption were based on the assumption that the sorption and the interactions between Kemiron and As followed the same conditions upon which the models were derived. The best fit curves were obtained with Gauss Newton analyses and confirmed by linear least squares methods. This confirmation was done by plotting the predicted data (from the selected model) on the y-axis and the experimental data on the x-axis. A correlation coefficient (r^2) was then be derived for a straight line fit through the origin with a slope 1. The empirical constants q_{max}, K_L, K_f and 1/n of the models were determined from the Gauss Newton algorithm. Appendix B indicates the experimental and the predicted data used to evaluate the empirical constants as well as the sum of squares of residual errors.

Table 5.13 summarizes the model fits to experimental data as well as the results from the linearization process used to determine the best model to adopt. Figures 5.23 to

5.25 are example plots of the linearilization results. The Langmuir model ($r^2 = 0.99$) fits As(V) adsorption onto Kemiron better than the Freundlich model ($r^2 < 0.92$) with maximum adsorption densities ranging between 68 mg As(V)/g solid at pH 9 and 88 mg As(V)/g solid at pH 7. The Freundlich model ($r^2 > 0.95$) on the other hand fits As(III) adsorption better than the Langmuir model ($r^2 < 0.95$) with the coefficient K_f increasing between pH values of 6 and 9. The differences between the r^2 values for the two models were not as significant for As(III) (as great as 0.07) as they were for As(V) (as great as 0.15). The sum of squares of residual error can also be used to infer best fits to experimental data where a value closest to zero is preferred. The standard error of estimate of the Langmuir models to As(V) sorption were ~2.87, 1.85, and 2.46 at pH values of 9, 8, and 7 respectively. The standard error of estimate of Freundlich models to As(III) sorption were 3.45, 1.68, and 3.00 at pH values of 6, 7, and 9 respectively. This also suggests good fits between the experimental data and the models selected.

Given the model fits, what can we infer about As(III) and As(V) sorption? The Langmuir model assumes monolayer coverage as well as uniform surface sites whereas the Freundlich model accounts for site heterogeneity. For the pH range studied in these isotherms, As(III) would exist mainly as an uncharged species. Given its first pK_a value of 9.23, the isotherm at pH 9 would include much higher concentrations of the negatively charged anion $H_2AsO_3^{2-}$. Although the differences between the Langmuir and Freundlich fits to As(III) isotherm data are not great, geochemistry can be used to explain the better results obtained from the Freundlich model. The surface complex formed between the uncharged As(III) species and the adsorbent could be due to a site type that is different from that involved with the complexation of negatively charged species. Over the pH

range studied, all As(V) species were negatively charged and it is possible that they interact with a uniform site type, hence the better fits obtained with the Langmuir model. Although the adsorption of As(V) and As(III) seems to follow Langmuir and Freundlich models respectively, there is a clear indication that a linear adsorption isotherm model would fit a relatively narrower range of initial concentrations. This latter point has implications for the modeling previously done with the rate of uptake data where a linear adsorption model was assumed. Given the limited concentration range used, that assumption was appropriate for the purposes of this research.

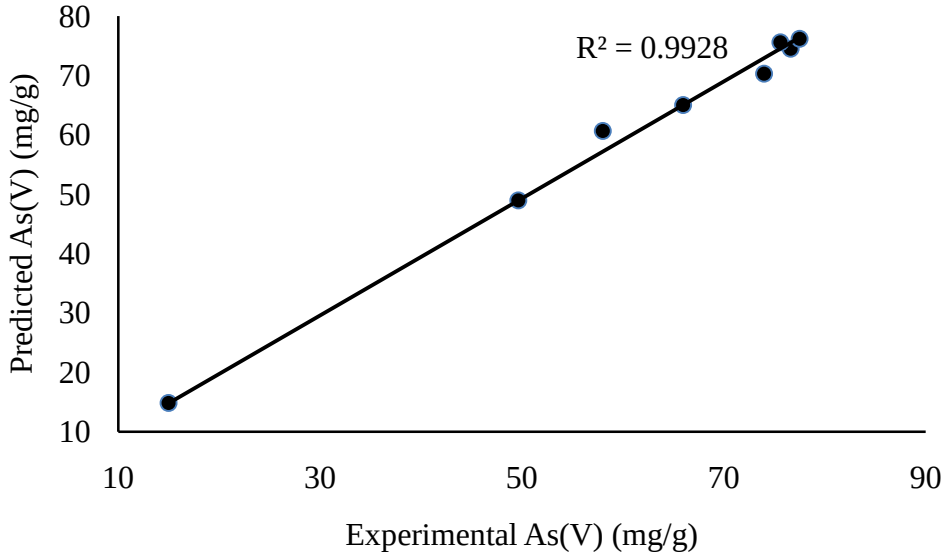

Figure 5.23: Experimental data and predicted data of As(V) sorption at pH 8. Conditions: ≤ 38 μm Kemiron ; I = 0.001 N $NaNO_3$; Langmuir model used.

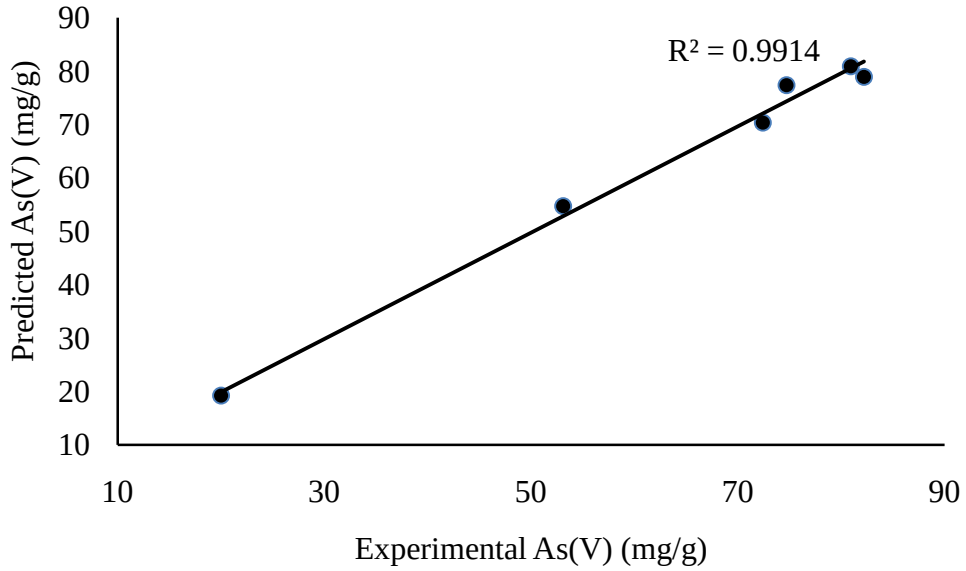

Figure 5.24: Experimental data and predicted data of As(V) sorption at pH 7. Conditions: ≤ 38 μm Kemiron; I = 0.001 N $NaNO_3$; Langmuir model used.

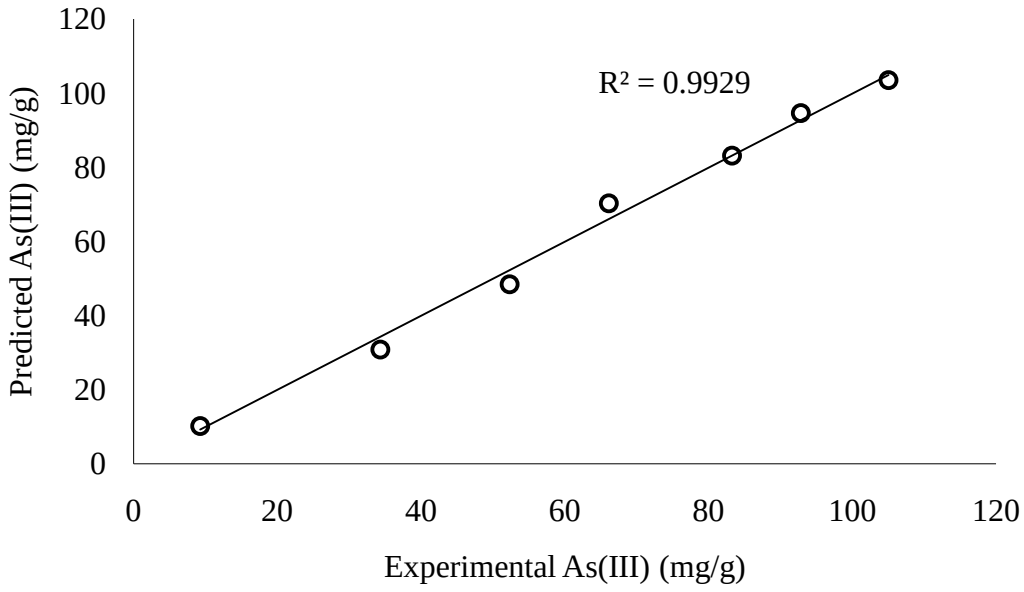

Figure 5.25: Experimental data and predicted data of As(III) sorption at pH 6. Conditions: ≤ 38 μm Kemiron; I = 0.001 N $NaNO_3$; Freundlich model used.

Table 5.7: Isotherm parameters of As onto 38 μm Kemiron particles. Conditions: binary systems of 0.001 N $NaNO_3$; CO_2 absent and at room temperature.

		Freundlich parameters			Langmuir parameters		
Species	pH	K_f	1/n	r^2	q_{max} (mg/g)	K_L	r^2
As(III)	6	29.46	0.34	0.99	103	0.25	0.94
	7	35.81	0.31	0.98	115	0.23	0.95
	9	42.54	0.28	0.95	123	0.21	0.92
As(V)	7	44.71	0.15	0.84	87	0.34	0.99
	8	35	0.24	0.86	82	0.31	0.99
	9	20	0.33	0.92	68	0.39	0.99

5.7 Effect of Presence of Competing Ions and Co-Contaminants

Figure 5.26 shows the effect of 5 mg/L (63 μM) Se(IV) or 5 mg/L (85 μM) Ni(II) on 5 mg/L (65μM) As(III) sorption to Kemiron. On a molar basis, all three concentrations were comparable and both Ni(II) and Se(IV) resulted in reduced As(III) sorption across all pH values with Se(IV) having a greater effect and with a lower percentage reduction due to the presence of either ion as the pH increased. For example, at pH 7 As(III) sorption was reduced from close to 80% to 70% in the presence of Ni(II) and to 50% in the presence of Se(IV). At pH 8, the As(III) sorption was reduced from approximately 85% to close to 80% in the presence of Ni(II) and 65% in the presence of Se(IV). In solution Se(IV) would form H_2SeO_3 which dissociates based on its pK_a values of 2.63 and 8.4 and hence in the pH range considered in this study, the main form of Se(IV) would be $HSeO_3^-$ and SeO_3^{2-}.

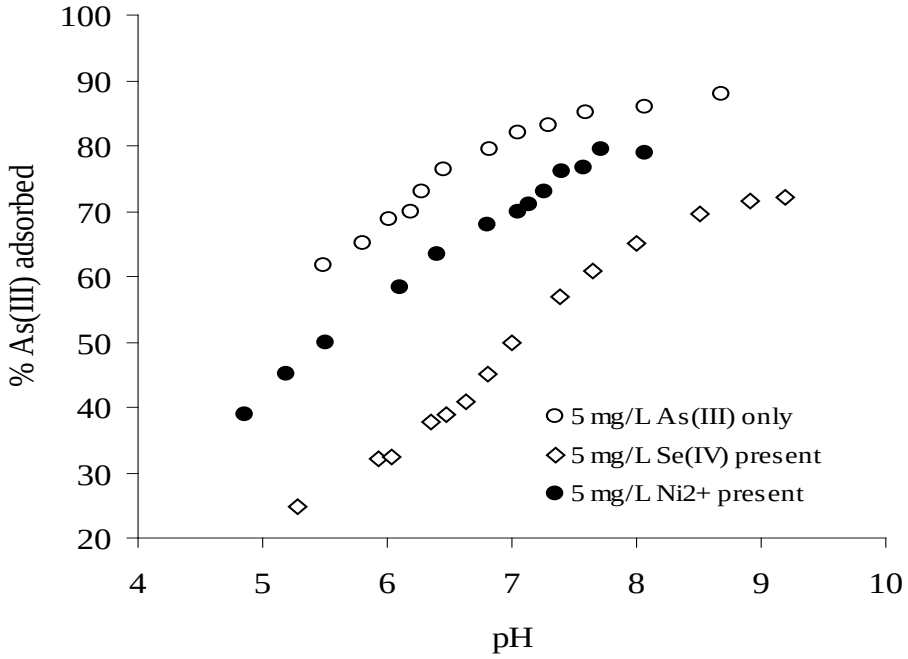

Figure 5.26: Effect of Se(IV) or Ni^{2+} on As(III) adsorption. Conditions: 0.1 g/L Kemiron (<38 μm), I = 0.001 N $NaNO_3$, CO_2 excluded.

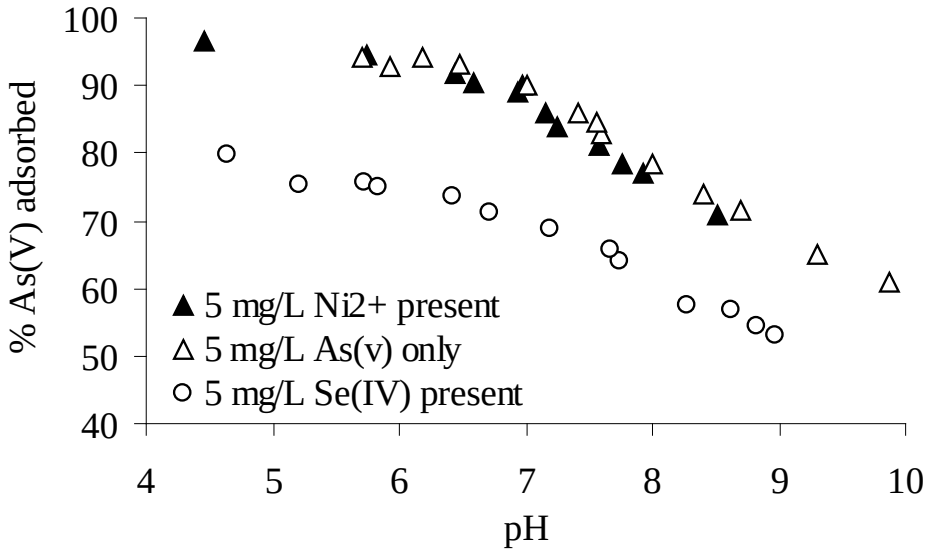

Figure 5.27: Effect of Se(IV) or Ni^{2+} on As(V) adsorption. Conditions: 0.1 g/L Kemiron (<38 μm), I = 0.001 N $NaNO_3$, CO_2 excluded.

The higher percentage of positively charged surface sites below the pzc, would attract the negatively charged Se(IV) species and this is confirmed in Figure 5.28 where Se(IV) sorption onto Kemiron increased as pH decreased with the slope of the sorption edge beginning to change around pH 8 and approximately 90% of Se(IV) being sorbed at pH 7. On a molar basis, the moles of sorbate (As(III) + Se(IV)) used in Figure 5.26 is similar to that of just 10 mg/L As(III) which is approximately 60% at pH 7 from Figure 5.18, and to that of just 10 mg/L Se(IV) which is also approximately 60% at pH 7 from Figure 5.28.

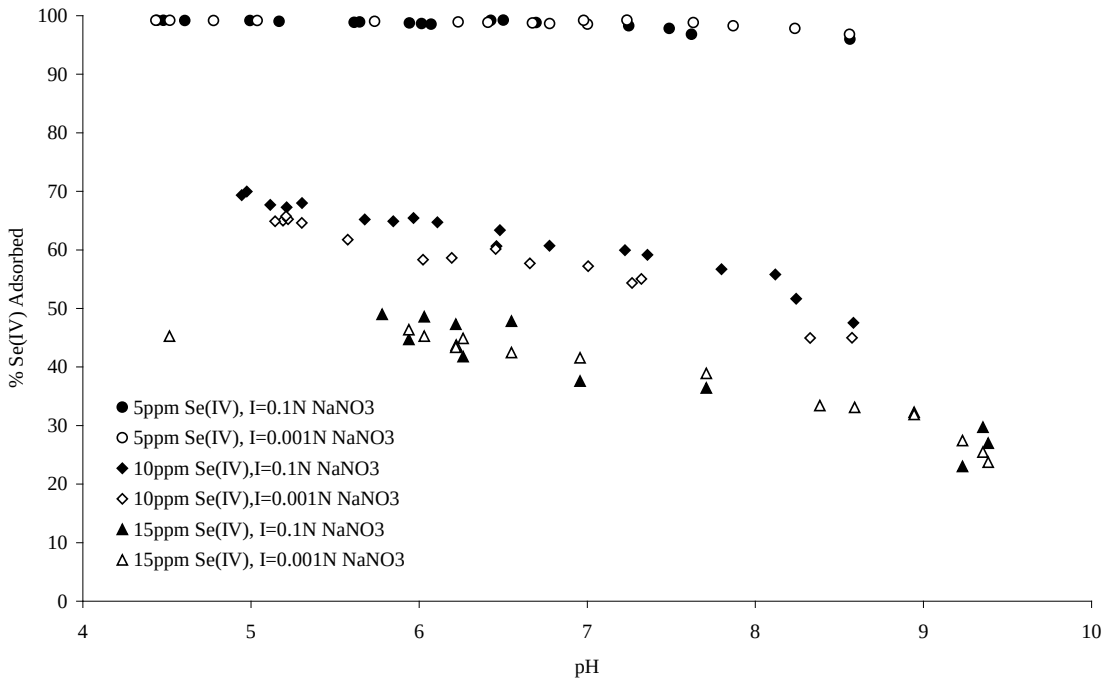

Figure 5.28: Se(IV) sorption as a function of pH. Conditions: 0.1 g/L Kemiron (<38 μm), I = 0.001 N $NaNO_3$ and 0.1 N $NaNO_3$, CO_2 excluded.

Figure 5.27 shows the effect of 5 mg/L (63 μM) Se(IV) or 5 mg/L (85 μM) Ni(II) on 5 mg/L (65μM) As(V) sorption to Kemiron. In the presence of 5 mg/L Se(IV), As(V) adsorption dropped by 20% between pH 4.5 and 9 which was less than that observed for

As(III) (40% between pH 5 and 7 and by 20% between pH 7 and 9). Ni(II) did not reduce As(V) sorption across the pH range studied unlike what was observed in Figure 5.26 for As(III). Although Ni(II) sorption to Kemiron by itself was not examined, it is expected to sorb as a typical cation which means its sorption would increase as pH increases (i.e., as the surface becomes increasingly negative it would attract more of the positively charged Ni(II) ions).

Figure 5.29 shows the effect of either 1000 mg/L (16.7 mM) CO_3^{2-} or 1000 mg/L (10.4 mM) SO_4^{2-} on 5 mg/L As(III) sorption to 0.1 g/L Kemiron. The molar concentration of carbonate used was approximately 1.6 times that of sulfate and may be one reason why the effect of carbonate was greater. Even though the carbonate and sulfate concentrations are more than two orders of magnitude greater than that of As(III), the amount of As(III) reduced is not as pronounced as seen in the case of either Ni(II) or Se(IV) above. Sulfate sorption to mineral oxides typically increases as pH decreases whereas that of carbonate plateaus around pH 6.5 and the amount sorbed of either of the two is reduced as ionic strength increases (Zhang and Sparks, 1990; He et al., 1997;Villalobos and Leckie, 2000). The affinity of carbonate and sulfate for adsorption to mineral oxides is considered low to moderate (Sposito, 1989), however, they have been seen to reduce the sorption of other anions (e.g. selenite) when present in extremely high concentrations (Balistrieri and Chao, 1987; Appelo et al. 2002). In some cases, carbonate enhanced oxyanion sorption to mineral oxides, as was seen in the case of phosphate on goethite (Wijna et al., 2000).

The effect of sulfate on As(III) sorption decreased as pH increased and can be explained in terms of a competitive sorption mechanism where sulfate affinity for the

surface decreased as pH increased (He *et al.*, 1997) at the same time that As(III) affinity reached its maximum. Villalobos and Leckie (2000) found that carbonate sorption to goethite peaked close to the first acidity constant for H_2CO_3 in the pH 6 region and hence its sorption curve is similar to that of As(III), just that the peak occurs around pH 6 versus between pH 8 and 9 and seen in Figure 5.19. Along with the higher carbonate concentration used when compared with sulfate, this would also explain why carbonate reduces As(III) sorption more than sulfate.

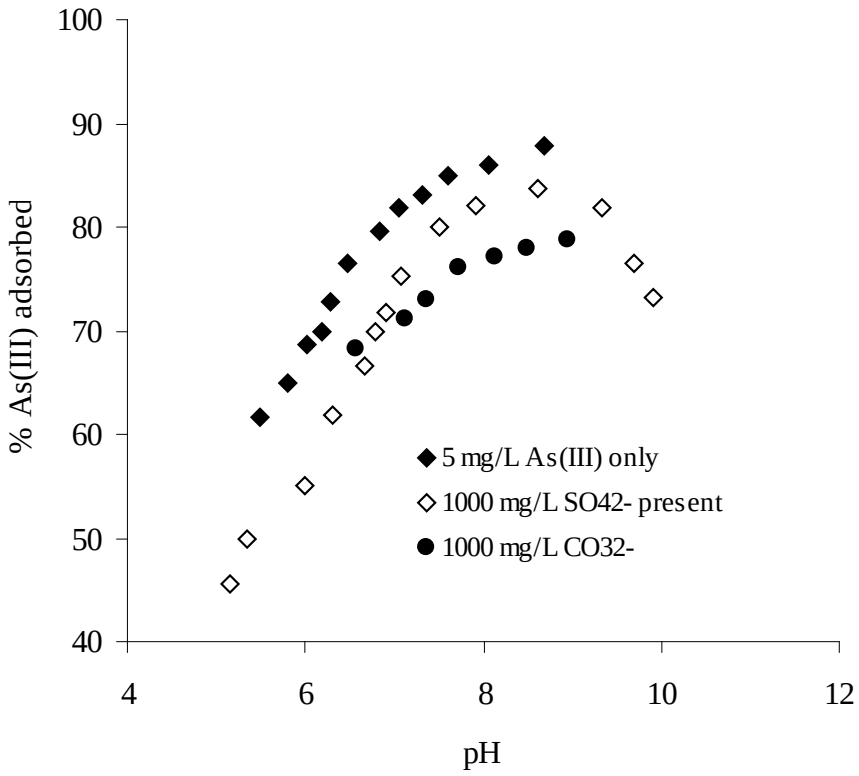

Figure 5.29: Effect of CO_3^{2-} or SO_4^{2-} on As(III) adsorption. Conditions: 0.1 g/L Kemiron (<38 μm), I = 0.001 N $NaNO_3$ and 0.1 N $NaNO_3$, CO_2 excluded from SO_4^{2-} experiments.

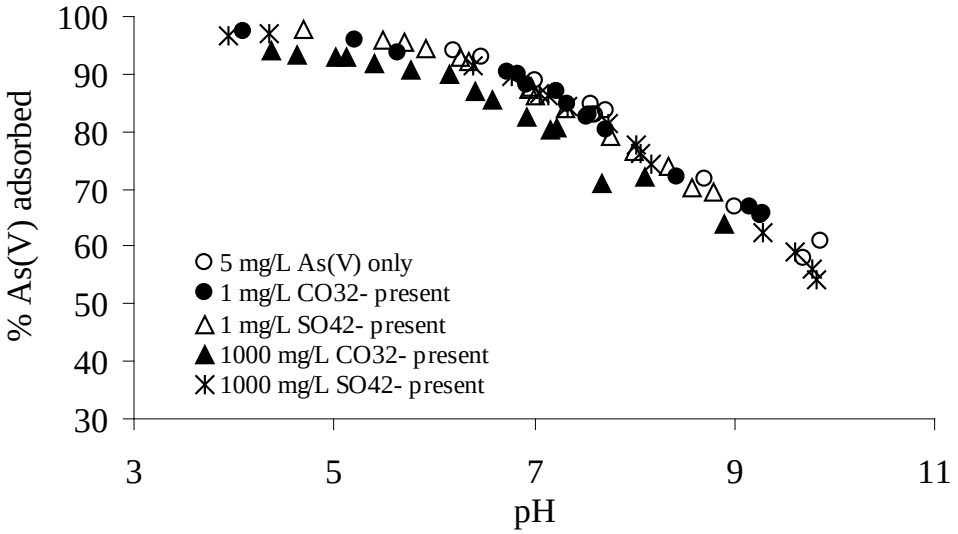

Figure 5.30: Effect of CO_3^{2-} or SO_4^{2-} on As(V) adsorption. Conditions: 0.1 g/L Kemiron (<38 μm), I = 0.001 N $NaNO_3$ and 0.1 N $NaNO_3$, CO_2 excluded from SO_4^{2-} experiments.

The presence of CO_3^{2-} (1 or 1000 mg/L) and SO_4^{2-} (1 or 1000 mg/L) had very little or no effect on the percentage of 5 mg/L As(V) sorbed (Figure 5.30). These ions are generally found closer to the higher concentration range in landfill leachate and the results from Figures 5.29 and 5.30 suggest that As(V) removal would be favored over As(III), however, Section 5.4 did show the rate of As(III) sorption to be faster than that of As(V) though the differences (from a practical standpoint) may not be significant.

The idea of introducing ions of opposite charge into systems in order to increase the mass of adsorption has been explored by many researchers and has shown to work many of the times. For instance, Schindler *et al.* (1990) showed that the presence of anions in solutions might enhance cation adsorption by forming mixed metal/ligand surface complexes whilst Davis and Bhatnagar (1995) showed that humic acids increased Cd adsorption onto the hematite surface.

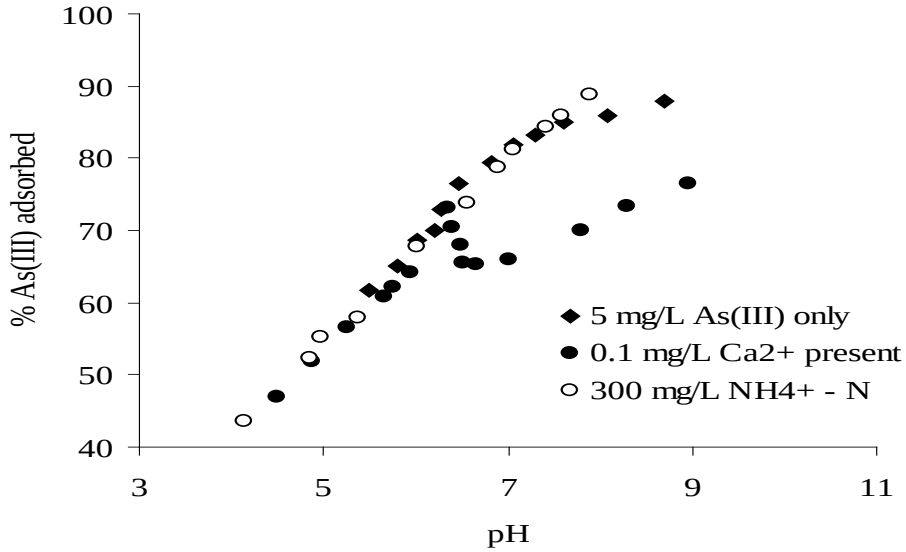

Figure 5.31: Effect of Ca^{2+} or NH_4^+ - N on As(III) adsorption. Conditions: 0.1 g/L Kemiron (<38 μm), I = 0.001 N $NaNO_3$ and 0.1 N $NaNO_3$, CO_2 excluded.

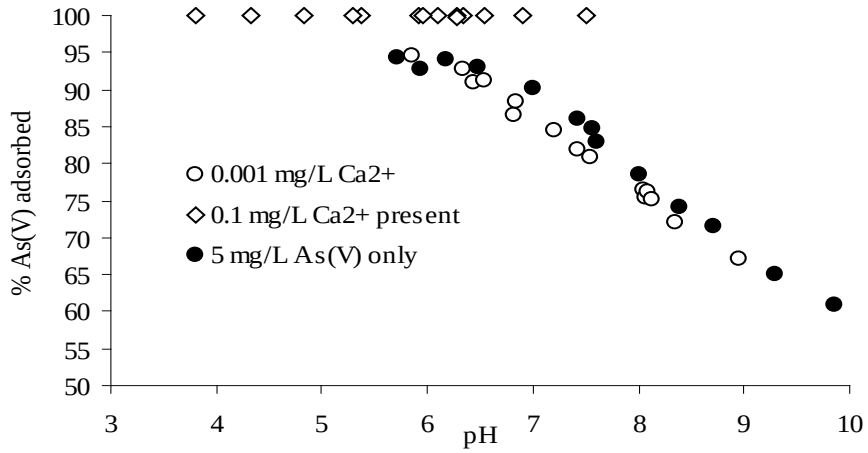

Figure 5.32: Effect of Ca^{2+} or NH_4^+ - N on As(V) adsorption. Conditions: 0.1 g/L Kemiron (<38 μm), I = 0.001 N $NaNO_3$ and 0.1 N $NaNO_3$, CO_2 excluded.

Typical landfill leachate contains Ca^{2+} and NH_4^+ in significant concentrations so the impact they have on sorption is important to understand in addition to their potential for enhancing sorption behavior. Figure 5.31 shows the effect of 0.1 mg/L Ca^{2+} and 300 mg/L NH_4^+-N on 5 mg/L As(III). The presence of 0.1 mg/L Ca^{2+} did not increase the amount of As(III) sorbed between pH 4 to 7. It actually caused about a 20% drop in the

amount of As(III) sorbed at pH 7 and above. The presence of 300 mg/L NH_4^+ did not impact the amount of As(III) sorbed from pH 4 to 8 significantly (Figure 5.31).

Figure 5.32 shows the effect of Ca^{2+} (0.001 mg/L and 0.1 mg/L) on 5 mg/L As sorption. These results indicated that while 0.001 mg/L of Ca^{2+} had no impact on the amount of As(V) sorbed between pH 5.5 and 9, the presence of 0.1 mg/L of Ca^{2+} increased the sorption of As(V) up to 100% between pH 4 to 7. This enhanced sorption could be due to the formation of a more favorable surface complex involving As(V) and Ca^{2+} species, or the favorable surface charge achieved by the presence of Ca^{2+} on the surface. Compared to the As(III) case, As(V) sorption is more favorable when Ca^{2+} is present and this could be a potential asset given high calcium levels in leachate.

5.8 Impact of Oxidation Reduction Potential (ORP) on As(V) Adsorption

The impact of ORP on As(V) removal was assessed in a binary system at two different ORP values, 295 mV and of -100 mV. Both tests were conducted at pH 7 for a total As(V) concentration of 5 mg/L. The results indicated that 90% of initial 5 mg/L As(V) was adsorbed at 295 mV, while only about 60% of the 5 mg/L As(V) was adsorbed at -100 mV.

The amount of As adsorbed (shown in Table 5.8) in the presence of Ca^{2+}, CO_3^{2-}, COD, NH_4^+ - N, Se(IV), Ni^{2+} or by the increase or decrease of ORP or pH was used to select the key factors for further testing in the landfill leachate system. A baseline of 12% increase or decrease in the As sorption when there was a change in value of a factor was used for the selection. Ca^{2+}, Ni^{2+}, Se(IV), ORP, and pH were the parameters that qualified for the further test in the synthetic landfill leachate systems.

Table 5.8: The impact of the various factors on the fractions of As adsorbed. Conditions: in binary system at pH 7, I = 0.001 N $NaNO_3$, at room temperature.

			% As Adsorbed			
Parameter	Low (-)	High (+)	As(V) (-)	As(V) (+)	As(III) (-)	As(III) (+)
pH	5	10	95	62	55	90
ORP	-150 mV	+295 mV	60	90	-	80
COD	5 mg/L	1000 mg/L	82	72	-	-
Se(IV)	0 mg/L	5 mg/L	90	70	82	50
Ni^{2+}	0 mg/L	5 mg/L	90	90	82	70
Ca^{2+}	0.001 mg/L	0.1 mg/L	88	100	80	68
CO_3^{2-}	1 mg/L	1000 mg/L	90	81	81	71
SO_4^{2-}	1 mg/L	1000 mg/L	90	90	81	75
NH_4^+ - N	-	300 mg/L	-	-	80	80

+ : data obtained under a high condition of the parameters.
- : data obtained under a low condition of the parameters.

5.9 Batch Equilibrium Sorption of Arsenic onto Kemiron in Landfill Leachate

Prior to the batch As adsorption experiment using synthetic landfill leachate, an initial batch test was done with natural landfill leachate from Polk County's North Central facility, Florida. The objective was to determine if Kemiron could remove As in the natural landfill leachate. Samples were collected from 3 locations within the leachate system and the concentrations of total arsenic are reported in Table 5.9. Geochemical parameters measured at the North Central Landfill leachate are also listed on Table 5.10 though these were not measured for the Phase 1 leachate used in Figure 5.34.

Table 5.9: As concentrations in landfill leachate sampled from the Polk County North Central landfill on 4/27/06.

Sample	As in filtrate through 0.45 μm Millipore filter (ppb)	As in acid digested filtrate (through 0.45 μm Millipore filter) (ppb)	As in unfiltered, digested leachate (ppb)
Phase 1	29 ± 2	92 ± 14	90 ± 7
Phase 2	76 ± 4	61 ± 3	64 ± 3
Leachate Tank	98 ± 5	126 ± 6	114 ± 6

Table 5.10: Concentrations of some of the contaminants in the leachate. Source: Polk County North Central leachate tank (Data obtained from Polk County Environmental Services Department, Solid Waste Division). 1 μM = 74.9 μg/L As.

Date	As (μM)	Ni (μM)	Cr (μM)	Bicarbonate (mg/L as $CaCO_3$)	pH	DO (mg/L)
3/14/02	1.60	1.44	0.14	1318	6.92	2.83
3/06/03	0.53	1.23	< 0.02	1873	7.21	6.21
3/26/04	0.95	2.52	0.38	2913	7.51	4.82

The sorption experiment was carried out using the filtered Phase 1 leachate solution without taking any precautions to eliminate biological effects. This solution had an undigested total As concentration of 0.029 mg/L and an acid digested total concentration of 0.092 mg/L. When used to make the 0.1 g/L Kemiron slurry to which 1 mg/L As(V) was added, the result is shown in Figure 5.34. For the given equilibration period between 40 and 50% of the As(V) was sorbed to the Kemiron in the presence of the Polk County Landfill leachate. The shape of the sorption edge was similar to that seen for As(V) in earlier parts of this chapter. Although the percentage sorbed and overall surface coverage was reduced in this leachate solution, the result suggested that the potential is there provided the right conditions or pretreatment steps are undertaken. In the next section,

research using synthetic leachate solutions is presented. These solutions capture some of the major constituents of leachate systems.

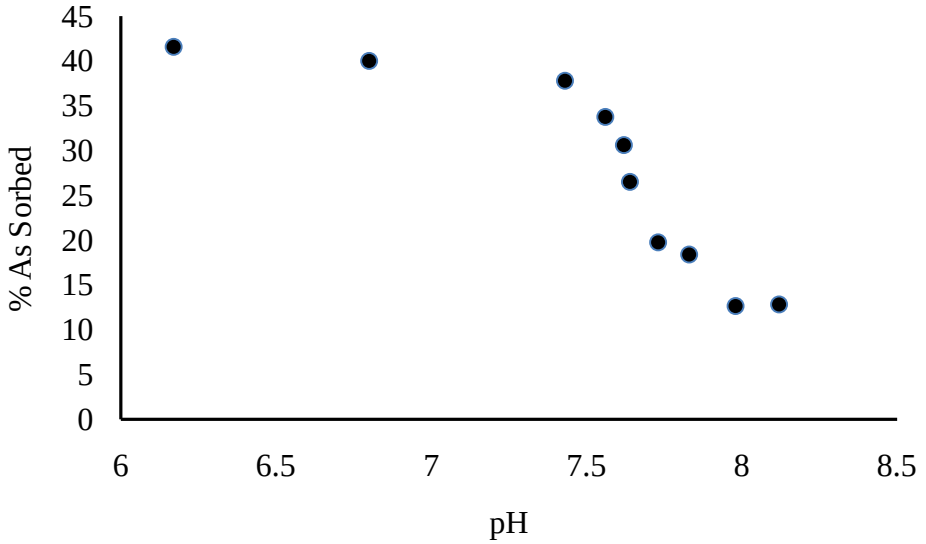

5.33: Adsorption edge of 1 mg/L As(V) on 0.1 g/L Kemiron in a Polk County landfill leachate solution. Conditions: Kemiron adsorbent grain size of ≤ 38 μm at room temperature.

5.9.1 Effects of Landfill Age and pH on Adsorption

To test for the impact of age of the synthetic leachate on As(V) adsorption, 5 mg/L As(V) was subjected to the same conditions in both an acidogenic and a methanogenic landfill leachate solution. The procedure here followed the same steps as the equilibration tests and the results are shown in Figures 5.34 and 5.35. Age had no impact on the As(V) removal. However, there was a slight increase in the percentage adsorption of As(III) in the older landfill leachate (acidogenic) compared to the amount sorbed in the methanogenic leachate as shown in Figure 5.35. pH on the other hand continued to have significant influence on As adsorbed in the synthetic landfill leachate solutions as the As(V) and As(III) sorption followed the same trends as were seen in

Figures 5.18 and 5.19. Compared to the clean systems with just DI water, both As(III) and As(V) sorption decreased in the presence of leachate by roughly 20% across all pH values.

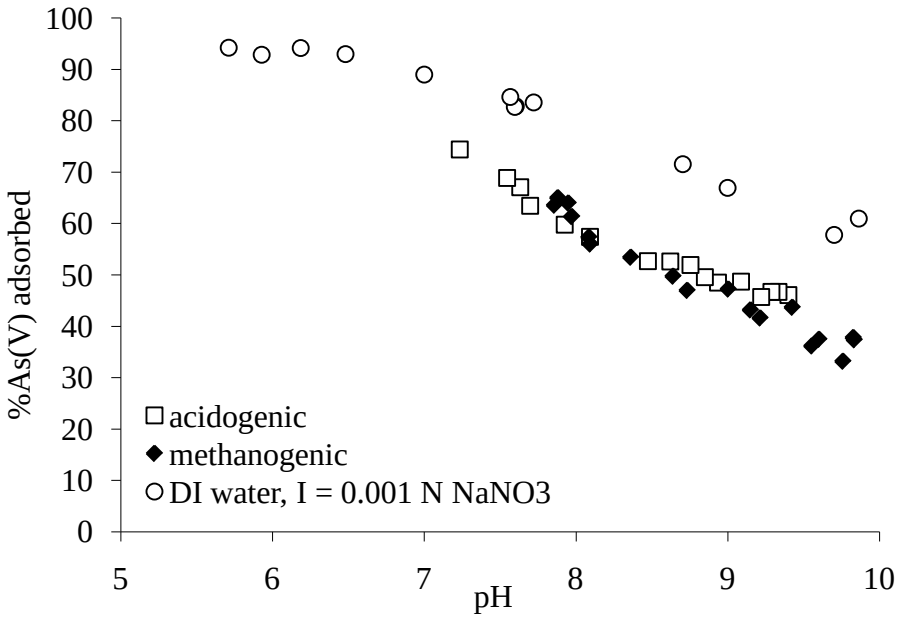

Figure 5.34: Effect of pH or age (acidogenic or methanogenic) of landfill leachate on 5 mg/L As(V) adsorption. Conditions: 0.1 g/L Kemiron adsorbent, grain size of ≤ 38 μm at room temperature.

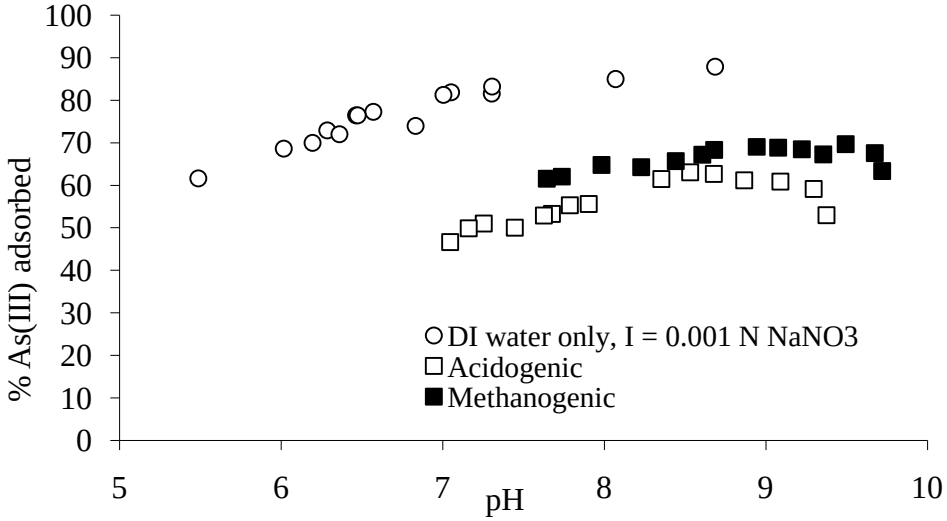

Figure 5.35: Effect of pH or age of landfill leachate on 5 mg/L As(III) adsorption. Conditions: 0.1 g/L Kemiron adsorbent, grain size of ≤ 38 μm at room temperature.

5.9.2 Effect of Se(IV) Present in the Landfill Leachate

To test for the impact of age of the leachate on As(V) adsorption, 5 mg/L As(V) was subjected to the same conditions in both acidogenic and the methanogenic landfill leachate in the presence of the two contaminants. The procedure here followed the same steps as the equilibration tests. Observation made is shown in Figure 5.37. Here, no apparent differences existed in the percentages of As(V) adsorbed in both leachate systems. However, there was about 20% drop in As(V) removal when compared with the As(V) sorbed in the pure system. The trend of As(V) removal in the landfill leachate also conformed to that of the ternary system with 5 mg/L of Se(IV) present. This thus suggests that Se(IV) as the co-contaminant may be the main controlling factor in the As(V) removal in the landfill leachate (see Figure 5.34).

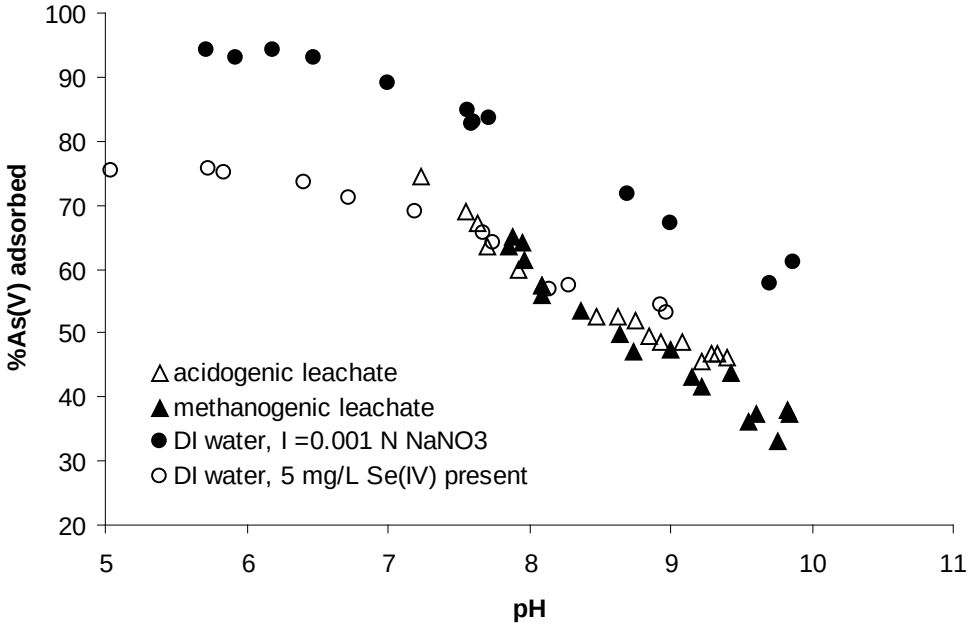

Figure 5.36: Effect of Se(IV) in As(V) removal in the synthetic landfill leachate. Condition: 0.1 g/L Kemiron, ≤ 38μm particle size, at room temperature.

5.9.3 Effect of Ca^{2+} on Arsenic Removal in Landfill Leachate

The impact of Ca^{2+} in the leachate was also evaluated and Figure 5.37 shows that Ca^{2+} had no impact on As(V) in the old landfill leachate after the Ca^{2+} concentration was increased by 1200 mg/L.

5.9.4 Effect of ORP (E_h) on Arsenic Adsorption in Synthetic Landfill Leachate

Figure 5.38 shows a scatter plot of ORP versus percentage As(V) sorbed onto 0.1 g/L Kemiron (≤ 38μm particle size) in the presence of acidogenic synthetic leachate. Experiments were conducted in such a way that pH and ORP were varied by the addition of nitric acid or sodium sulfide respectively. There was no significant trend or

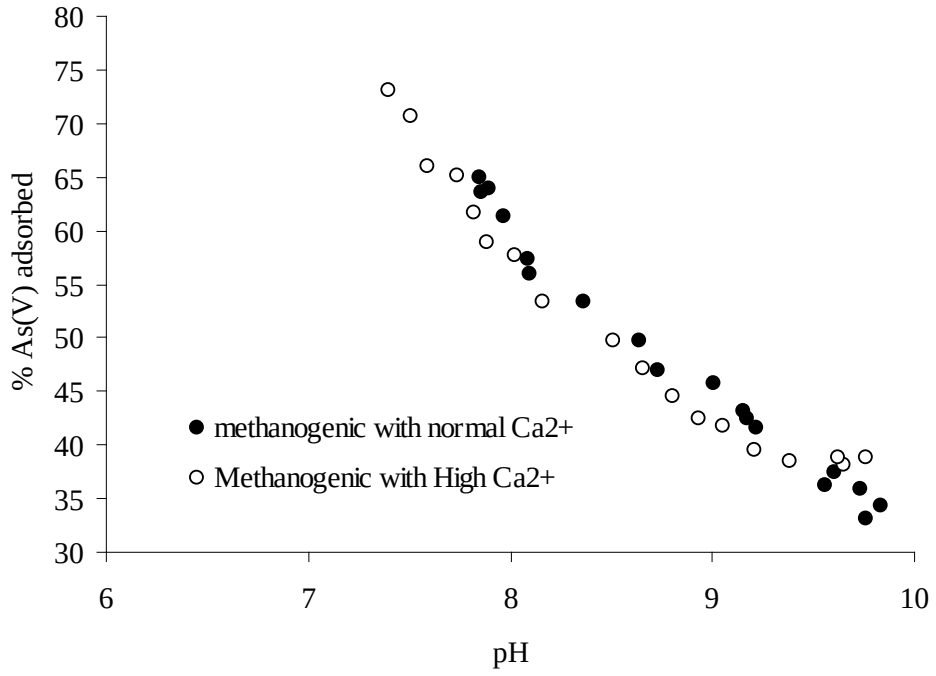

Figure 5.37: Effect of Ca^{2+} on 5 mg/L As(V) adsorption in synthetic landfill leachate. Condition: 0.1 g/L Kemiron, ≤ 38μm particle size, at room temperature.

correlation between the ORP of the batch system and the percentage of As(V) sorbed in the acidogenic leachate. Figure 5.39 plots the percentage As(V) removed as a function of pH and distinguishes data points where ORP was greater than 0 mV and less than 0 mV, crudely representing oxidizing and reducing environments respectively (Christensen *et al.*, 2001).

The plot in Figure 5.40 suggests that arsenic sorption decreased up until pH values around 10 and then sharply rose again in the pH 11 range. The steep slope of the sorption curve above pH 10 suggests that there may be other mechanisms like precipitation dominating As(V) removal. The amount of As(V) removed in this pH range was also not affected by whether the ORP values were greater than, or less than 0. This again suggests that another removal mechanism might be important.

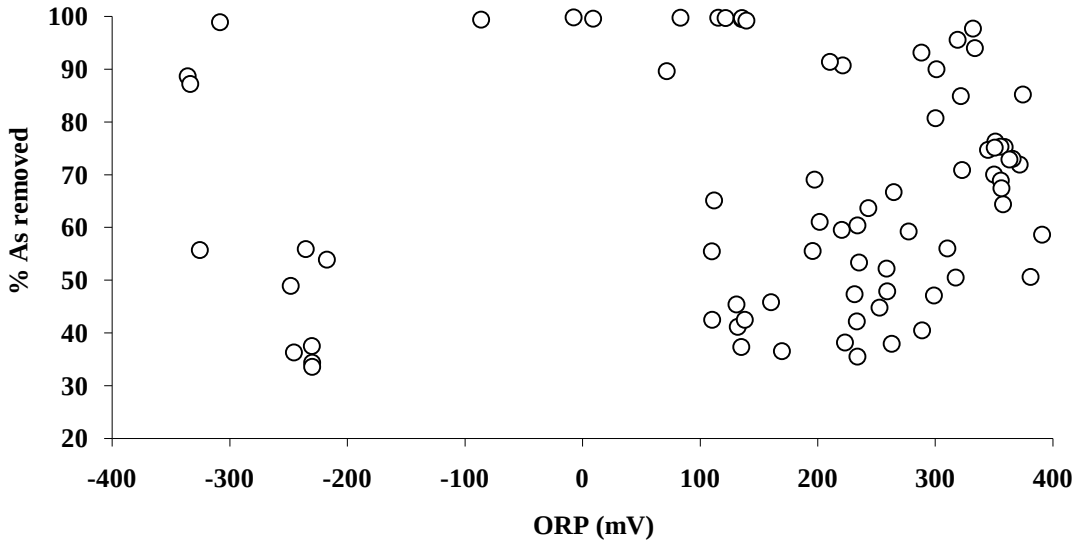

Figure 5.38: The impact of ORP on As removal in synthetic landfill leachate. Condition: 0.1 g/L Kemiron, ≤ 38μm particle size, room temperature, 5 mg/L As(V) initially, pH not controlled, acidogenic leachate conditions..

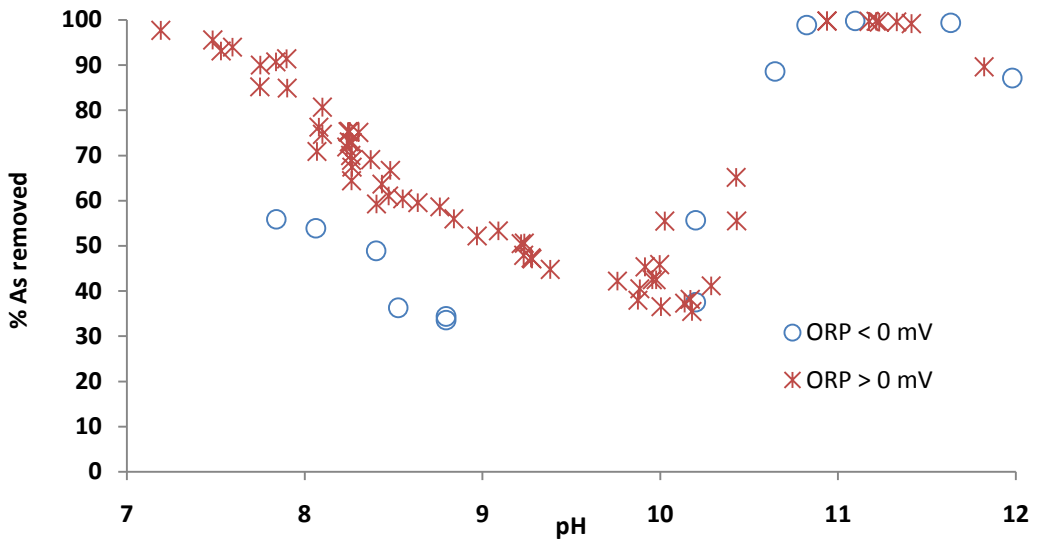

Figure 5.39: Impact of pH and ORP on As removal in synthetic landfill leachate. Condition: 0.1 g/L Kemiron, ≤ 38µm particle size, at room temperature, 5 mg/L As(V) initially, acidogenic leachate conditions.

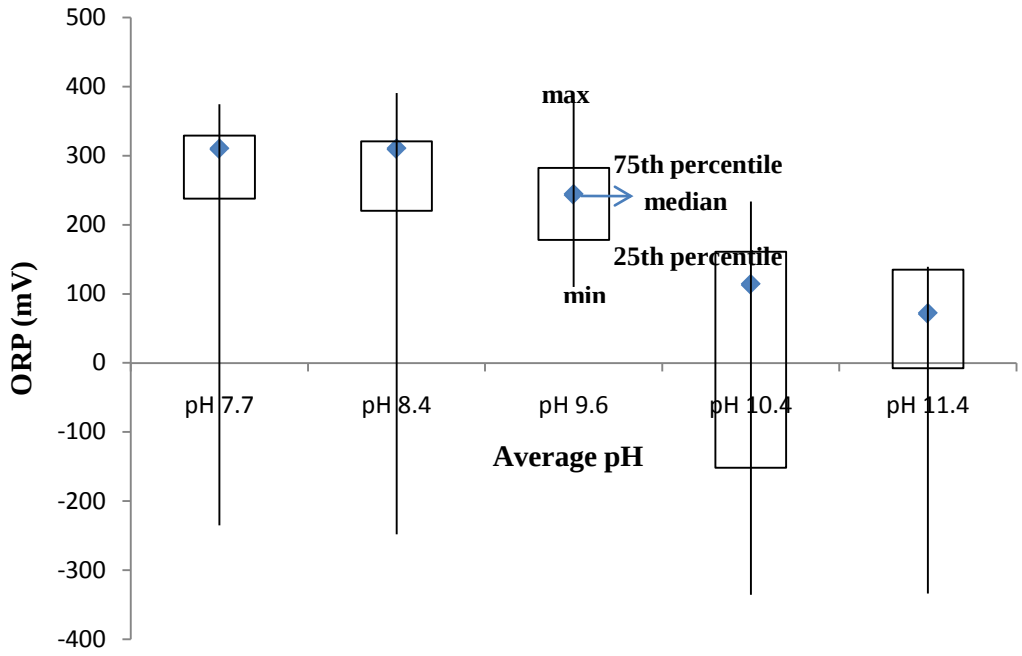

Figure 5.40: Box plot of ORP (mV) as a function of pH. Plot shows values that fall within the 25th and 75th percentile (box), the minimum and maximum loading (line) and the median (diamond). The pH plotted represents the average for the given pH range evaluated from 7-8, 8-9, 9-10, and 10-11. Condition: 0.1 g/L Kemiron, ≤ 38µm particle size, at room temperature, 5 mg/L As(V) initially.

These high pH ranges were not studied in the simpler batch systems as Kemiron dissolution would be an issue and the likelihood of such high pH values in leachate solutions may not be that common. The experiments were conducted in such a way that addition of chemicals to change ORP were not done under controlled pH conditions. Instead, the systems were allowed to equilibrate and the final pH recorded after 72 hours along with the amount of arsenic removed. Below pH 10, the amount of arsenic removed increases as pH decreases, with higher percentage removals seen in samples that had ORP values greater than 0 mV. Figures 5.35 and 5.36 show reductions in As(V) and As(III) sorption in the presence of the acidogenic leachate to levels that are much lower than those observed in Figure 5.40, especially for the points with ORP values > 0 mV. Abiotic redox transformations of the As(V)/As(III) and/or Fe(III)/Fe(II) species could be occurring during these experiments. Dissolution of Kemiron and precipitation of an amorphous iron oxide phase could be one mechanism to enhance total arsenic removal. Figure 5.41 presents a box plot of ORP (mV) as a function of pH for the same set of data shown in Figures 5.39 and 5.40. In general, the majority of ORP values tend to decrease as pH increases.

Geochemical modeling is used in Section 5.11 to discuss the aqueous equilibrium speciation expected for arsenic as a function of pH and ORP.

5.10 Effect of Hydrogen Sulfide on Arsenic Adsorption

Figures 5.42 – 5.44 were derived using Geochemist Workbench software and they show arsenic speciation as a function of E_h (in volts) and sulfide concentration or pH. E_h and ORP are the same and the graphs below use the default plots from Geochemist workbench. Figures 5.42 sand 5.43 show arsenic speciation as a function of sulfide

concentrations for pHs of 5 and 10 respectively when temperature was set at 25^{o}C and atmospheric pressure was set at 1.013 bar. Experiments were conducted under total sulfide concentrations of 1 x 10^{-5} and 1 x 10^{-3} M which would translate into lower values when plotted as HS^- concentrations. Given the ORP and pH values measured in experiments, $H_2AsO_4^-$, $HAsO_4^{2-}$, $As(OH)_3$, $As(OH)_4^-$, and AsS_2^- could exist based on Figures 5.42 and 5.43 with less likelihood of the sulfide complex because of the total sulfide concentration added. According to the results generated with Geochemist Workbench software, no precipitates formed when sulfide was included (from sodium sulfide salt) along with the composition of the synthetic leachate solution, 5 mg/L total As, and assuming a total dissolved Fe concentration ~ 10^{-3} M (a very conservative estimate based on EDS elemental composition and the fact that experiments were run with 0.1 g/L Kemiron). The data generated with the Geochemical workbench can be in appendix C.

Benjamin (2002) assumed that adsorption and precipitation of the same target contaminant occur in parallel and the total contaminant removed would be the sum of the amount removed by each process. In the absence of precipitation as is predicted by the simulations, it could be inferred that the total As removed in the synthetic leachate solution was purely due to adsorption onto the Kemiron particles.

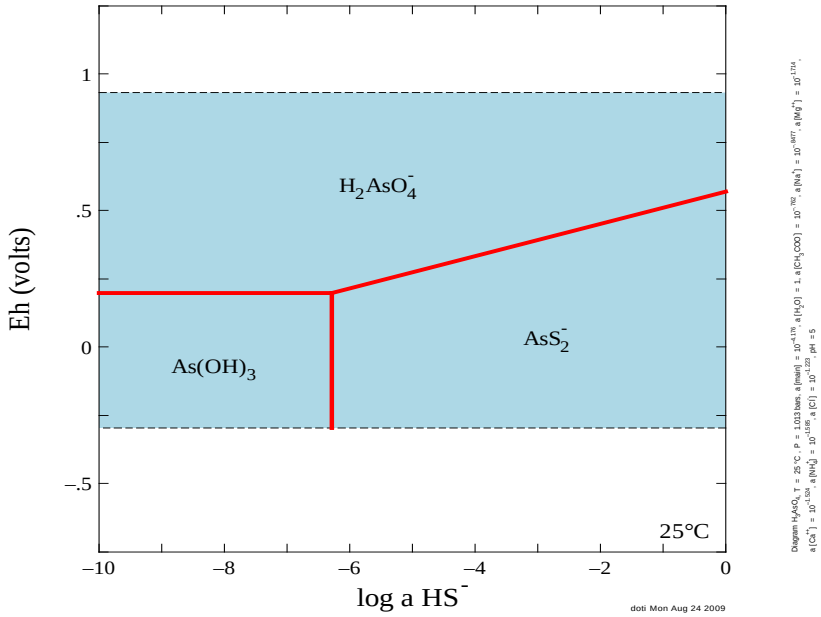

Figure 5.41: E_h –log {HS^-} diagram of inorganic arsenic at pH 5. Conditions: at 25°C, at a pressure of 1.013 bar.

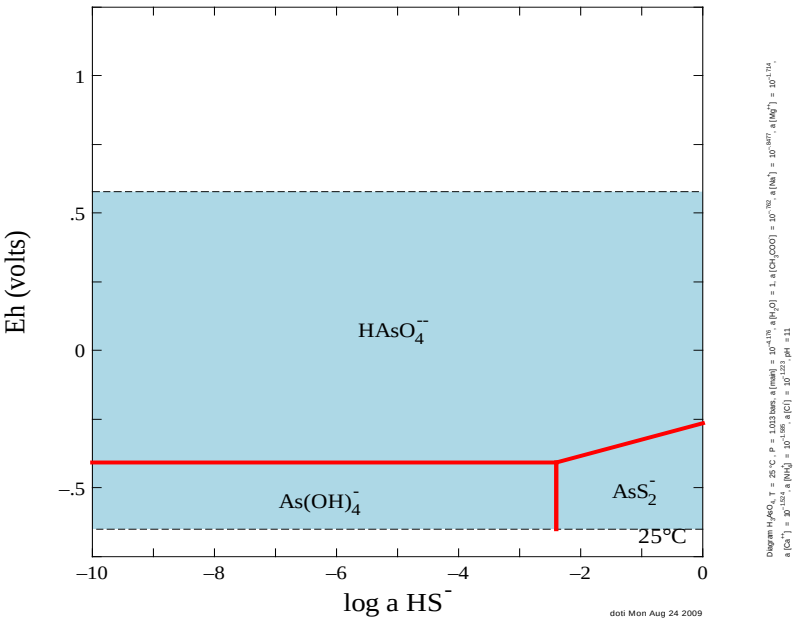

Figure 5.42: E_h – log {HS^-} diagram of inorganic arsenic at pH 10. Conditions: at 25°C, and at a pressure of 1.013 bar.

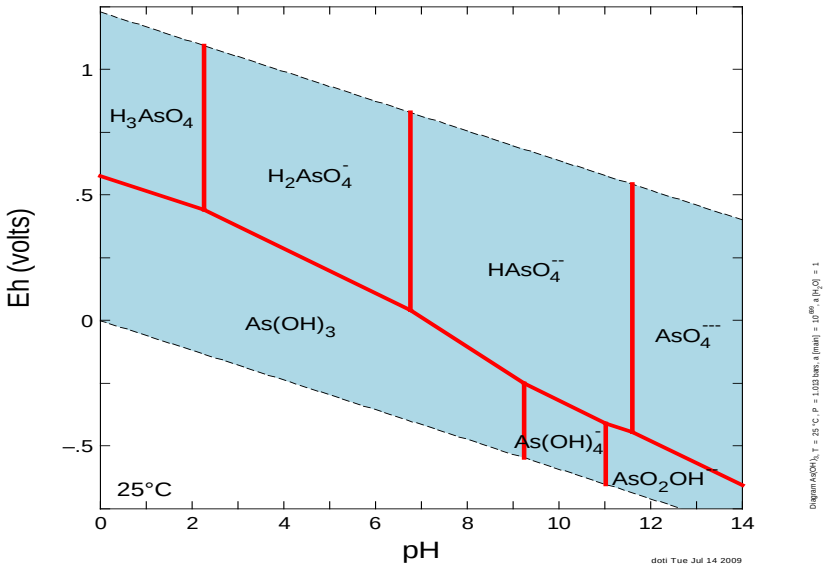

Figure 5.43: E_h – pH diagram of inorganic arsenic. $P_{O_2\ (g)}$ = 0.21 bar, at 25°C, and P_{H_2} (g) = 1 bar.

5.11 Kinetics of Arsenic in Landfill Leachate

A batch kinetic study was done for As(V) onto 38 µm in the acidogenic synthetic landfill leachate. The objective was to model and estimate diffusion coefficient of As(V) in the landfill leachate. Another objective was to compare the coefficients of As(V) in the binary system with that in the landfill leachate to evaluate the impact of the medium on the arsenic removal.

5.11.1 As(V) Diffusion Coefficient Estimation in Landfill Leachate

The rate of diffusion of As(V) into Kemiron was evaluated and modeled based on the assumption that As(V) migration was intraparticle diffusion controlled. We adopted Crank's (1975) fractional uptake solution to Fick's second law of diffusion to model.

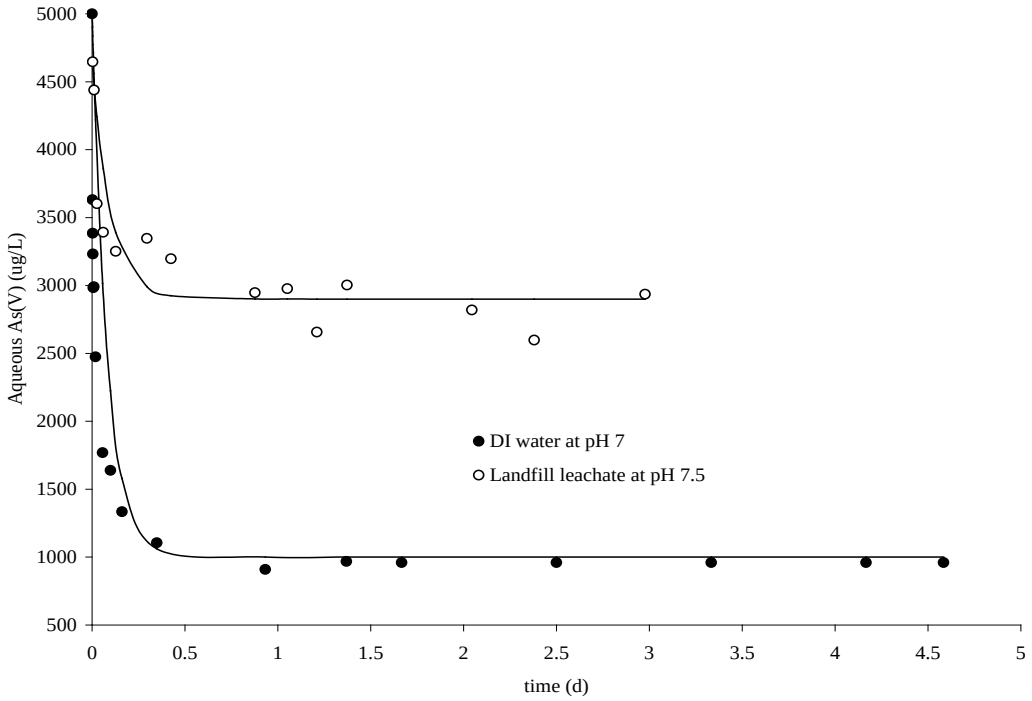

Figure 5.44: Rate of 5 mg/L As(V) removal onto ≤ 38 μm particle size. Conditions: in a synthetic acidogenic landfill leachate at pH 7.5, ORP of 240 mV, and at room temp.

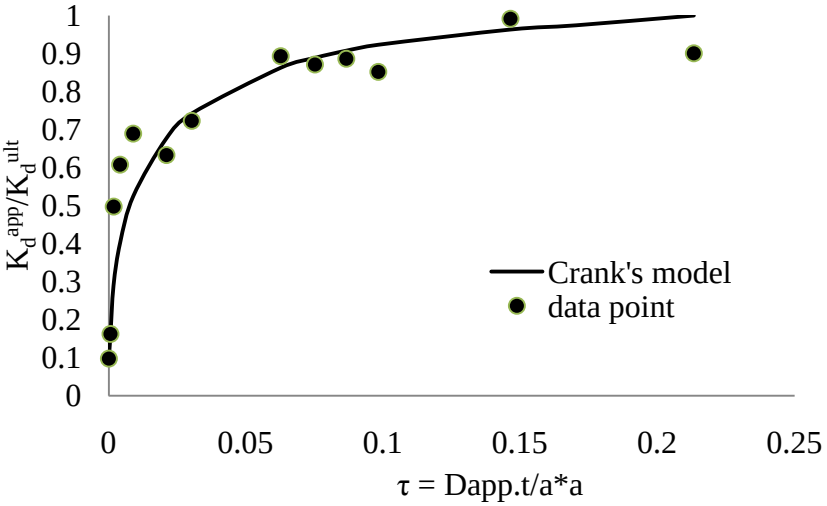

Figure 5.45: Fractional removal model of As onto Kemiron in the synthetic leachate.

Figure 5.45 shows two different removal rates for As; the initial faster rate which is followed by a slower rate. Most of the removal occurred within the first 12 hours of

reaction. The apparent diffusion coefficient (D_{app}/a^2) of the As was estimated to be 8.3 x 10^{-7} s^{-1} compared (fit shown in Figure 5.46) with 3.2 x $10^{-7}s^{-1}$ of As(V) or 2.5 x $10^{-7}s^{-1}$ of As(III) in the binary system. Hence, in the presence of the leachate D_{app} is similar to that for the DI water, but there was a significant drop in the sorption capacity.

5.12 Maximum As Removal onto ≤38 μm Particle Size in Landfill Leachate

Previous sections showed that Se(IV) reduced As sorption to Kemiron in both clean systems and under synthetic landfill conditions. Experiments were therefore conducted to further evaluate the effect of Se(IV) on As removal as a function of pH and ORP for a total As concentration of 5 mg/L (added as As(V) and in the presence of the acidogenic synthetic leachate. The results of the experimental runs are plotted in Figure 5.47. Areas indicated as having 0% arsenic sorbed should be viewed as areas where no data exists. Maximum arsenic removal (≥90%) occurred at pH 8 (ORPs of 200, 0 and 350 mV), and between pH 11and 12 (ORPs of -300 and 0 mV).

Loadings of As onto the Kemiron particles (≤ 38 μm) under the optimum ORP and pH values and in the presence of Se(IV) are tabulated in Table 5.11. The loadings measured are comparable to loadings seen for arsenic on other adsorbent surfaces in less complex systems like surface water or DI water (Table 5.12). It should be noted that particle size varies in the results presented in Table 5.12 and our work using a "fine fraction" which has been shown to reach equilibrium faster than larger porous particles. Our loadings in the presence of synthetic leachate solutions are comparable to loadings seen in the literature. The Kemiron sorbent costs between $2 to $4 per pound which falls within the range seen for commercially available sorbents ($0.50 to $50 per pound).

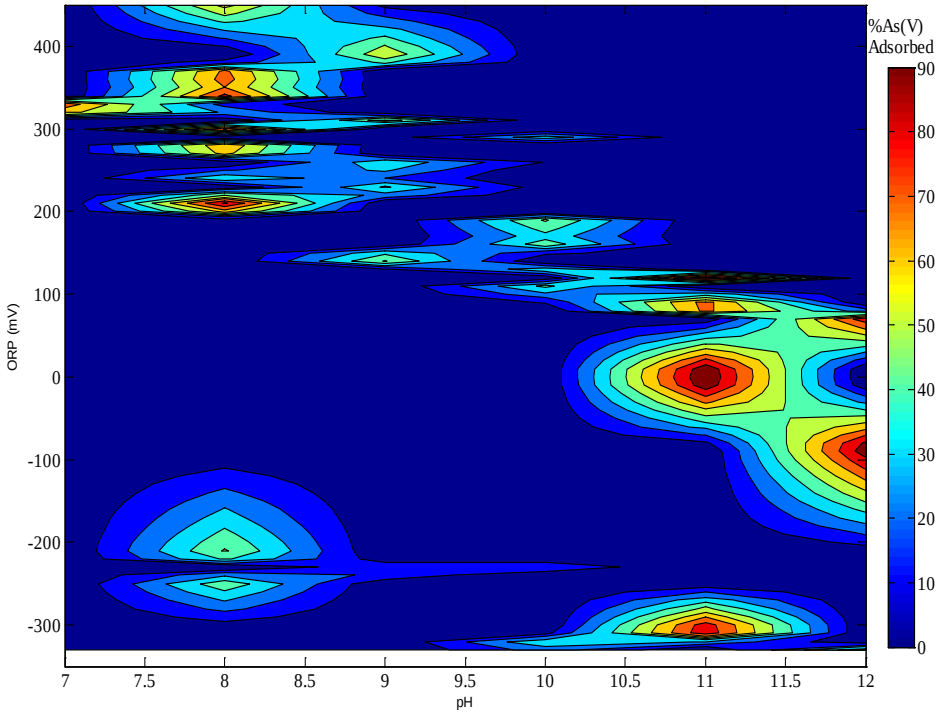

Figure 5.46: Contours of %As sorbed in young synthetic landfill leachate. Conditions: at various ORP and pH values and at room temperature.

Table 5.11: Maximum adsorption densities of As. Conditions: under optimum pH and ORP conditions at room temperature, Kemiron particle size ≤ 38 μm, 0.1 g/L Kemiron, 5 mg/L As(V).

Arsenic loadings (mg As/g Kemiron)	Conditions	
	ORP (mV)	pH
47.5	320	7
23.8	350	7.5
47.5	200	8
47.5	350	8
29.0	400	9.0
47.5	0	11
47.5	-300	11
47.5	-100	12

Table 5.12: As loadings at equilibrium/ breakthrough. Condition: DI/surface water as seen on other adsorbents under various pH and at room temperature.

Adsorbent	As species	Initial conc (mg/L)	Loading (mg/g)	pH	Test type	reference
GFH	As(V)	0.1 - 0.11	0.99 – 1.5	8.6	Column	Badruzzaman *et al.* (2004)
Zeolite (H24)	As(V)	10 - 150	35.8	6.5	Batch	Chutia *et al.* (2009)
Zeolite (H90)	As(V)	10 – 150	34.8	3.2	Batch	Chutia *et al.* (2009)
U. cylindricum	As(III)	10 - 400	67.2	6.0	Batch	Tuzen *et al.* (2009)
Iron coated zeolite	As(V)	2.0	0.68 – 0.53	4.0	Batch	Jeon *et al.* (2009)
Kemiron	As	5.0	47.5 in leachate		Batch	This work

Though they offer rapid equilibration times, the less than 38 µm particles are not very practical in full scale treatment since their separation from cleaned solutions would pose a challenge. From the standpoint of further developing this research as a viable treatment technology for landfill leachate, experiments with larger particle sizes will have to be considered since these can be packed into fixed bed reactors thereby eliminating challenges related to separation of the sorbent from the treated solutions. The rate of uptake experiments presented in this work, coupled with the modeling of this data, show that the time to reach equilibrium in these larger particles will be longer. This has implications for the envisioned treatment process, however, it is likely that optimized particle sizes and configurations can assist with reducing mass transfer resistances within the pore structures. Landfill leachate is a very complex water to be treated for arsenic and this work is the first study that we have seen looking at the use of sorption

technology for such applications. Whilst we found that As(V) could be removed by Kemiron in the presence of filtered leachate from a real landfill, the majority of our experiments were done in relatively clean systems designed to capture some of the key characteristics of leachate solutions. In thinking of building on the work done here, researchers should think of combined systems that would be most appropriate for treating leachate which may reduce the presence of ions that can potentially compete with arsenic for sorption sites.

Chapter 6

Summary, Conclusion, and Recommendation for Future Research

6.1 Introduction

This chapter summarizes all of the experimental results obtained according to their chapters. These experimental results provide the first step in a project aimed at removing arsenic from landfill leachate by adsorption onto mineral oxides either packed into fixed bed column reactors or mixed into leachate at the landfill site.

6.2 Summary

The nitrogen BET surface area of the Kemiron (particle sizes ≤ 38 μm and 500 – 600 μm) was ~40 m^2/g with ~ 44% of the pore sizes in the 500 – 600 μm fraction less than 3 nm. EDS analysis showed that Kemiron was made up of 40 % Fe, 42% O, 8% carbon and 6 % S. XRD analysis indicated that Kemiron was an agglomeration of microparticles and was classified as amorphous though there was some similarity to goethite.

The kinetic studies of As(III) and As(V) onto ≤ 38 μm and 500 – 600 μm grain sizes exhibited an inverse relation between the grain sizes and the rate of sorption at pH 7. For the ≤ 38 μm grain size both As(III) and As(V) sorption reached equilibrium in ~ 36 hours whereas ~ 374 days was required for the larger grain sizes. For the larger grain sizes As(III) reached equilibrium faster likely because of its major uncharged species

(H_3AsO_3). These penetrated pore spaces easier than the negatively charged As(V) species. Given that 44% of surface area was in pore sizes less than 3 nm, the reduction in particle size by a factor of ~15 from an average of 550 μm had a major impact on the time to equilibrium. For a standard fixed bed treatment system, column diameters to particle diameters must be greater than 10 and more research should be done on either determining the optimum particle size for packing into columns (faster approach to equilibrium whilst still preventing column clogging) or alternative ways for removing fines if mixed with leachate in a stirred reactor. Alternatively, redesign of sorbent particles should consider access to particle surface area.

Crank's model solution to Fick's law of diffusion was used to estimate diffusion coefficients for As adsorption. D_{app}/a^2 for As(V) and As(III) were similar for each grain size though As(III) values were always slightly larger than As(V) values. The larger particles had smaller D_{app}/a^2 which is expected given the inclusion of the particle radius, a. D_{app}/a^2 for As(III) and As(V) on the ≤ 38 μm particles was 25 and 32 x 10^{-8} s^{-1} respectively and on the 500-600 μm it was 0.07 and 0.02 10^{-8} s^{-1} respectively. If average particle radius values were assumed for each grain size (e.g. 19 μm and 550 μm) the 4 order of magnitude difference between D_{app} would not be accounted for. Given that the $\leq$ 38 μm particles may contain more smaller sized particles this could reduce the differences seen for D_{app}. Tortuosity or constrictivity factors could also be used to account for a larger radius needed for the larger particle sizes.

The results of the rate of adsorption involving the various concentrations of As(V) onto the 500 – 600 μm grain size indicated that the adsorption capacity was dependent on the initial As(V) concentrations. The pseudo equilibrium graphs of As(V) sorption onto

the 500 – 600 μm showed a shift of the equilibration times to the right as the initial As(V) increased. That indicated that the equilibration times got higher as the initial concentration increased.

As(III) and As(V) sorption to Kemiron was pH dependent with As(V) sorption increasing as pH decreased and As(III) sorption having a maximum around pH 8. Ionic strength (0.1 N and 0.001 N $NaNO_3$) had no impact on the removal of either As species, suggesting an innersphere type complexation removal mechanism.

Table 5.7 summarizes the Freundlich and Langmuir isotherm fits for As(V) and As(III) onto the ≤ 38 μm particles. The Langmuir model ($r^2 = 0.99$) fit As(V) adsorption onto Kemiron better than the Freundlich model ($r^2 < 0.92$) with maximum adsorption densities ranging between 68 mg As(V)/g solid at pH 9 and 88 mg As(V)/g solid at pH 7, where r^2 is the correlation between the experimental and predicted values. The Freundlich model ($r^2 > 0.95$) on the other hand fit As(III) adsorption better than the Langmuir model ($r^2 < 0.95$) with the coefficient K_f increasing between pH values of 6 and 9 and adsorption densities as high as ~100 mg As(III)/g sorbent under given experimental conditions.

Both Ni(II) and Se(IV) resulted in reduced As(III) sorption across all pH values with Se(IV) having a greater effect and with a lower percentage reduction due to the presence of either ion as the pH increased. In the presence of 5 mg/L Se(IV), As(V) adsorption dropped by 20% between pH 4.5 and 9 which was less than that observed for As(III) (40% between pH 5 and 7 and by 20% between pH 7 and 9). Ni(II) did not reduce As(V) sorption across the pH range studied unlike what was observed for As(III). The presence of either 1000 mg/L CO_3^{2-}, 1000 mg/L SO_4^{2-}, or 300 mg/L NH_4^+ - N had

no major impact on As(V) (carbonate caused a reduction of less than 10% across the pH range). With the exception of NH_4^+ - N, they all reduced sorption of As(III) across the pH range by up to 20% in some cases. Ca^{2+} increased As(V) sorption and reduced As(III) sorption. Whilst ions like carbonate and sulfate will be in high concentrations in leachate solutions, co-contaminants like Se(IV) and Ni(II) will compete with As, especially As(III) for sorption sites.

There was no difference between acidogenic and methanogenic leachate systems on either As(V) or As(III) sorption and both caused about a 30% reduction in sorption at pH 8 with that number decreasing to ~ 10% at pH 7 for As(V). The effect of calcium on increased As(V) sorption was not observed in the presence of leachate. In the synthetic landfill leachate pH and ORP were identified as the most influential factors for As(V) removal. Subsequently maximum As(V) removal was achieved at optimum values of pHs 8 and 7.5 and between pH 11and 12 under ORPs of between 200 and 400 mV and between ORPs of -300 and 100 mV respectively. Leachate systems usually lie between pH values of 5 and 8 with positive ORP values, suggesting that the potential for this to work is great for older leachates and for younger leachates pH manipulation may have to be considered to increase removal efficiency. High removal amounts were seen in the high pH range, and the use of CO_2 to treat such a high pH solution afterwards could be considered. Similarly, oxidation of As(III) to As(V) would also reduce the effect of co-contaminants on overall arsenic removal.

6.3 Conclusion

This research showed that Kemiron could be used to remove As(V) and As(III) from solutions with loadings seen as high as ~90 mg As/g Kemiron in relatively clean systems and could also remove arsenic from complex matrices like landfill leachate. Compared to As(V), As(III) sorption was more sensitive to the presence of co-contaminants (Ni(II) and Se(IV)) and high concentrations of ions like CO_3^{2-}, SO_4^{2-} and NH_4^+ - N showed reduced sorption whereas As(V) sorption was only reduced in the presence of Se(IV). Synthetic acidogenic and methanogenic leachate solutions reduced sorption of both As(V) and As(III), with a greater impact seen on As(III) above pH 7, but with little difference seen between the two types of leachate on either ion. Using the acidogenic conditions which had higher concentrations of major ions, As(V) sorption could be manipulated by changes in ORP and pH with the most appropriate pH values seen between 5 and 8. Assuming a loading of 45 mg As/g sorbent (this would be 50% of that seen in the clean system which is a conservative estimate given our results thus far) then the amount of Kemiron needed per year would be 66 kg which, at $4/lb ($9/kg), would cost $600 if treating a 0.1 mg/L As leachate solution (assuming a volume of 7,986,529 gallon/yr as was the case of a Florida landfill). Compared to offsite disposal costs of $110/gallon the potential cost savings for an onsite sorption process could be huge provided the equipment and maintenance costs are not great.

6.4 Recommendations for Future Research

Future research work could be categorized into two sections: experimental lab and pilot studies, and modeling.

More experiments are needed to test the application in column systems and in the presence of other co-contaminants. Attempts to optimize particle size and particle morphology are also possible bearing in mind the eventual cost of the material. Tests on real landfill leachate should also be conducted, but done in conjunction with other researchers trying to remove other contaminants (e.g. organics) or materials (e.g filtration or flocculation pretreatment step). Microbial activity was not considered in this research and their effect on the process should be determined. These tests can be scaled up for pilot testing.

More mechanistic sorption models would capture surface complexation that responds to pH changes. A linear adsorption model was assumed for finding apparent diffusivities yet experiments show that this model would not apply to As(III) and As(V) sorption. Hence, future work could couple a mass transfer model with a more mechanistic adsorption model.

References

Abdallah, E. A. M. and G. A. Gagnon (2009) Arsenic removal from groundwater through iron oxyhydroxide coated waste products. *Can. J. Civ. Eng.*, 36(5), 881-888.

Agrawal, A. and K. K. Sahu (2006) Kinetic and isotherm studies of cadmium adsorption on manganese nodule residue. *Journal of Hazardous Materials*, 137(2), 915-924.

Alcantar, N. and T. Pichler (2007) Personal communication.

Al Yaqout, A. F. and M. F. Hamoda (2005) Prediction of contaminants migration at unlined landfill sites in an arid climate - A case study. *Water Air Soil Pollut.*, 162(1-4), 247-264.

Alvarez-Vazquez, H., B. Jefferson and S. J. Judd (2004) Membrane bioreactors vs conventional biological treatment of landfill leachate: a brief review. *J. Chem. Technol. Biotechnol.*, 79(10), 1043-1049.

Andrew, A. S., J. L. Burgess, M. M. Meza, E. Demidenko, M. G. Waugh, J. W. Hamilton and M. R. Karagas (2006) Arsenic exposure is associated with decreased DNA repair in vitro and in individuals exposed to drinking water arsenic. *Environ. Health Perspect.*, 114(8), 1193-1198.

Appelo, C. A. J., M. J. J.Van der Weiden, C. Tournassat, and L. Charlet (2002) Surface complexation of ferrous iron and carbonate on ferrihydrite and the mobilization of arsenic. *Environmental Science and Technology*, 36(14), 3096-3103

Ashrafizadeh, S. N., Z. Khorasani and M. Gorjiara (2008) Ammonia removal from aqueous solutions by Iranian natural zeolite. *Sep. Sci. Technol.*, 43(4), 960-978.

Badruzzaman, M., P. Westerhoff and D. R. U. Knappe (2004) Intraparticle diffusion and adsorption of arsenate onto granular ferric hydroxide (GFH). *Water Research*, 38(18), 4002-4012.

Bajpai, S. and M. Chaudhuri (1999) Removal of arsenic from ground water by manganese dioxide-coated sand. *Journal of Environmental Engineering-ASCE*, 125(8), 782-784.

Balistrieri, L.S. and T.T. Chao (1987) Selenium adsorption by goethite. *Soil Sci. Soc. Am. J.*, 1987(51), 1145-1151.

Ball, W. P. (1990) Equilibrium sorption and diffusion rate studies with halogenated organic chemical and sandy aquifer material. Doctoral dissertation, Stanford University, Order number 9017828.

Ball, W. P. and P. V. Roberts (1991) Long-Term sorption of Halogenated Organic Chemicals by aquifer material. 2. Intraparticle Diffusion. *Environ. Sci. Technol.,* 25(7), 1237-1249.

Bang, S., G. P. Korfiatis and X. G. Meng (2005) Removal of arsenic from water by zero-valent iron. *Journal of Hazardous Materials,* 121(1-3), 61-67.

Bayard, R., V. Chatain, C. Gachet, A. Troadec and R. Gourdon (2006) Mobilisation of arsenic from a mining soil in batch slurry experiments under bio-oxidative conditions. *Water Research,* 40(6), 1240-1248.

Benjamin, M. M. (2002) *Water Chemistry.* McGraw-Hill, New York.

Bodek, I., W. J. Lyman, W. F. Reehl, and D. H. Rosenblatt (1988) *Environmental Inorganic Chemistry,* Pergamon Press, NY, USA.

Boni, M. R., A. Chiavola and S. Sbaffoni (2006) Pretreated waste landfilling: Relation between leachate characteristics and mechanical behaviour. *Waste Manage.,* 26(10), 1156-1165.

Catalano, J. G., Z. Zhang, P. Fenter and M. J. Bedzyk (2006) Inner-sphere adsorption geometry of Se(IV) at the hematite (100)-water interface. *Journal of Colloid and Interface Science,* 297(2), 665-671.

Chakraborty, S., M. Wolthers, D. Chatterjee and L.Charlet (2007) Adsorption of arsenite and arsenate onto muscovite and biotite mica. Elkin 06. *International Electrokinetics Conference*, June 25-29, Nancy, France, 309(2), 392.

Chapra, C. S. and R. P. Canale (1998) Numerical Methods for Engineers. *McGraw-Hill Co.: Singapore,* 3rd ed.

Chiou, H. Y., Y. M. Hsueh, K. F. Liaw, S. F. Horng, M. H. Chiang, Y. S. Pa, J. S. N. Lin, C. H. Huang and C. J. Chen (1995) Incidence of Internal Cancers and Ingested Inorganic Arsenic - A 7-Year Follow-Up-Study In Taiwan. *Cancer Res.,* 55(6), 1296-1300.

Chowdhury, U. K., B. K. Biswas, T. R. Chowdhury, G. Samanta, B. K. Mandal, G. C. Basu, C. R. Chanda, D. Lodh, K. C. Saha, S. K. Mukherjee, S. Roy, S. Kabir, Q. Quamruzzaman and D. Chakraborti (2000) Groundwater arsenic contamination in Bangladesh and West Bengal, India. *Environ. Health Perspect.,* 108(5), 393-397.

Christensen, T. H., P. L. Bjerg, S. A. Banwart, R. Jakobsen, G. Heron and H. J. Albrechtsen (2000) Characterization of redox conditions in groundwater contaminant plumes. *J. Contam. Hydrol.,* 45(3-4), 165-241.

Christensen, T. H., P. Kjeldsen, H. J. Albrechtsen, G. Heron, P. H. Nielsen, P. L. Bjerg and P. E. Holm (1994) Attenuation of Landfill Leachate Pollutants In Aquifers. *Crit. Rev. Environ. Sci. Technol.,* 24(2), 119-202.

Chutia, P., S. Kato, T. Kojima and S. Satokawa (2009) Arsenic adsorption from aqueous solution on synthetic zeolites *J. Hazard. Mater.,* 162(1), 440-447.

Cincotti, A., A. Mameli, A. M. Locci, R. Orru and G. Cao (2006) Heavy metals uptake by Sardinian natural zeolites: Experiment and modeling. *Industrial and Engineering Chemistry Research,* 45(3), 1074-1084.

Cooke, A. J., R. K. Rowe, B. E. Rittmann, J. VanGulck and S. Millward (2001) Biofilm growth and mineral precipitation in synthetic leachate columns. *Journal of Geotechnical and Geoenvironmental Engineering,* 127(10), 849-856.

Crank, J. (1975) The Mathematics of Diffusion. *Oxford University Press: Oxford, U.K.,* 2nd ed.

Cunningham, J. A., C. J. Werth, M. Reinhard and P. V. Roberts (1997) Effects of Grain-Scale Mass Transfer on the Transport of Volatile Organics Through Sediments 1. Model Development. *Water Resour. Res.,* 33(12), 2713-2726

Davis, A. P. and V. Bhatnagar (1995) Adsorption of Cadmium and Humic-Acid onto Hematite. *Chemosphere,* 30(2), 243-256.

Davis J.A. and D.B. Kent (1990) Surface complexation modeling in aqueous geochemistry. In: Hochella M.F., Jr., White A.F., eds. Reviews in mineralogy, Vol. 23: *Mineral-water interface geochemistry*. Washington, DC: Mineralogical Society of America, 177-260.

Duggan, J. (2005) The potential for landfill leachate treatment using willows in the UK - A critical review. *Resour. Conserv. Recycl.,* 45(2), 97-113.

Dzombak, D. A. and F. M. Morel (1990) *Surface Complexation Modeling, Hydrous Iron Oxide*. Wiley-Interscience, New York.

El-Fadel, M., E. Bou-Zeid, W. Chahine and B. Alayli (2002) Temporal variation of leachate quality from pre-sorted and baled municipal solid waste with high organic and moisture content. *Waste Manage.,* 22(3), 269-282.

Entezari, M. H. and T. R. Bastami (2006) Sono-sorption as a new method for the removal of lead ion from aqueous solution. *Journal of Hazardous Materials*, 137(2), 959-964.

Fan, H. J., I. W. Chen, M. H. Lee and T. Chiu (2007) Using FeGAC/H2O2 process for landfill leachate treatment. *Chemosphere*, 67(8), 1647-1652.

Fan, H. J., H. Y. Shu, H. S. Yang and W. C. Chen (2006) Characteristics of landfill leachates in central Taiwan. *Science of The Total Environment*, 361(1-3), 25-37.

Ghosh, A., M. Mukiibi and W. Ela (2004) TCLP underestimates leaching of arsenic from solid residuals under landfill conditions. *Environmental Science and Technology*, 38(17), 4677-4682.

Gimenez, J., M. Martinez, J. de Pablo, M. Rovira and L. Duro (2007) Arsenic sorption onto natural hematite, magnetite, and goethite. *Journal of Hazardous Materials*, 141(3), 575-580.

Goldberg, S. (2002) Competitive adsorption of arsenate and arsenite on oxides and clay minerals. *Soil Science Society of America Journal*, 66(2), 413-421.

Gregg, S. J. and K. S. W. Singh (1982) *Absorption, Sorption Area and Porosity* Academic Press, London and New York.

Hayes, K. F., and Leckie, J. O. (1987) Modeling ionic strength effects on cation adsorption at hydrous oxide/solution interface. *Journal of Colloid and Interface Science*, 115(2), 564-72.

Hayes, K.F., C. Papelis, and J. O. Leckie (1998) Modelling ionic strength effects on anion adsorption at hydrous oxide/solution interfaces. *J. Colloid Interface Sci.*, 125:717-726.

He, L.M., L. W. Zelazny, V. C. Baligar, K. D. Ritchey, and D. C. Martens (1997) Ionic strength effects on sulfate and phosphate adsorption on gamma-alumina and kaolinite: Triple-layer model. *Soil Science Society of America Journal*, 61(3), 784-793.

Hiemstra, T., de wit, J. C. M., and van Riemsdijk, W. H. (1989a) Multisite proton adsorption modeling at the solid/solution interface of (hydr)oxides: A new approach II. application to various important (hydr)oxides. *Journal of Colloid and Interface Science*, 133(1), 105-116.

Jeon, C. S., K. Baek, J. K. Park, Y. K. Oh and S. D. Lee (2009) Adsorption Characteristics of Iron-coated Zeolite. *J. Hazard. Mater.*, 163(2-3), 804-808.

Jones, G. W. and T. Pichler (2007) Relationship between pyrite stability and arsenic mobility during aquifer storage and recovery in southwest central Florida. *Environmental Science and Technology,* 41(3), 723-730.

Kanel, S. R., B. Manning, L. Charlet and H. Choi (2005) Removal of arsenic(III) from groundwater by nanoscale zero-valent iron. *Environmental Science and Technology,* 39(5), 1291-1298.

Kargi, F. and M. Y. Pamukoglu (2003) Simultaneous adsorption and biological treatment of pre-treated landfill leachate by fed-batch operation. *Process Biochem.,* 38(10), 1413-1420.

Kjeldsen, P., M. A. Barlaz, A. P. Rooker, A. Baun, A. Ledin and T. H. Christensen (2002) Present and long-term composition of MSW landfill leachate: A review. *Crit. Rev. Environ. Sci. Technol.,* 32(4), 297-336.

Kjeldsen, P., P. L. Bjerg, K. Rugge, T. H. Christensen and J. K. Pedersen (1998) Characterization of an old municipal landfill (Grindsted, Denmark) as a groundwater pollution source: landfill hydrology and leachate migration. *Waste Manage. Res.,* 16(1), 14-22.

Kjeldsen, P. and M. Christophersen (2001) Composition of leachate from old landfills in Denmark. *Waste Manage. Res.,* 19(3), 249-256.

Kuleyin, A. and O. N. Ergun (2007) Studies on removal of ammonium ions from synthetic aqueous solutions and field leachate samples using clinoptilolite. *Fresenius Environmental Bulletin,* 16(2), 168-175.

Kurttio, P., E. Pukkala, H. Kahelin, A. Auvinen and J. Pekkanen (1999) - Arsenic Concentrations in Well Water and Risk of Bladder and Kidney Cancer in Finland. *Environmental Health Perspectives* 107(9), 710.

LaBolle, E. M. and G. E. Fogg (2001) Role of Molecular Diffusion in Contaminant Migration and Recovery in an Alluvial Aquifer System. *Transport in Porous Media,* 42(1-2), 155-179.

Lamm, S. H. and M. B. Kruse (2005) Arsenic ingestion and bladder cancer mortality - What do the dose-response relationships suggest about? *Human and Ecological Risk Assessment,* 11(2), 433-450.

Letavayova, L., V. Vlckova and J. Brozmanova (2006) Selenium: From cancer prevention to DNA damage. *Toxicology,* 227(1-2), 1-14.

Lewis, D. R., J. W. Southwick, R. Ouellet-Hellstrom, J. Rench and R. L. Calderon (1999) Drinking water arsenic in Utah: A cohort mortality study. *Environ. Health Perspect.,* 107(5), 359-365.

Maji, S. K., A. Pal and T. Pal (2007) Arsenic removal from aqueous solutions by adsorption on laterite soil. *J. Environ. Sci. Health Part A-Toxic/Hazard. Subst. Environ. Eng.,* 42(4), 453-462.

Martinez, M., J. Gimenez, J. de Pablo, M. Rovira and L. Duro (2006) Sorption of selenium(IV) and selenium(VI) onto magnetite. *Applied Surface Science,* 252(10), 3767-3773.

McBride, M. B. (1997) A critique of diffuse double layer models applied to colloid and surface chemistry. *Clays and Clay Minerals,* 45(4), 598-608.

Mead, M. N. (2005) - Arsenic: In Search of an Antidote to a Global Poison. *Environ. Health Perspect.,* 113(6), A378 - A386.

Moghaddam, A. H. and C. N. Mulligan (2008) Leaching of heavy metals from chromated copper arsenate (CCA) treated wood after disposal. *Waste Manage.,* 28(3), 628-637.

Mor, S. (2006) Leachate characterization and assessment of groundwater pollution near municipal solid waste landfill site. *Environ. Monit. Assess.,* 118(1-3), 435-456.

Naeem, A., P. Westerhoff and S. Mustafa (2007) Vanadium removal by metal (hydr)oxide adsorbents. *Water Research,* 41(7), 1596-1602.

Navas-Acien, A., E. K. Silbergeld and E. Guallar (2008) Arsenic Exposure and Prevalence of Type 2 Diabetes in US Adults. *Epidemiology,* 19(6), S308-S308.

Oliveira, A. F., A. C. Q. Ladeira, V. S. T. Ciminelli, T. Heine and H. A. Duarte (2006) Structural model of arsenic(III) adsorbed on gibbsite based on DFT calculations. *Journal of Molecular Structure-Theochem,* 762(1-3), 17-23.

Papini, M. P., Kahie, Y. D., Troia, B., Majone, M. (1999) Adsorption of lead at variable pH onto a natural porous medium: Modeling of batch and column experiments. *Environmental Science and Technology* 33(24), 4457-4464

Payne, K. B. and T. M. Abel-Fattah (2005) Adsorption of arsenate and arsenite by iron-treated activated carbon and zeolites: Effects of pH, temperature, and ionic strength. *Journal of Environmental Science and Health Part A-Toxic/Hazardous Substances and Environmental Engineering,* 40(4), 723-749.

Pohland, F. G. and S. R. Harper (1989) Treatment of Landfill Leachate with an Upflow Anaerobic Reactor Combining a Sludge Bed and a Filter - Discussion. *Water Sci. Technol.,* 21(12), 1543-1550.

Pokhrel, D. and T. Viraraghavan (2004) Leachate generation and treatment - A review. *Fresenius Environ. Bull.,* 13(3B), 223-232.

Poulsen, T. G., P. Moldrup, K. Sorensen and J. A. Hansen (2002) Linking landfill hydrology and leachate chemical composition at a controlled municipal landfill (Kastrup, Denmark) using state-space analysis. *Waste Manage. Res.*, 20(5), 445-456.

Pujari, P. R. and V. Deshpande (2005) Source apportionment of groundwater pollution around Landfill site in Nagpur, India. *Environ. Monit. Assess.*, 111(1-3), 43-54.

Rahman, M., M. Vahter, N. Sohel, M. Yunus, M. A. Wahed, P. K. Streatfield, E. C. Ekstrom and L. A. Persson (2006) Arsenic exposure and age- and sex-specific risk for skin lesions: A population-based case-referent study in Bangladesh. *Environ. Health Perspect.*, 114(12), 1847-1852.

Reitzel, S., G. Faquhar and E. McBean (1992) Temporal Characterization Of Municipal Solid-Waste Leachate. *Can. J. Civ. Eng.*, 19(4), 668-679.

Renou, S., J. G. Givaudan, S. Poulain, F. Dirassouyan and P. Moulin (2008) Landfill leachate treatment: Review and opportunity. *J. Hazard. Mater.*, 150(3), 468-493.

Rigby, S. P. (2005) Predicting surface diffusivities of molecules from equilibrium adsorption isotherms. *Colloid Surf. A-Physicochem. Eng. Asp.*, 262(1-3), 139-149.

Rittmann, B. E. and P. L. McCarty (2001) *Environmental Biotechnology: Principles and Applications.* McGraw-Hill, New York.

Rossman, T. G., A. N. Uddin and F. J. Burns (2004) Evidence that arsenite acts as a cocarcinogen in skin cancer. *Toxicology And Applied Pharmacology*, 198(3), 394-404.

Salem, Z., K. Hamouri, R. Djemaa and K. Allia (2008) Evaluation of landfill leachate pollution and treatment. *Desalination*, 220(1-3), 108-114.

Sari, A. and M. Tuzen (2009) Biosorption of As(III) and As(V) from aqueous solution by macrofungus (Inonotus hispidus) biomass: Equilibrium and kinetic studies. *J. Hazard. Mater.*, 164(2-3), 1372-1378.

Savarimuthu, X., M. M. Hira-Smith, Y. Yuan, O. S. von Ehrenstein, S. Das, N. Ghosh, D. N. G. Mazumder, and A. H. Smith (2006) Seasonal variation of arsenic concentrations in tubewells in West Bengal, India. *Journal of Health Population and Nutrition*, 24(3), 277-281.

Schindler, S., H. Elias and H. Paulus (1990) Kinetics and Mechanism of Ligand Substitution in Binuclear Copper(Ii) Complexes As Model Compounds for Hemocyanin. *Z.Naturforsch.(B)*, 45(5), 607-618.

Sierra-Alvarez, R., J. A. Field, I. Cortinas, G. Feijoo, M. T. Moreira, M. Kopplin and A. J. Gandolfi (2005) Anaerobic microbial mobilization and biotransformation of arsenate adsorbed onto activated alumina. *Water Research,* 39(1), 199-209.

Simeonova, P. P. and M. I. Luster (2004) Arsenic and atherosclerosis. *Toxicol. Appl. Pharmacol.,* 198(3), 444-449.

Smedley, P. L., and D. G. Kinniburgh (2002) A review of the source, behaviour and distribution of arsenic in natural waters. *Applied Geochemistry*, 17(5), 517-568.

Smith, A., C. Steinmaus, J. Liaw, G. Marshall, Y. Yuan, C. Ferreccio and O. Von Ehrenstein (2006) Early childhood carcinogenic exposures causing lung cancer in young adults. *Epidemiology,* 17(6), S316-S317.

Smith, E. and R. Naidu (2009) Chemistry of inorganic arsenic in soils: kinetics of arsenic adsorption-desorption. *Environ. Geochem. Health,* 31, 49-59.

Smith, E. H. (1998) Surface complexation modeling of metal removal by recycled iron sorbent. *Journal of Environmental Engineering-ASCE,* 124(10), 913-920.

Sing, K. S. W., D. H. Everett, R. A. W. Haul, L. Moscou, R. A. Pierotti, J. Rouquérol, and T. Siemieniewska (1985) Reporting physisorption data for gas/solid systems with special reference to the determination of surface area and porosity. *International Union of Pure and Applied Chemistry. Pure and Appl. Chem.* 57, 603- 619.

Sperlich, A., A. Werner, A. Genz, G. Amy, E. Worch and M. Jekel (2005) Breakthrough behavior of granular ferric hydroxide (GFH) fixed-bed adsorption filters: modeling and experimental approaches. *Water Research,* 39(6), 1190-1198.

Sposito G. (1989) The chemistry of soils. Oxford Univ. Press, New York.

Statom, R. A., G. D. Thyne and J. E. McCray (2004) Temporal changes in leachate chemistry of a municipal solid waste landfill cell in Florida, USA. *Environ. Geol.*, 45(7), 982-991.

Steinmaus, C. M., Y. Yuan and A. H. Smith (2005) The temporal stability of arsenic concentrations in well water in Western Nevada. *Environ. Res.*, 99(2), 164-168.

Sugden, K. D., K. M. Rigby and B. D. Martin (2004) Oxidative activation of the human carcinogen chromate by arsenite: A model for synergistic metal activation leading to oxidative DNA damage. *Toxicology in Vitro,* 18, 741-748.

Thirunavukkarasu, O. S., T. Viraraghavan and K. S. Subramanian (2003a) Arsenic removal from drinking water using granular ferric hydroxide. *Water SA,* 29(2), 161-170.

Thirunavukkarasu, O. S., T. Viraraghavan and K. S. Subramanian (2003b) Arsenic removal from drinking water using iron oxide-coated sand. *Water Air and Soil Pollution,* 142(1-4), 95-111.

Tseng, W. P. (1989) Blackfoot Disease In Taiwan - A 30-Year Follow-Up-Study. *Angiology,* 40(6), 547-558.

Tuzen, M., A. Sari, D. Mendil, O. D. Uluozlu, M. Soylak and M. Dogan (2009) Characterization of biosorption process of As(III) on green algae Ulothrix cylindricum. *J. Hazard. Mater.,* 165(1-3), 566-572.

Vaughan, R. L., B. E. Reed and E. H. Smith (2007) Modeling As(V) removal in iron oxide impregnated activated carbon columns. *J. Environ. Eng.-ASCE,* 133(1), 121-124.

Villalobos, M and J. O. Leckie (2000) Carbonate adsorption on goethite under closed and open CO_2 conditions. *Geochimica et Cosmochimica Acta,* 64(22): 3787-3802.

Villalobos, M., M. A. Trotz and J. O. Leckie (2003) Variability in goethite surface site density: evidence from proton and carbonate sorption. *Journal of Colloid and Interface Science,* 268(2), 273-287.

Wasserman (2004) Water arsenic exposure and children's intellectual function in Araihazar, Bangladesh (vol 112, pg 329, 2004). *Environ. Health Perspect.,* 112(17), A980-A980.

Weber, W. J., Y. C. Jang, T. G. Townsend and S. Laux (2002) Leachate from land disposed residential construction waste. *Journal of Environmental Engineering-ASCE,* 128(3), 237-245.

Wijnja, H. and C. P. Schulthess (2000) Interaction of carbonate and organic anions with sulfate and selenate adsorption on an aluminum oxide. *Soil Science Society of America Journal,* 64(3), 898-908.

Wiszniowski, J., D. Robert, J. Surmacz-Gorska, K. Miksch and J. V. Weber (2006) Landfill leachate treatment methods: A review. *Environmental Chemistry Letters,* 4(1), 51-61.

Xiao, Y., X. M. Bai, Z. Y. Ouyang, H. Zheng and F. F. Xing (2007) The composition, trend and impact of urban solid waste in Beijing. *Environ. Monit. Assess.,* 135(1-3), 21-30.

Xu, Y., L. Axe, N. Yee and J. A. Dyer (2006) Bidentate complexation modeling of heavy metal adsorption and competition on goethite. *Environmental Science and Technology,* 40(7), 2213-2218.

Zhang, C. J. and P. J. D. Lindan (2003) Multilayer water adsorption on rutile TiO2(110): A first-principles study. *Journal of Chemical Physics*, 118(10), 4620-4630.

Zhang, G. S., J. H. Qu, H. J. Liu, R. P. Liu and R. C. Wu (2007) Preparation and evaluation of a novel Fe-Mn binary oxide adsorbent for effective arsenite removal. *Water Research*, 41(9), 1921-1928.

Zhang, H. and H. M. Selim (2005) Kinetics of arsenate adsorption-desorption in soils. *Environmental Science and Technology*, 39(16), 6101-6108.

Zhang, P.and D. L. Sparks (1990) Kinetics and mechanisms of sulfate adsorption/desorption on goethite using pressure-jump relaxation. *Soil Sci. Soc. Am. J.* 54:1266-1273 b.

Appendices

Appendix A: Mercury Porosimetry Results

Table A.1: Cumulative pore area and pore size distribution. Conducted by Micromeritics Instrument Corporation, on 2/27/2006 using mercury intrusion porosimeter.

dp (μm)	Cumulative pore area (m^2/g)	dp (μm)	Cumulative pore area (m^2/g)
327.6878	0	0.082366656	0.613288164
227.54985	0.000391807	0.077124146	0.68414408
173.5191125	0.001992231	0.072485175	0.735545158
89.2352375	0.007810588	0.068383612	0.79736352
59.79998125	0.008456222	0.067093756	0.819862127
44.96617813	0.008889776	0.063579523	0.873644352
32.78413125	0.009327926	0.060412372	0.936363518
25.78112344	0.009644276	0.055784235	1.026214719
21.25665156	0.009885686	0.051826349	1.116279244
17.21953594	0.010087615	0.048360913	1.214369059
13.91776875	0.010356329	0.045349207	1.288767934
11.32151797	0.010593125	0.042679626	1.383346796
9.037774219	0.010916039	0.040343109	1.459046245
7.860540625	0.011092873	0.038285596	1.538657069
7.232928906	0.011251267	0.036297885	1.643633485
6.033024219	0.011566636	0.034231061	1.739577532
4.900156641	0.011741296	0.033016724	1.801502585
3.881474219	0.011960343	0.031560455	1.878663898
3.209735352	0.012347241	0.030240915	1.976126671
2.51315957	0.012966263	0.029024652	2.076627731
2.068713281	0.01343941	0.027905322	2.136651039
1.602570605	0.014325585	0.026871759	2.226849556
1.317486621	0.015491906	0.025912503	2.332393408
1.056382031	0.017722609	0.02417337	2.496361017
0.839917383	0.019865477	0.022654832	2.63280344
0.672953271	0.024533082	0.021322115	2.84517765
0.555413916	0.031453006	0.020129604	3.033255816
0.432398877	0.041619271	0.019490553	3.147248745
0.350161328	0.055746056	0.018878058	3.262808561
0.284233057	0.077651411	0.018030894	3.454088926
0.2059545776	0.092751451	0.009816467	7.680464745
0.226553027	0.116956413	0.009632477	7.867991924
0.183068579	0.169815227	0.009430498	8.088423729
0.150857471	0.238609686	0.009144685	8.420746803
0.139377173	0.271915466	0.008918386	8.653759956
0.129389758	0.309654266	0.008702028	8.925909042

Appendix A (continued)

Table A.1 (continued).

dp (μm)	Cumulative pore area (m^2/g)	dp (μm)	Cumulative pore area (m^2/g)
0.120856372	0.349265516	0.008537014	8.925909042
0.017255145	3.611133575	0.008359469	9.178256989
0.016468413	3.831953287	0.008207018	9.337397575
0.015751926	4.065076351	0.007989118	9.601500511
0.015093037	4.287619591	0.007799093	9.928987503
0.014374319	4.519478798	0.007618278	10.29830074
0.013828618	4.726214409	0.007507674	10.44942856
0.013268764	5.01078701	0.007339589	10.6950779
0.012940515	5.163272858	0.007222354	11.24076939
0.012631678	5.361508369	0.007108595	11.42803192
0.012408337	5.524181843	0.006985001	11.67472553
0.012073802	5.759036064	0.006839588	11.89489937
0.011721764	5.903332233	0.006712788	12.23061752
0.011463208	6.146080494	0.006602528	12.53014565
0.011179498	6.391561508	0.006507509	12.70552349
0.010876588	6.620385647	0.006403679	13.03821087
0.010655597	6.842644215	0.00623812	13.3563509
0.010440336	6.976864815	0.006132047	13.50846195
0.010231044	7.225616455	0.006029965	13.89335632
0.010004567	7.451769352	0.00594064	13.97526073

Table A.2: Cumulative pore volume and pore size distribution. Conducted by Micromeritics Instrument Corporation, on 2/27/2006 using mercury intrusion porosimeter.

dp (μm)	Cumulative pore volume (mL/g)	dp (μm)	Cumulative pore volume (mL/g)
327.6878	3.85505E-30	0.003015605	0.418612689
227.54985	0.027193252	0.003119041	0.416973919
173.5191125	0.107428282	0.003230148	0.415266722
89.2352375	0.298528105	0.003318718	0.415266722
59.79998125	0.310555875	0.003412499	0.415266722
44.96617813	0.316233605	0.00365387	0.415266722
32.78413125	0.32049188	0.003767985	0.415266722
25.78112344	0.322807789	0.003889517	0.415266722
21.25665156	0.324227214	0.004018863	0.415266722
17.21953594	0.325198412	0.004109827	0.415266722

Appendix A (continued)

Table A.2 (continued).

dp (μm)	Cumulative pore volume (mL/g)	dp (μm)	Cumulative pore volume (mL/g)
0.015093037	0.385733902	0.017968045	0.415266722
0.014374319	0.386587948	0.018821135	0.415266722
0.013828618	0.387316763	0.019417583	0.415266722
0.013268764	0.38828066	0.02006114	0.415266722
0.012940515	0.388780236	0.021246402	0.415266722
0.012631678	0.389413893	0.022551984	0.415266722
0.012408337	0.389923066	0.024061369	0.415266722
0.012073802	0.390641779	0.025809195	0.415266722
0.011721764	0.391070992	0.026721527	0.415266722
0.011463208	0.391774505	0.027748093	0.415266722
0.011179498	0.392469287	0.028854703	0.415266722
0.010876588	0.393100172	0.030049753	0.415266722
0.010655597	0.393698394	0.031345477	0.415266722
0.010440336	0.394052327	0.032796786	0.415266722
0.010231044	0.394695073	0.03398844	0.415266722
0.010004567	0.395267129	0.036058444	0.415266722
0.009816467	0.39583376	0.038059836	0.415266722
0.009632477	0.396289647	0.04012941	0.415266722
0.009430498	0.396814913	0.042477521	0.415266722
0.009144685	0.397586524	0.045199429	0.415266722
0.008918386	0.398112655	0.04812095	0.415266722
0.008702028	0.398712069	0.051586279	0.415266722
0.008537014	0.399255842	0.055623175	0.415266722
0.008359469	0.399591953	0.060252893	0.415266722
0.008207018	0.400138855	0.063355811	0.415266722
0.007989118	0.400801867	0.066916986	0.415266722
0.007799093	0.401530713	0.068212219	0.415266722
0.007618278	0.401821971	0.072270886	0.415266722
0.007507674	0.40228644	0.076850433	0.415136099
0.007339589	0.402707458	0.082242633	0.414662212
0.007222354	0.403287828	0.088143085	0.41402784
0.007108595	0.403623283	0.095059583	0.413348764
0.006985001	0.40405789	0.106266272	0.412734091
0.006839588	0.404438376	0.112904944	0.412186325
0.006712788	0.405007094	0.120423975	0.411470085
0.006602528	0.405505627	0.129109424	0.410816699
0.006507509	0.405793041	0.139088293	0.410134822

Appendix A (continued)

Table A.2 (continued).

13.91776875	0.326244295	0.004170942	0.415266722
11.32151797	11.32151797	11.32151797	11.32151797
9.037774219	9.037774219	9.037774219	9.037774219
7.860540625	7.860540625	7.860540625	7.860540625
7.232928906	7.232928906	7.232928906	7.232928906
6.033024219	6.033024219	6.033024219	6.033024219
4.900156641	4.900156641	4.900156641	4.900156641
3.881474219	3.881474219	3.881474219	3.881474219
0.113243518	0.113243518	0.113243518	0.113243518
0.106497888	0.106497888	0.106497888	0.106497888
0.095366675	0.095366675	0.095366675	0.095366675
0.088414441	0.088414441	0.088414441	0.088414441
0.082366656	0.082366656	0.082366656	0.082366656
0.077124146	0.077124146	0.077124146	0.077124146
0.072485175	0.072485175	0.072485175	0.072485175
0.068383612	0.068383612	0.068383612	0.068383612
0.067093756	0.067093756	0.067093756	0.067093756
0.063579523	0.063579523	0.063579523	0.063579523
0.060412372	0.060412372	0.060412372	0.060412372
0.055784235	0.055784235	0.055784235	0.055784235
0.051826349	0.051826349	0.051826349	0.051826349
0.048360913	0.048360913	0.048360913	0.048360913
0.045349207	0.045349207	0.045349207	0.045349207
0.042679626	0.042679626	0.042679626	0.042679626

Appendix B: N_2(g) Porosimetry Data for ≤ 38 μm Grain Size

Table B.1: BET surface area input report (≤ 38 μm grain size)

TriStar 3000 V6.07 A Unit 1 Port 1 Serial #: 2059			
Started: 9/13/2007 4:33:24PM.		Analysis Adsorptive: N2	
Completed: 9/13/2007 7:11:10PM.		Analysis Bath Temp.: 77.300 K	
Report Time: 9/14/2007 10:19:13AM.		Sample Mass: 1.6713 g	
Warm Free Space: 6.5257 cm³ Measured.			
Cold Free Space: 20.4456 cm³ Measured			
Equilibration Interval: 10 s Low.		Pressure Dose: None	
Sample Density: 1.000 g/cm³.		Automatic Degas: Yes	
Stage	Soak Temperature (°C)	Ramp Rate (°C/min)	Soak Time (min)
1	80	10	180

Table B.2: Relative pressure isotherm tabular report (≤ 38 μm grain size)

Relative Pressure (P/Po)	Absolute Pressure (mmHg)	Quantity Adsorbed (cm³/g STP)	Elapsed Time (h:min)	Saturation Pressure (mmHg)
			01:04	737.62726
0.048377386	35.68448	7.5086	01:24	
0.073976302	54.56694	8.1308	01:32	
0.102309658	75.46639	8.7114	01:39	
0.123118993	90.81593	9.1012	01:45	
0.147660233	108.91821	9.5345	01:51	
0.172691625	127.38205	9.9580	01:58	
0.198041172	146.08057	10.3714	02:03	
0.223502487	164.86153	10.7776	02:09	
0.249290584	183.88353	11.1791	02:15	
0.275267857	203.04507	11.5779	02:21	
0.301460081	222.36517	11.9751	02:26	

Table B.3: BET surface area output report (≤ 38 μm grain size)

BET Surface Area:	37.5978 ± 0.1598 m^2/g
Slope:	0.114518 ± 0.000483 g/cm^3 STP
Y-Intercept:	0.001266 ± 0.000092 g/cm^3 STP
C:	91.479128
Qm:	8.6368 cm^3/g STP
Correlation coefficient:	0.9999
Molecular cross-sectional area:	0.1620 nm^2

Appendix B (continued)

Table B.4: BET isotherm result (≤ 38 μm grain size)

Relative Pressure (P/Po)	Quantity Adsorbed (cm^3/g STP)	1/[Q(Po/P – 1]
0.048377386	7.5086	0.006770
0.073976302	8.1308	0.009825
0.102309658	8.7114	0.013083
0.123118993	9.1012	0.015427
0.147660233	9.5345	0.018170
0.172691625	9.9580	0.020962
0.198041172	10.3714	0.023810
0.223502487	10.7776	0.026707
0.249290584	11.1791	0.029705
0.275267857	11.5779	0.032806
0.301460081	11.9751	0.036038

Table B.5: Cumulative pore volume result (500 – 600 μm grain size)

Relative Pressure (P/Po)	Quantity Adsorbed (cm^3/g STP)
0.0566	39.84724
0.0981	44.87312
0.1477	49.89687
0.1969	54.37599
0.2467	58.75347
0.29	63.08098
0.3999	71.83011
0.4959	79.75732
0.6	88.20927
0.6976	97.22081
0.7969	109.2003
0.8952	126.6693
0.9931	155.1257
0.9	141.6986
0.8001	127.7297
0.70299	110.2745
0.59716	96.34435
0.491606	85.88597
0.395091	73.95985
0.292459	64.61581

Appendix C: Non-Linear Regression Analysis of Isotherm Data

Table C.1: Nonlinear regression fit to Langmuir isotherm model at pH 9. Conditions: As(V) species; 38 µm Kemiron particle size in binary systems of 0.001 N $NaNO_3$; CO_2 absent, and at room temperature.

Aqueous	K_L = 0.39, q_{max} = 67.95		
As(V)(mg/L)	q(mg/g)	Predicted (q mg/g)	Residual error
0.800	18.00	18.6574515	1.6939
5.30505	46.2556	47.9036208	0.2681
14.46464	54.18855	58.1544328	-3.6347
25.01477	59.7002	61.3619097	-2.0021
31.86075	64.21011	62.3754093	1.2638
43.2572	67.5292	63.3832014	3.3370

Table C.2: Nonlinear regression fit to Langmuir isotherm model at pH 8. Condition: As(V) species; 38 µm Kemiron particle size in binary systems of 0.001 N $NaNO_3$; CO_2 absent, and at room temperature.

Aqueous	K_L = 0.31, q_{max} = 81.77		
As(V)(mg/L)	q(mg/g)	Predicted (q mg/g)	Residual error
0.702	15	14.84385	0.5789
4.86068	49.6552657	48.94122	0.8215
9.693	58	60.66914	-3.1047
13.39593	65.9746503	65.00001	0.2801
22.3973375	74	70.27777	2.6687
42.10535	76.6098981	74.49094	0.7443
53.181067	75.5904437	75.56313	-1.4340
62.23	77.5062344	76.16918	-0.1742

Appendix C (continued)

Table C.3: Nonlinear regression fit to Langmuir isotherm model at pH 7. Condition: As(V) species; 38 µm Kemiron particle size in binary systems of 0.001 N $NaNO_3$; CO_2 absent, and at room temperature.

Aqueous	K_L = 0.34, q_{max} = 87.25		
As(V)(mg/L)	q(mg/g)	Predicted (q mg/g)	Residual error
0.823456	20	19.215473	1.0650
4.969	53.1	54.734978	-1.5032
12.603485	72.40837	70.390978	1.8021
24.44568	74.7	77.368467	-3.0952
30.2038	82.2	78.956456	2.7638
41.91872	80.934201	80.927202	-0.5411

Table C.4: Nonlinear regression fit to Freundlich isotherm model at pH 9. Condition: As(III) species; 38 µm Kemiron particle size in binary systems of 0.001 N $NaNO_3$; CO_2 absent, and at room temperature.

Aqueous	K_f = 42.54, *1/n* = 0.28		
As(III)(mg/L)	q(mg/g)	Predicted (q mg/g)	Residual error
0.009200967	9.751959	10.82010158	-1.7253
0.60808	40.79814	36.04042262	3.7819
3.641226667	61.97635	60.24887908	0.9425
11.59478	81.80263	84.01648729	-2.5532
19.987175	94.12435	98.23369582	-4.0937
30.461075	109.7598	110.8659051	-0.7297
39.268075	123.0015	119.2514106	4.3870

Appendix C (continued)

Table C.5: Nonlinear regression fit to Freundlich isotherm model at pH 7. of As(III). Condition: 38 µm Kemiron particle size in binary systems of 0.001 N $NaNO_3$; CO_2 absent, and at room temperature.

Aqueous	K_f = 35.67, *1/n* = 0.35		
As(III)(mg/L)	q(mg/g)	Predicted (q mg/g)	Residual error
0.023381	9.612393455	8.892546334	-1.6022
0.997515	37.18053878	32.02433913	1.3971
4.17858	56.73898635	52.22156098	1.0211
11.49344	74	73.76582615	-2.1786
29.95287	103.4	102.2966378	0.9700
38.1549	110.185385	111.1075207	-0.2022

Table C.6: Nonlinear regression fit to Freundlich isotherm model at pH 6. Condition: As(III) species; 38 µm Kemiron particle size in binary systems of 0.001 N $NaNO_3$; CO_2 absent, and at room temperature.

Aqueous	K_f = 40.10, *1/n* = 0.29		
As(III)(mg/L)	q(mg/g)	Predicted (q mg/g)	Residual error
0.0574205	9.277358	10.15114251	-1.8812
1.3029017	34.34369	30.81896051	2.1142
4.631712	52.3225	48.3904839	2.7322
13.204807	66.13327	70.24409421	-4.6577
21.22822	83.26322	83.16737564	0.0816
30.493129	92.84054	94.60276874	-1.2326
39.291775	105.0341	103.5305812	2.4992

Appendix D: Output of Geochemical Impact of HS^- on Leachate Solution.

Generated with Geochemical Workbench.

Table D.1: Summary of input and output data.

Temperature = 25°C		Pressure = 1.013 bars	
pH = 5.0		log f_{O2} = -61.752	
Eh = 0.0200 volts		pe = 0.3381	
Ionic strength	=	4036200.159965	
Activity of water	=	0.997976	
Solvent mass	=	1.000000 kg	
Solution mass	=	193877.440114 kg	
Solution density	=	1.014 g/cm3	
Chlorinity	=	0.059797 molal	
Dissolved solids	=	999995 mg/kg sol'n	
Rock mass	=	0.000000 kg	
Carbonate alkalinity	=	0.00 mg/kg as $CaCO_3$	
No minerals in system.			

Table D.2: Species with respective concentrations generated.

Aqueous species	Molality	mg/kg sol'n	act. coef.	log act.
SO_4^{--}	$2.018*10^{6}$	$9.998*10^{5}$	0.1111	5.3506
HSO_4^-	$3.090*10^{2}$	$1.547*10^{2}$	0.7139	2.3436
$CO_{2(aq)}$	$1.088*10^{-1}$	$2.469*10^{-2}$	1.0000	-0.9635
Cl^-	$5.980*10^{-2}$	$1.093*10^{-2}$	0.6267	-1.4263
$NH_4SO_4^-$	$4.097*10^{-2}$	$2.411*10^{-2}$	0.7139	-1.5339
$NaSO_4^-$	$3.987*10^{-2}$	$2.448*10^{-2}$	0.7139	-1.5457
$CaSO_4$	$2.994*10^{-2}$	$2.102*10^{-2}$	1.0000	-1.5237
$MgSO_4$	$1.934*10^{-2}$	$1.201*10^{-2}$	1.0000	-1.7136
HCO_3^-	$6.229*10^{-3}$	$1.960*10^{-3}$	0.7502	-2.3304
$FeSO_4$	$9.356*10^{-4}$	$7.331*10^{-4}$	1.0000	-3.0289
$As(OH)_3$	$6.671*10^{-5}$	$4.333*10^{-5}$	1.0000	-4.1758
HSe^-	$3.761*10^{-5}$	$1.551*10^{-5}$	0.7139	-4.5710
$N_{2(aq)}$	$3.188*10^{-5}$	$4.606*10^{-6}$	1.0000	-4.4965
H^+	$1.050*10^{-5}$	$5.458*10^{-8}$	0.9524	-5.0000
$NiSO_4$	$2.896*10^{-6}$	$2.311*10^{-6}$	1.0000	-5.5383
H_2SO_4	$2.180*10^{-6}$	$1.103*10^{-6}$	1.0000	-5.6616
H_2Se	$1.770*10^{-6}$	$7.391*10^{-7}$	1.0000	-5.7521
$H_2S_{(aq)}$	$1.814*10^{-7}$	$3.188*10^{-8}$	1.0000	-6.7414
CO_3^{--}	$1.563*10^{-7}$	$4.838*10^{-8}$	0.1354	-7.6743
$Fe(SO_4)_2^-$	$9.527*10^{-8}$	$1.218*10^{-7}$	0.7139	-7.1674
Na^+	$3.600*10^{-8}$	$4.268*10^{-9}$	0.7139	-7.5901

Appendix D (continued)

Table D.2 (continued).

NH_4^+	$2.613*10^{-8}$	$2.431*10^{-9}$	0.5738	-7.8241
$As(OH)_4^-$	$5.457*10^{-9}$	$4.024*10^{-9}$	0.7139	-8.4094
Ca^{++}	$3.037*10^{-9}$	$6.278*10^{-10}$	0.2106	-9.1942
HS^-	$3.024*10^{-9}$	$5.158*10^{-10}$	0.6731	-8.6914
Mg^{++}	$1.664*10^{-9}$	$2.086*10^{-10}$	0.3071	-9.2917
OH^-	$1.529*10^{-9}$	$1.341*10^{-10}$	0.6731	-8.9877
AsS_2^-	$1.456*10^{-9}$	$1.044*10^{-9}$	0.7139	-8.9833
$CaCl^+$	$1.682*10^{-10}$	$6.554*10^{-11}$	0.7139	-9.9205
$NaHCO_3$	$1.616*10^{-10}$	$7.003*10^{-11}$	1.0000	-9.7915
Fe^{++}	$1.252*10^{-10}$	$3.605*10^{-11}$	0.2106	-10.5792
$H_2AsO_4^-$	$8.932*10^{-10}$	$6.493*10^{-11}$	0.7139	-10.1954
$CaHCO_3^+$	$6.270*10^{-11}$	$3.269*10^{-11}$	0.7945	-10.3026
$HAsS_2$	$5.227*10^{-11}$	$3.775*10^{-11}$	1.0000	-10.2818
$MgCl^+$	$3.791*10^{-11}$	$1.168*10^{-11}$	0.7139	-10.5676
$MgHCO_3^+$	$3.423*10^{-11}$	$1.506*10^{-11}$	0.7139	-10.6120
NaCl	$2.422*10^{-11}$	$7.302*10^{-12}$	1.0000	-10.6157
$HAsO_4^{--}$	$1.002*10^{-11}$	$7.232*10^{-12}$	0.1111	-11.9535
$FeHCO_3^+$	$3.438*10^{-12}$	$2.073*10^{-12}$	0.7139	-11.6100
$FeCl^+$	$3.316*10^{-12}$	$1.562*10^{-12}$	0.7139	-11.6257
NH_3	$7.915*10^{-13}$	$6.953*10^{-14}$	1.0000	-12.1015
Ni^{++}	$4.751*10^{-13}$	$1.439*10^{-13}$	0.2106	-12.9998
HCl	$2.977*10^{-13}$	$5.598*10^{-14}$	1.0000	-12.5263
H_3AsO_4	$1.135*10^{-13}$	$8.308*10^{-14}$	1.0000	-12.9451
$FeCl_2$	$4.656*10^{-14}$	$3.044*10^{-14}$	1.0000	-13.3320
AsO_2OH^{--}	$3.416*10^{-14}$	$2.184*10^{-14}$	0.1111	-14.4208
Se^{--}	$2.755*10^{-14}$	$1.122*10^{-14}$	0.1111	-14.5143
$FeSO_4^+$	$2.262*10^{-14}$	$1.772*10^{-14}$	0.7139	-13.7919
$CaCO_3$	$2.225*10^{-14}$	$1.149*10^{-14}$	1.0000	-13.6526
$MgCO_3$	$8.940*10^{-15}$	$3.888*10^{-15}$	1.0000	-14.0487
$H_{2(aq)}$	$8.441*10^{-15}$	$8.777*10^{-17}$	1.9293	-13.7882
$FeCO_3$	$2.672*10^{-15}$	$1.597*10^{-15}$	1.0000	-14.5732
$NaCO_3^-$	$2.434*10^{-15}$	$1.042*10^{-15}$	0.7139	-14.7601
S_4^{--}	$1.059*10^{-15}$	$7.002*10^{-16}$	0.1111	-15.9296
$FeOH^+$	$2.439*10^{-16}$	$9.167*10^{-17}$	0.7139	-15.7590
S_5^{--}	$1.694*10^{-16}$	$1.401*10^{-16}$	0.1111	-16.7253
$MgOH^+$	$1.156*10^{-16}$	$2.463*10^{-17}$	0.7139	-16.0833
AsO_4^{---}	$5.646*10^{-17}$	$4.046*10^{-17}$	0.0050	-18.5493
SeO_3^{--}	$4.986*10^{-17}$	$3.265*10^{-17}$	0.0004	-19.7071
S_2^{--}	$2.735*10^{-17}$	$9.046*10^{-18}$	0.1111	-17.5174
$CaOH^+$	$1.830*10^{-17}$	$5.390*10^{-18}$	0.7139	-16.8838
NaOH	$1.659*10^{-17}$	$3.423*10^{-18}$	1.0000	-16.7801
S^{--}	$1.586*10^{-17}$	$2.623*10^{-18}$	0.1603	-17.5946
S_6^{--}	$1.306*10^{-17}$	$1.296*10^{-17}$	0.1111	-17.8384

Appendix D (continued)

Table D.2 (continued).

S_3^{--}	$9.001*10^{-18}$	$4.466*10^{-18}$	0.1111	-18.0000
$HSeO_3^-$	$5.465*10^{-18}$	$3.607*10^{-18}$	0.7139	-17.4088
$NiOH^+$	$3.018*10^{-18}$	$1.179*10^{-18}$	0.7139	-17.6666
$FeHSO_4^{++}$	$3.934*10^{-18}$	$3.103*10^{-19}$	0.1603	-19.2002
$Fe(OH)_2^+$	$1.667*10^{-19}$	$7.727*10^{-20}$	0.7139	-18.9244
$FeOH^{++}$	$2.244*10^{-20}$	$8.431*10^{-21}$	0.1603	-20.4440
$H2SeO_3$	$1.506*10^{-20}$	$1.002*10^{-20}$	1.0000	-19.8221
$Fe(OH)_3$	$5.317*10^{-21}$	$2.931*10^{-21}$	1.0000	-20.2744
$FeCO_3^+$	$8.650*10^{-21}$	$5.169*10^{-22}$	0.7139	-21.2093
$Mg_2CO_3^{++}$	$9.931*10^{-23}$	$5.564*10^{-23}$	0.1603	-22.7979
$Fe(OH)_2$	$9.928*10^{-23}$	$4.602*10^{-23}$	1.0000	-22.0031
Fe^{+++}	$8.332*10^{-23}$	$2.400*10^{-23}$	0.0669	-23.2537
$FeCl^{++}$	$3.934*10^{-23}$	$1.853*10^{-23}$	0.1603	-23.2001
$CH_{4(aq)}$	$3.782*10^{-23}$	$3.129*10^{-24}$	1.9293	-22.1369
$Ni(OH)_2$	$2.650*10^{-23}$	$1.268*10^{-23}$	1.0000	-22.5767
$FeCl_2^+$	$1.480*10^{-24}$	$9.675*10^{-25}$	0.7139	-23.9761
$Fe(OH)_4^-$	$1.751*10^{-25}$	$1.119*10^{-25}$	0.7139	-24.9030
Mg_2OH^{+++}	$2.281*10^{-26}$	$7.718*10^{-27}$	0.0493	-26.9494
$FeCl_3$	$3.954*10^{-27}$	$3.308*10^{-27}$	1.0000	-26.4030
CH_3COO^-	$1.042*10^{-27}$	$3.172*10^{-28}$	0.7502	-27.1072
HCH_3COO	$4.458*10^{-28}$	$1.381*10^{-28}$	1.0000	-27.3509
$Ni(OH)_3^-$	$1.518*10^{-29}$	$8.590*10^{-30}$	0.7139	-28.9652
$FeCl_4^-$	$2.497*10^{-30}$	$2.546*10^{-30}$	0.7139	-29.7489
$Fe(OH)_3^-$	$2.188*10^{-30}$	$1.206*10^{-30}$	0.7139	-29.8063
Ni_2OH^{+++}	$4.064*10^{-31}$	$2.818*10^{-31}$	0.0493	-31.6984
$Ni(NH_3)_2^{++}$	$5.302*10^{-32}$	$2.537*10^{-32}$	0.1603	-32.0705
$NaCH_3COO$	$1.319*10^{-35}$	$5.581*10^{-36}$	1.0000	-34.8797
$MgCH_3COO^+$	$1.042*10^{-35}$	$4.479*10^{-36}$	0.7139	-35.1285
$FeCH_3COO^+$	$6.588*10^{-36}$	$3.904*10^{-36}$	0.7139	-35.3276
$Ni(OH)_4^{--}$	$9.124*10^{-37}$	$5.965*10^{-37}$	0.1111	-36.9942
SeO_4^{--}	$7.892*10^{-38}$	$5.819*10^{-38}$	0.1111	-38.0572
$CaCH_3COO^+$	$4.607*10^{-38}$	$2.355*10^{-38}$	0.7139	-37.4830
$Fe_2(OH)_2^{++++}$	$2.309*10^{-38}$	$1.735*10^{-38}$	0.0151	-39.4587
$FeHSeO_3$	$4.371*10^{-40}$	$4.144*10^{-40}$	1.0000	-39.3594
$HSeO_4^-$	$9.967*10^{-42}$	$7.401*10^{-42}$	0.7139	-41.1478
$AsH_{3(aq)}$	$8.308*10^{-42}$	$3.340*10^{-42}$	1.0000	-41.0805
$FeCH_3COO^{++}$	$1.713*10^{-46}$	$1.015*10^{-46}$	0.1603	-46.5611
$NiSeO_4$	$4.147*10^{-49}$	$4.313*10^{-49}$	1.0000	-48.3823
$Fe_3(OH)_4^{5+}$	$7.115*10^{-54}$	$8.645*10^{-54}$	0.0012	-56.0640
$Mg_4(OH)_4^{++++}$	$1.004*10^{-55}$	$8.560*10^{-56}$	0.0151	-56.8202
NO_2^-	$1.053*10^{-57}$	$2.498*10^{-58}$	0.6267	-57.1806
$Ni_4(OH)_4^{++++}$	$2.202*10^{-59}$	$3.440*10^{-59}$	0.0151	-60.4792
HNO_2	$1.097*10^{-59}$	$2.659*10^{-60}$	1.0000	-58.9599

Appendix D (continued)

Table D.2 (continued).

$O_{2(aq)}$	$1.157*10^{-65}$	$1.910*10^{-66}$	1.9293	-64.6512
$Fe(CH_3COO)_2^+$	$1.893*10^{-70}$	$1.699*10^{-70}$	0.7139	-69.8691
NO_3^-	$1.023*10^{-74}$	$3.272*10^{-75}$	0.6267	-74.1930
$Ni(NH_3)_6^{++}$	$1.369*10^{-76}$	$1.136*10^{-76}$	0.1603	-76.6585
$FeNO_2^{++}$	$3.254*10^{-77}$	$1.709*10^{-77}$	0.1603	-77.2826
$CaNO_3^+$	$4.578*10^{-83}$	$2.411*10^{-83}$	0.7139	-82.4857
$NiNO_3^+$	$1.904*10^{-87}$	$1.186*10^{-87}$	0.7139	-86.8667
$Fe(CH_3COO)_3$	$1.055*10^{-95}$	$1.268*10^{-95}$	1.0000	-94.9768
$FeNO_3^{++}$	$2.228*10^{-96}$	$1.355*10^{-96}$	0.1603	-96.4470
$(O\text{-phth})^{--}$	$2.345*10^{-106}$	$1.985*10^{-106}$	0.1111	-106.5842
$H(O\text{-phth})^-$	$9.318*10^{-107}$	$7.936*10^{-107}$	0.7139	-106.1770
$H_2(O\text{-phth})$	$5.924*10^{-109}$	$5.076*10^{-109}$	1.0000	-108.2274
$Na(O\text{-phth})^-$	$4.699*10^{-114}$	$4.535*10^{-114}$	0.7139	-113.4743
$Ca(O\text{-phth})$	$4.377*10^{-114}$	$4.610*10^{-114}$	1.0000	-113.3588
ClO_4^-	$5.403*10^{-147}$	$2.771*10^{-147}$	0.6731	-146.4393
$Ni(NO_3)_2$	$7.354*10^{-163}$	$6.930*10^{-163}$	1.0000	-162.1335

Table D.3: The initial input species with respective concentrations.

	In fluid			Sorbed	Kd	
Original basis	total moles	moles	mg/kg	moles	mg/kg	L/kg
$As(OH)_4^-$	$6.67*10^{-5}$	$6.67*10^{-5}$	$4.92*10^{-5}$			
Ca^{++}	0.0299	0.0299	0.00619			
Cl^-	0.0598	0.0598	0.0109			
Fe^{++}	0.000936	0.000936	0.000270			
H^+	309.0	309.0	1.60			
H_2O	55.7	55.7	5.17			
HCO_3^-	0.115	0.115	0.0362			
Mg^{++}	0.0193	0.0193	0.00242			
NO_3^-	0.0410	0.0410	0.0131			
Na^+	0.0399	0.0399	0.00473			
Ni^{++}	$2.90*10^{-6}$	$2.90*10^{-6}$	$8.77*10^{-7}$			
$O_{2(aq)}$	-0.197	-0.197	-0.0325			
SO_4^{--}	$2.02*10^6$	$2.02*10^6$	$1.00*10^6$			
SeO_3^{--}	$3.94*10^{-5}$	$3.94*10^{-5}$	$2.58*10^{-5}$			

Appendix D (continued)

Table D.4: Gases with respective fugacities generated.

Gases	fugacity	log fug.
$CO_{2(g)}$	3.082	0.489
$N_{2(g)}$	0.04878	-1.312
Steam	0.03125	-1.505
$H_2S_{(g)}$	$1.940*10^{-6}$	-5.712
$H_{2(g)}$	$2.108*10^{-11}$	-10.676
$S_{2(g)}$	$1.958*10^{-16}$	-15.708
$CH_{4(g)}$	$4.823*10^{-20}$	-19.317
$O_{2(g)}$	$1.769*10^{-62}$	-61.752

Appendix E: Raw Experimental Data

Table E.1: As(V) sorption data on 0.1 g/L Kemiron.

5 ppm As(V), 0.001 N		5 ppm As(V), 0.1 N		5 ppm2 As(V), 0.1 N	
Final pH	**% sorbed**	**Final pH**	**% sorbed**	**Final pH**	**% sorbed**
9.70	57.83	9.34	67.01	8.78	64.58
9.86	60.99	8.94	66.51	7.90	73.51
8.70	71.60	8.26	75.66	7.87	71.36
7.60	82.86	7.90	80.28	7.73	74.80
7.57	84.68	8.08	76.77	7.41	78.53
7.60	82.74	7.33	85.95	7.26	78.25
7.57	83.75	7.47	86.64	7.00	81.10
7.72	83.62	6.57	92.31	6.90	83.03
7.42		6.98	91.29	6.70	84.07
5.71	94.25	4.55	98.33	6.68	84.39
6.19	94.16	4.31	98.55	6.25	86.61
6.48	93.03			5.74	89.41
5.93	92.85			5.59	87.92
10 ppm As(V), 0.001 N		10 ppm As(V), 0.1 N		10 ppm As(V), 0.1 N	
Final pH	**% sorbed**	**Final pH**	**% sorbed**	**Final pH**	**% sorbed**
9.50	36.70	8.71	37.27	9.81	35.97
9.68	41.07	7.11	47.19	9.92	39.20
8.68	48.01	6.89	46.17	9.38	39.58
8.46		6.65	47.50	8.73	45.57
7.96	49.53	6.63	47.21	7.58	54.42
8.85	45.89	6.02	46.92	7.76	51.28
7.49	54.49	6.01	44.68	6.69	61.73
7.78	57.33	6.00	47.04	5.29	69.71
7.83	54.44	5.27	58.82	5.88	65.96
5.46	66.80	5.22	58.18	5.91	68.10
4.32	72.02	5.20	59.44		
6.11	65.16	5.00	61.38		
4.48	72.07				

Appendix E (continued)

Table E.2: 5 ppm As(III) sorption data on 0.1 g/L Kemiron.

10 ppm As(III), 0.001 N sodium nitrate		10 ppm As(III), 0.1 N sodium nitrate	
Final pH	% As(V) removed	pH	% As(V) removed
9.7	61.5	8.5	55.0
9.2	65.2	7.9	59.4
6.6	55.6	7.8	56.9
7.0	61.8	7.5	54.9
7.0	58.9	7.3	57.4
7.3	63.1	6.1	50.2
7.4	62.6	5.9	44.3
8.0	69.0	5.9	44.6
7.1	59.5	5.1	41.7
6.6	56.7	4.8	39.8
6.2	53.4	4.5	38.3
5.7	41.0	4.3	35.0
4.7	36.7		
4.6	31.1		
4.6	30.3		
4.2	27.3		
4.1	26.9		
1 ppm As(III), 0.1 N sodium nitrate			
8.9	98.4		
8.7	98.9		
7.7	98.2		
5.9	98.4		
5.8	96.1		
5.8	98.3		
5.8	97.5		
5.6	95.1		
5.1	92.4		
5.1	96.8		
4.7	91.1		
4.5	88.4		
4.3	83.5		
4.1	86.6		
5 ppm As(III), 0.1 N sodium nitrate			
9.6	78.1		
9.6	81.9		
9.7	80.7		
8.7	87.4		
7.3	81.6		

Appendix E (continued)

Table E.2 (continued).

6.9	78.4
6.0	69.1
6.3	71.8
6.6	74.3
6.8	76.4
4.0	38.2
4.2	43.8

Table E.3: 5 ppm As(III) Isotherm data on 0.1 g/L Kemiron, I = 0.01 N $NaNO_3$.

pH	**Ceq(mg/l)**	**q(mg/g)**	**pH**	**Ceq(mg/l)**	**q(mg/g)**
6	0.06	9.28	7	0.02	9.61
6	1.30	34.34	7	1.00	37.18
6	4.63	52.32	7	4.18	56.74
6	13.20	66.13	7	40.22	95.97
6	21.23	83.26			
6	30.49	92.84			
6	39.29	105.03			
pH	**Ceq(mg/l)**	**q(mg/g)**	**pH**	**Ceq(mg/l)**	**q(mg/g)**
8	0.01	9.75	9	0.01	9.75
8	0.75	39.46	9	0.61	40.80
8	11.49	82.79	9	3.64	61.98
8	29.95	98.12	9	11.59	81.80
8	38.15	116.19	9	19.99	94.12
			9	30.46	104.76
			9	39.27	113.00

Appendix E (continued)

Table E.4: 5 ppm As(V) Sorption on 0.1 g/L Bayoxide, I = 0.01 N $NaNO_3$.

0.1g/L BayOxide	
5 ppm initial As(V) concentration	
Final	**% As(V)**
pH	5 ppm
9.3	18.2
9.6	18.5
8.9	
8.8	21.9
8.2	24.0
7.0	26.4
7.0	28.5
6.7	30.0
6.8	31.2
6.3	29.1
6.6	31.8
6.4	34.6
5.4	37.6
5.3	36.3
4.7	41.1
10 ppm initial As(V) concentration	
Final	**% As(V)**
pH	10 ppm
8.7	3.6
8.3	3.0
7.7	5.4
7.1	9.3
6.7	9.8
6.5	
6.4	12.3
6.4	11.3
6.4	14.6

Appendix E (continued)

Table E.5: 5 ppm As(V) Sorption to 0.1 g/L Kemiron in the presence of Se(IV), I = 0.001 N $NaNO_3$.

w5 ppm Se(IV) **Final pH**	**% As(V) removed**
8.97	53.12
8.93	54.51
8.14	56.90
8.28	57.56
7.74	64.11
7.67	65.76
7.19	68.86
6.72	71.11
6.41	73.55
5.05	75.32
5.73	75.57
5.84	75.08
5.05	
4.65	79.73

w 0.5 ppm Se(IV) **Final pH**	**% As(V) removed**
8.27	70.88
8.28	67.82
8.96	63.50
8.09	74.92
7.82	76.61
7.73	78.57
7.58	79.16
7.21	86.64
7.07	85.18
6.96	87.60
6.57	89.04
6.35	88.79
5.99	97.07

Appendix E (continued)

Table E.6: 5 ppm As(V) Sorption to 0.1 g/L Kemiron in the presence of Ca^{2+}, I = 0.001 N $NaNO_3$.

W 0.1 ppm Ca^{2+}

Final pH	% As(V) removed
3.81	99.99
5.38	99.95
6.09	99.98
6.55	99.99
5.29	99.96
5.92	100.00
6.34	100.00
6.28	100.00
6.91	100.00
5.96	100.00
6.28	99.65
4.83	100.00
4.33	100.00

w 0.001 ppm Ca^{2+}

Final pH	% As(V) removed
8.95	66.98
8.05	76.42
8.35	71.93
8.06	75.49
8.08	76.15
8.14	75.15
7.54	80.95
6.81	86.49
7.43	81.90
7.21	84.43
6.84	88.42
6.43	91.06
6.55	91.19
6.34	92.66
5.85	94.45

Appendix E (continued)

Table E.7: 5 ppm As(V) sorption to 0.1 g/L Kemiron in the presence of CO_3^{2-}, I = 0.001 N $NaNO_3$.

0.1 ppm CO32-	
Final pH	% As(V) sorbed
8.27	70.1
7.52	77.9
7.42	79.7
7.37	80.6
3.59	96.6
3.91	95.6
6.14	91.2
6.52	88.8
6.54	90.8
6.88	89.0
6.89	86.8
6.91	89.6
7.13	86.7
6.32	91.5
5.75	94.0
1 ppm CO_3^{2-}	
9.27	65.3
9.28	65.8
9.16	66.8
8.42	72.1
7.73	80.3
7.53	82.3
7.55	83.0
7.23	86.8
7.33	84.6
6.83	90.1
6.93	88.1
6.73	90.4
4.09	97.3
5.65	93.7
5.21	95.9
100 ppm CO_3^{2-}	
9.99	58.0
9.91	61.0
9.42	66.8
7.99	82.1
8.14	82.6

Appendix E (continued)

Table E.7 (continued).

0.1 ppm CO32-	
Final pH	% As(V) sorbed
8.11	83.1
7.88	86.0
7.49	86.6
7.31	90.2
6.96	90.2
6.73	91.4
6.33	93.5
5.96	94.8
3.82	97.7

Table E.8: 5 ppm As(V) sorption to 0.1 g/L Kemiron in the presence of SO_4^{2-}, I = 0.001 N $NaNO_3$.

1 ppm SO_4^{2-}	
Final pH	% As(V) sorbed
8.57	70.3
8.79	69.7
8.33	73.9
8.00	76.4
7.75	79.0
7.01	86.3
7.32	83.9
6.97	87.7
6.95	87.4
6.34	92.2
6.26	92.9
5.91	94.5
5.69	95.7
5.48	95.8
4.69	97.7
100 ppm SO_4^{2-}	
7.80	78.9
8.79	70.3
7.85	79.8

Appendix E (continued)

Table E.8 (continued).

7.50	83.5
7.14	87.6
5.76	92.0
4.96	91.7
6.90	86.2
6.79	89.0
4.71	95.1
6.73	88.6
4.28	94.6
6.42	89.9

Table E.9: 5 ppm As(V) or As(III) sorption to 0.1 g/L Kemiron in the presence of 5 ppm Ni. I = 0.001N $NaNO_3$.

As(V)	
pH	%As(V) Sorbed
7.93	76.9
7.76	78.3
7.57	81.0
7.25	84.0
7.15	86.0
6.94	88.9
6.59	90.3
6.43	91.9
5.74	94.4
6.97	90.2
4.46	96.7
As(III)	
pH	% As(III) Sorbed
8.13	79.8
7.72	76.5
7.59	74.8
7.43	74.2
7.35	73.5
6.93	71.8
6.84	68.8
5.70	56.3
7.03	71.1
7.03	72.6
7.24	74.2
7.86	82.2

Appendix E (continued)

Table E.10: 5 ppm As(V) sorption to 0.1 g/L Kemiron (≤ 38 μm) as a function of pH and ORP in a synthetic landfill leachate solution.

Final ORP	Final pH	% As(V) removed	Final ORP	Final pH	% As(V) removed
-336	10.6	89	234	10.2	36
-334	12.0	87	234	8.6	60
-325	10.2	56	235	9.1	53
-308	10.8	99	243	8.4	64
-248	8.4	49	253	9.4	45
-245	8.5	36	259	9.0	52
-235	7.8	56	259	9.2	48
-230	10.2	38	263	9.9	38
-230	8.8	34	265	8.5	67
-230	8.8	34	277	8.4	59
-217	8.1	54	288	7.5	93
-86	11.6	99	289	9.9	41
-8	11.1	100	299	9.3	47
9	11.3	100	300	8.1	81
72	11.8	90	301	7.8	90
83	10.9	100	310	8.8	56
110	10.0	55	317	9.2	51
110	10.0	42	319	7.5	96
112	10.4	65	322	7.9	85
115	10.9	100	323	8.1	71
122	11.2	100	332	7.2	98
131	9.9	45	334	7.6	94
132	10.3	41	345	8.1	75
135	10.1	37	350	8.3	70
135	11.2	100	351	8.3	75
135	11.2	100	351	8.1	76
138	10.0	43	355	8.3	75
139	11.4	99	356	8.3	69
160	10.0	46	356	8.3	67
170	10.0	37	357	8.3	64
196	10.4	56	359	8.2	75
197	8.4	69	363	8.3	73
202	8.5	61	366	8.3	73
210	7.9	91	372	8.2	72
221	8.6	60	375	7.7	85
221	7.8	91	381	9.2	51
223	10.2	38	391	8.8	59
231	9.3	47			
233	9.8	42			

Appendix F: Non-Linear Regression of Freundlich Isotherm

```
disp('Gauss-Newton Method of non-linear Regression of Freundlich isotherm, pH 6')
disp('y=(a(1)*x^a(2))')
x=[0.0574205 1.3029017 4.631712 13.204807 21.22822 30.493129 39.291775];
y=[9.277358 34.34369 52.3225 66.13327 83.26322 92.84054 105.0341];
x
y
n=20
a=[10 0.1]'
for i=1:n
   disp(' ')
   i
   a
   dfda1=x.^a(2);
   dfda2=(a(1).*x.^a(2)).*log(x);
   DFDB=[dfda1' dfda2']
   D=[(y-(a(1).*x.^a(2)))']
   B=(inv(DFDB'*DFDB))*(DFDB'*D)
   a=a+B;
end
disp(' ')
a
x1=(0:0.5:45);
ytheo=(a(1).*x1.^a(2));
plot(x,y,'*')
hold on
plot(x1,ytheo,'r')
```

Appendix G: Non-Linear Regression of Langmuir Isotherm

```
disp('Gauss-Newton Method of non-linear Regression of Langmuir isotherm')
disp('y=(a(1)*x*a(2))/(1+a(1)*x)')
x=[0.8 5.30505 14.46464 25.01477 31.86075 43.2572];
y=[18 46.2556 54.18855 59.7002 64.21011 67.5292];
x
y
n=50
a=[1 100]'
for i=1:n
   disp(' ')
   i
   a
   dfda1=((a(2).*x)./((1+a(1).*x)))-(a(1).*x.*a(2).*x)./((1+a(1).*x)).^2;
   dfda2=a(1).*x./(1+a(1).*x);
   DFDB=[dfda1' dfda2']
   D=[(y-(a(1).*x.*a(2))./(1+a(1).*x))']
   B=(inv(DFDB'*DFDB))*(DFDB'*D)
   a=a+B;
end
disp(' ')
a
x1=(0:0.5:50);
ytheo=(a(1).*x1.*a(2))./(1+a(1).*x1);
plot(x,y,'O')
hold on
plot(x1,ytheo,'r')
```

About the Author

Douglas Oti received a Bachelor's Degree in Geological Engineering from the University of Science and Technology in 1998 in Ghana and an M.S. in Civil Engineering with a focus on Water Resources from North Carolina Agricultural and Technical State University in 2004. He was a T.A of various undergraduate Water Resources Courses while in the Master's program and entered the Ph.D. program at the University of South Florida in 2004.

While in the Ph.D. program Douglas was very active in various Student Associations including FSAWWA, ASCE and Engineers for a Sustainable World. In ESW he held a position of Vice President for projects in 2007-2008. He has presented his work at the Florida Air & Waste Management Association (A&WMA) conference as well as local college and university research symposia. He has so far published one peer reviewed article in the Journal of Environmental Science and Health, Part A: Toxic/Hazardous Substance and Environmental Engineering. He was also involved in teaching and mentoring undergraduate students in classrooms and in the lab for Environmental and Hydraulics courses. He was always the first to be in the lab and the last to leave.